CO.165
A-617

Folia

NEUROPATHOLOGICA

ω 718

Folia
Neuropathologica

terMedia

TERMEDIA Publishing House

BIBLOTEKA

Contents

Folia
Neuropathologica

Dysembryoplastic neuroepithelial tumour: insight into the pathology and pathogenesis

Iwona Sontowska[1], Ewa Matyja[2], Jacek Malejczyk[1], Wieslawa Grajkowska[3]

[1]Department of Histology and Embryology, Center for Biostructure Research, Medical University of Warsaw, [2]Department of Experimental and Clinical Neuropathology, Mossakowski Medical Research Centre Polish Academy of Sciences, Warsaw, [3]Department of Pathology, The Children's Memorial Health Institute, Warsaw, Poland

Abstract

Dysembryoplastic neuroepithelial tumour (DNT) is categorized as a benign glioneuronal neoplasm affecting children and young adults with chronic epileptic seizures. It is characterized by predominant intracortical localization and nodular architecture. Dysembryoplastic neuroepithelial tumour usually demonstrates a distinctive morphological pattern with a specific glioneuronal element but occasionally, its morphological picture is heterogeneous and unspecific. Thus, considering the morphology of DNT, three different histopathological subtypes are distinguished: simple, complex, and non-specific and diffuse. The DNT lesions are often related with focal cortical dysplasia (FCD) type IIIb, which is postulated to play a role in epileptogenicity. Moreover, the accompanying inflammation process might be implicated in DNT-related epileptogenesis.

Dysembryoplastic neuroepithelial tumour is generally characterized by favourable prognosis and good results of surgical treatment. The pathogenesis and molecular mechanisms involved in DNT development remain uncertain. The main molecular findings are connected with BRAF alterations and activation of RAS/ERK, PI3K/AKT and mTOR signalling pathways.

The present review summarizes the clinical, histopathological and molecular findings of DNT. The classification controversy, morphological heterogeneity and diagnostic problems are also discussed.

Key words: DNT, dysembryoplastic neuroepithelial tumour, histopathological variants, BRAF, mTOR, DNT – pathology and pathogenesis.

Introduction

Dysembryoplastic neuroepithelial tumour (DNT) is a benign, glioneuronal neoplasm that is included in the group of neuronal and mixed neuronal-glial tumours, according to the revised 4th edition of current 'WHO Classification of Tumours of the Central Nervous System' 2016 [46]. This slowly growing tumour corresponds histologically to WHO grade I [37].

Dysembryoplastic neuroepithelial tumour was first described in 1988 by Daumas-Duport *et al.* [17] as a distinct clinico-pathological entity associated with drug-resistant seizures, which affects children

Communicating author:
Wieslawa Grajkowska, PhD, Department of Pathology, The Children's Memorial Health Institute, Al. Dzieci Polskich 20, 04-730 Warsaw, Poland, phone: +48 22 815 19 60, e-mail: w.grajkowska@ipczd.pl

and young adults. Typically, the lesion is located in the cerebral cortex, particularly in the mesial temporal lobe. It exhibits multinodular architecture and appears in several different histopathological forms: 1) simple, 2) complex, 3) non-specific and diffuse. The most common clinical presentation is a drug-resistant epilepsy of a partial complex type, with early-onset and long duration from weeks to decades. The resection of the lesion is recommended in symptomatic cases. The stabilization of epileptic seizures has been demonstrated after total or even subtotal resection [12]. Occasionally, the recurrences and spontaneous or post radiation anaplastic transformation to high-grade gliomas have been noted [27].

Localization

Typically, the DNT lesion is located supratentorially in the cerebral cortex with a predilection for the mesial temporal lobe, less commonly for the frontal lobe [5,12,60]. It can be also found in other sites, including the septum pellucidum, caudate nucleus, brain stem and cerebellum [66]. Extremely rarely, the DNT located inside the ventricles, area of the corpus callosum and pericallosal region has been reported [2,11,23].

Clinical presentation

The main symptom of DNT is an early-onset, long-lasting, intractable epilepsy, mostly complex partial seizures with a frequent secondary generalization [5,12,41,59]. Seizures have their onset before the age of 20 years, usually in the childhood and continue for years to decades (mean duration of 10.8 years). The majority of cases are without focal neurologic deficits. Other symptoms, like dysarthria, facial asymmetry, focal weakness or numbness, visual field deficits or other visual symptoms are rarely encountered [16]. Moreover, the obstructive hydrocephalus could be seen in the septum pellucidum lesions [66].

Neuroimaging findings

Typically, DNT is a well-demarcated, multinodular lesion with predominant cerebral cortical location (Fig. 1A and B). It is hypointense on T1-weighted and hyperintense on T2-weighted magnetic resonance images (MRI) [35,36,59]. Dysembryoplastic neuroepithelial tumour is often composed of single or multiple cysts [59,67] and sometimes contains microcalcifications [16,59]. The deformations of the overlying part of the skull have been described. The oedema, mass
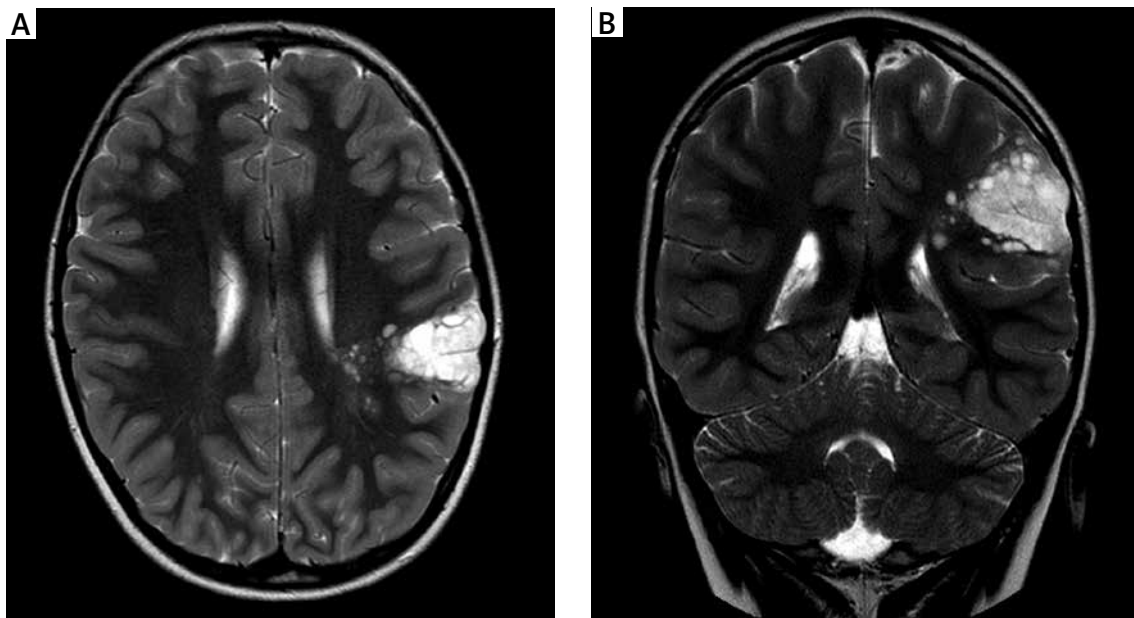

Fig. 1. Magnetic resonance images (MRI) of dysembryoplastic neuroepithelial tumour (DNT). **A)** The multinodular intracortical lesion of high signal intensity on axial T2-weighted MR image. **B)** Coronal T2-weighted MRI with hyperintense cortical abnormality (Courtesy of Professor M. Roszkowski).

effects on midline structures and contrast enhancement are not typical for DNT [36,67]. The internal septation and hyperintense "ring sign" at the periphery of the lesion might be revealed by MRI FLAIR sequence. The magnetic resonance spectroscopy (MRS) usually shows a low *N*-acetylaspartate peak and a lack of elevated choline-containing component (Cho) or Cho-Cr ratio (Cho/Cr) [67]. These features help to identify the DNT lesion and distinguish it from other low-grade gliomas.

Histopathology

Typically, DNT is characterized by intracortical nodules with columnar architecture of uniform oligodendrocyte-like cells within microcystic background (Fig. 2A and B). It exhibits a distinct morphology with a so-called specific glioneuronal element (Fig. 2C). This element consists predominantly of small oligodendrocyte-like cells arranged in a columnar orientation along parallel bundles of axons (Fig. 2D). They are usually oriented perpendicular to the cortical/pial surface [20]. Microcysts of various shape and size are lined by small, uniform cells of oligodendrocyte-like morphology (Fig. 2E and F). The large neurons are scattered within microcystic areas, sometimes making an impression that they "float" in mucin-filled background (Fig. 3A). The neurons usually exhibit morphology of normal pyramidal neurons (Fig. 3B) and may be considered as pre-existing cortical neuronal cells. Moreover, the various amount of astrocytes might be scattered in the DNT lesion. The above multinodular architecture of the lesion accompanied by the presence of "floating neurons" are the most distinctive morphological features of DNT.

Sometimes, the DNT may exhibit a growth pattern resembling diffuse gliomas. In some cases the DNT lesion consists of solid areas with oligodendrocyte-like cells and thin-walled microvessels (Fig. 3C). Delicate, so-called "chicken-wire" vasculature resembling oligodendroglioma can be visible (Fig. 3D). Microvascular proliferation with a telangiectatic pattern could be also seen. Some areas of DNT show hypercellularity with honeycomb appearance of monomorphic cells with round nuclei surrounded by clear haloes or ribbon-like palisades highly similar to oligodendroglioma (Fig. 3E and F). However, perinuclear satellitosis is not characteristic for DNTs lesions. Occasionally, the compact piloid tissue with pleomorphic neoplastic cells might resemble pilocytic astrocytoma.

Intriguingly, Komori *et al*. [33] claimed that DNT is rather a glial than glioneuronal tumour, similar to oligodendroglioma, thus it should be classified as a non-infiltrative oligodendroglioma. The research performed on DNT samples using morphometric evaluation and immunohistochemical studies documented staining for Neu-N, a neuronal nuclear antigen being a marker of neurons, and Olig-2, a transcription factor important for motoneuron [42,52] and oligodendrocyte differentiation [70]. They found that double immunohistochemical staining showed co-localization of Olig-2 and Neu-N. The distribution of Neu-N positive nuclei was similar in the tumour tissue and the adjacent cortex. Moreover, the density of Neu-N positive nuclei was lower in the tumours located in the white matter compared to those from grey matter. They suggest that probably Neu-N positive cells are entrapped in granular and pyramidal neuronal cells [33].

Three histopathological forms of DNT have been described, including: 1) simple, 2) complex and 3) non-specific and diffuse. The last form was created based on the statement that the diffuse form of DNT corresponds to a non-specific variant [8,19,29]. However, the diagnosis and definition of the non-specific type of DNT is controversial.

The simple form of DNT is composed of the specific glioneuronal element with oligodendrocyte-like cells arranged in columns. The bundles of axons and floating neurons are dispersed in a mucin-like background.

The complex form of DNT exhibits heterogeneous morphology with multinodular architecture. Except a specific glioneuronal element mentioned above, it is characterized by presence of glial nodules resembling oligodendrocytic or astrocytic population [18].

Diagnosis of a **non-specific and diffuse form of DNT** is challenging because of lack of the specific glioneuronal element and no multinodular structure. This form of DNT exhibits glial components similar to glial nodules of the complex DNT type. It is difficult to distinguish this DNT variant from other glial tumours. The non-specific and diffuse form of DNT might be histologically similar to glioma, ganglioglioma, pilocytic astrocytoma or diffuse astrocytoma [61,65]. Nevertheless, the clinical presentation with chronic seizures, cortical localization on neuroimaging and a follow-up are similar to typical DNT. Thus, the clinical data are mandatory to consider the identification of the non-specific and diffuse form of DNT [19].
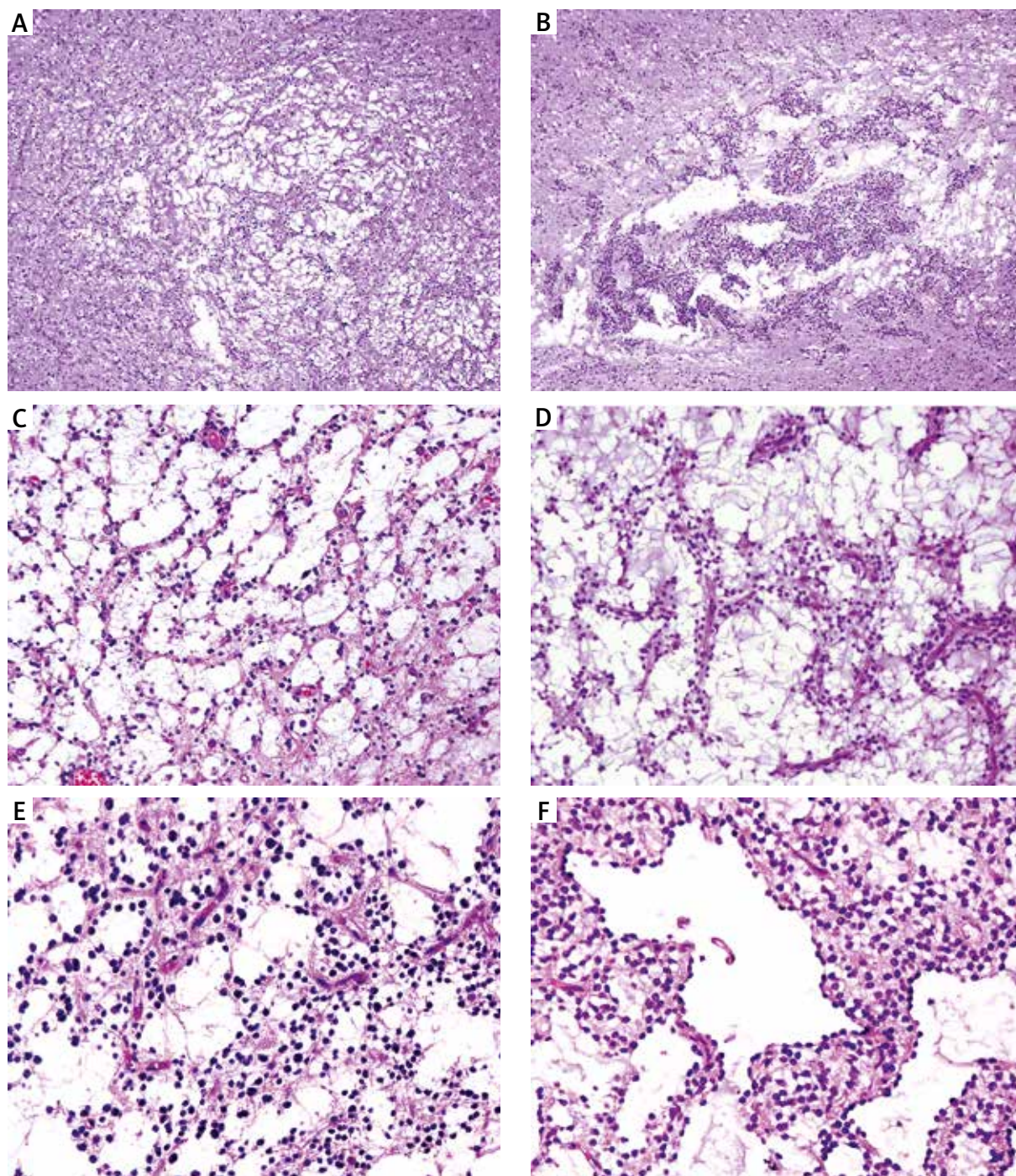
Fig. 2. Histopathology of dysembryoplastic neuroepithelial tumour (DNT), H&E staining. **A, B**) Intracortical nodules with microcystic, vacuolated background. **C**) Specific glioneuronal component with typical columnar architecture. **D)** Microcystic region consisting of mucin-rich background and a small oligodendrocyte-like component arranged along parallel rows of axons. **E)** Microcystic architecture with uniform oligodendrocyte-like cells and tiny vessels. **F)** Large microcysts lined by small oligodendrocyte-like cells (from own archival surgical material).
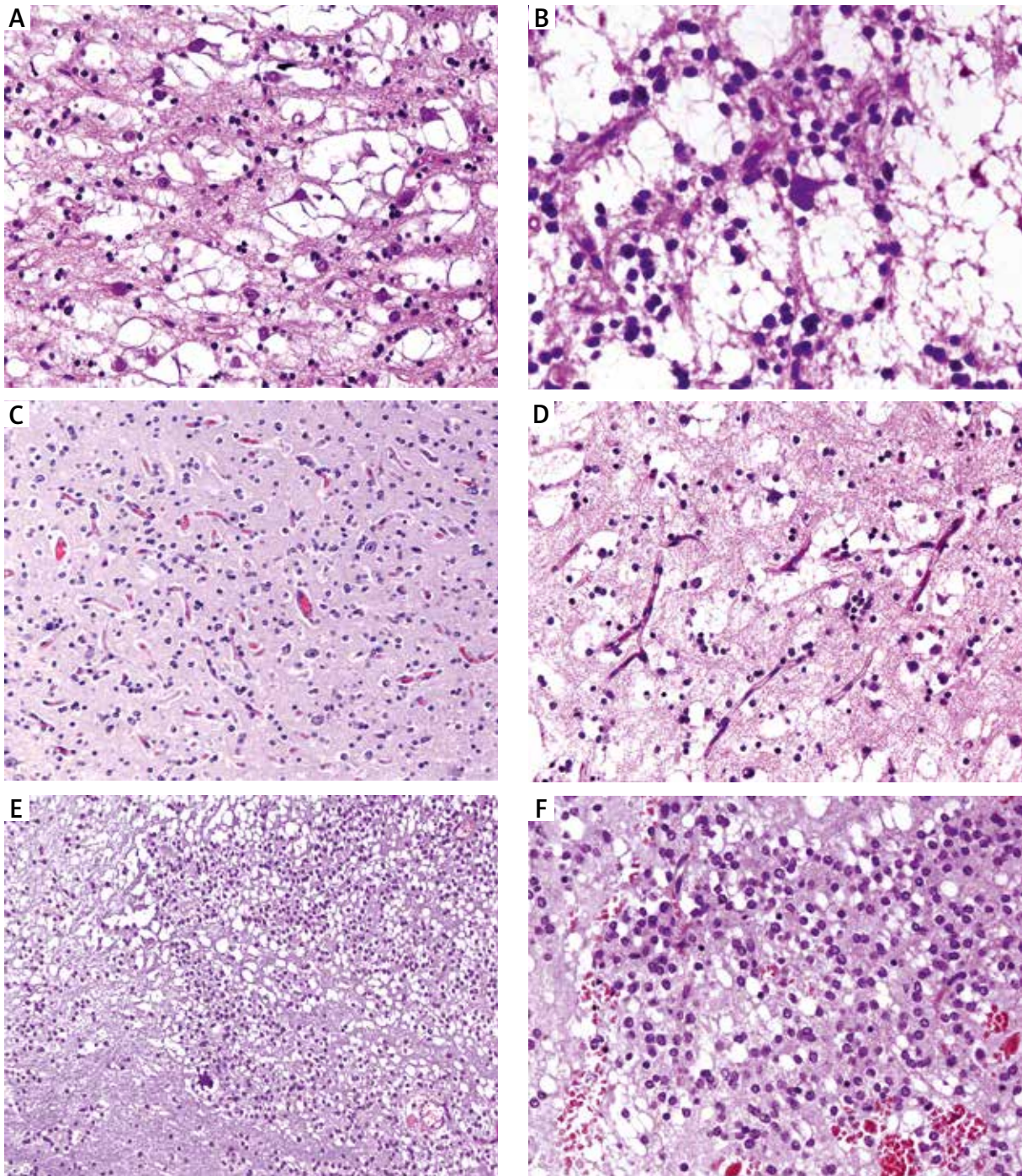
Fig. 3. Histopathology of dysembryoplastic neuroepithelial tumour (DNT), H&E staining. **A)** Specific glioneuronal element with alveolar arrangement of oligodendrocyte-like cells and numerous interspersed floating neurons. **B)** Typical glioneuronal element with an easily visible floating neuron. **C)** Solid growth pattern with oligodendrocyte-like cells and small, thin-walled vessels. **D)** Delicate branching capillaries and small, uniform cells resembling oligodendroglioma. **E)** Diffuse growth pattern with honeycomb appearance mimicking oligodendroglioma. **F)** Small, monomorphic cells with round nuclei surrounded by clear haloes similar to oligodendroglioma (from own archival surgical material).

In accordance with the benign nature of DNT, cytological atypia or mitotic activity are uncommon features and Ki-67 proliferative index is usually low, ranges from 0 to about 1.6% [22].

Moreover, DNT may be associated with focal cortical dysplasia (FCD), hippocampal sclerosis and ganglioglioma [50,51,63]. Cortical dysplasia accompanying DNT lesions is identified as FCD type IIIb, according to the criteria of the classification of the International League Against Epilepsy [6]. The foci of cortical dysplasia often coexist with the simple and non-specific type of DNT [18,19].

Differences between various forms of DNT also manifest in epileptogenicity. Chassoux et al. [15], using stereo-electroencephalography, compared epileptogenicity in different histological variants of DNT. Interestingly, they have found that the epileptogenic zone is localized in the tumour in a simple and complex form and is more widespread in most non-specific DNTs. The difference is pronounced especially in non-specific, temporal DNTs with extensive focal cortical dysplasia (FCD). However, the relationship with FCD does not unambiguously explain this discrepancy.

In addition, rare mixed tumours composed of a DNT lesion with components of rosette forming glioneuronal tumour [38], pilocytic astrocytoma [44] or pleomorphic xanthoastrocytoma [30] have been described.

Immunophenotypic profile

Markers useful in characterization of immunophenotype of DNT include S-100 protein, transcriptional factor OLIG-2, glial fibrillary acid protein (GFAP), NeuN, microtubule-associated protein 2 (MAP-2), CD34, nestin, and calbindin.

The small oligodendrocyte cells express S-100 protein (Fig. 4A) and OLIG-2, whereas they are negative for GFAP. The neuronal component consisting of "floating neurons" shows neuronal markers such as NeuN, MAP-2 and synaptophysin. GFAP can be expressed in the astrocytes scattered in the background (Fig. 4B).

MAP2 protein was observed in different proportions among DNT variants. It is expressed during development of the central nervous system as well as in neurons and glial cells in the adult brain [58,64]. MAP2 expression in oligodendrocyte-like cells and glial elements was observed significantly more often in non-specific DNTs than in the simple or complex form. Co-expression of MAP2 and CD34 was significantly more frequent in the non-specific than in complex and simple form [62]. However, the difference in MAP2 expression among different types of DNT has not been confirmed [65].

A cell-surface transmembrane protein CD34 can be found in some cases of DNT. It is commonly used as a marker of hematopoietic stem, progenitor cells and vascular endothelial cells, which is associated with increased proliferation and abrogated cell differentiation [45]. CD34 staining was observed in the perikaryal membrane of neuronal cells, cytoplasm of oligodendrocyte-like cells, pericellular stroma and stellate cells with astroglial morphology. Irrespective of the classification to the non-specific or
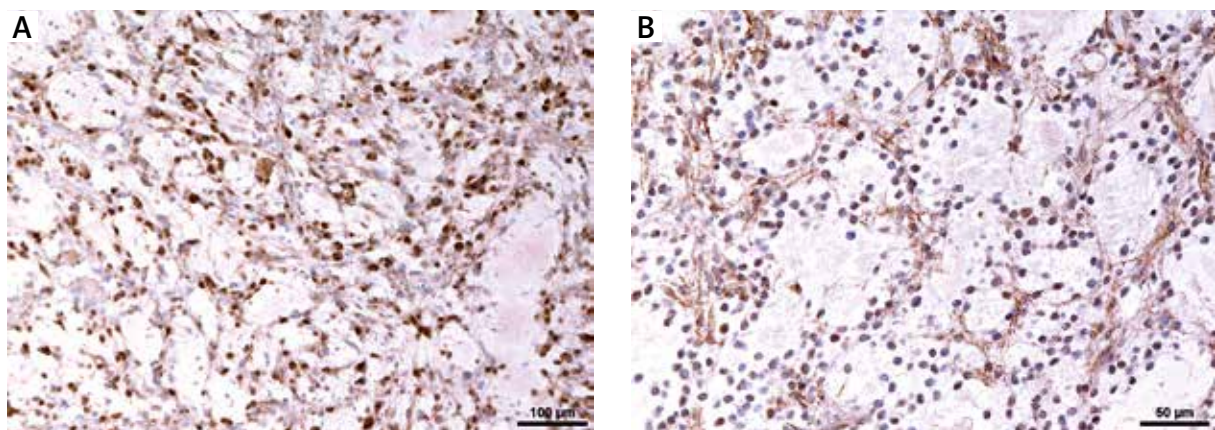

Fig. 4. Immunohistochemistry of dysembryoplastic neuroepithelial tumour (DNT). **A)** S-100 protein immunopositivity in oligodendrocyte-like elements. **B)** Glial fibrillary acid protein (GFAP) reactivity in the astrocytes scattered in the background (from own archival surgical material).

diffuse form, CD34 expression in both types of DNT was found to be similar. Statistically significant differences of immunohistochemical staining for CD34 among three main histological types of DNT were observed in two studies. The highest expression of CD34 was noticed for the non-specific type compared with simple and complex types [62,65].

Expression of CD34 and nestin was found to be the highest in the non-specific and diffuse form, but there was a difference in expression of these markers in the simple type [61,62]. However, Thom *et al.* [65] observed a statistically significant correlation between CD34 and nestin staining in particular forms. Nestin is expressed during development of the central nervous system and in the majority of proliferating brain progenitor cells, thus it is considered as a neural stem cell marker [40]. Expression of nestin and CD34 was considerably higher in the non-specific and diffuse DNTs, which may suggest that it is a less differentiated form. Nevertheless, it is not related to higher malignancy [65].

Furthermore, the non-specific type and mixed DNT/GG tumours were characterized by a significantly higher expression of calbindin [65], a calcium binding protein expressed in neuronal cells [4].

Molecular findings

The main molecular findings are connected with *BRAF* alterations and activation of RAS/ERK, PI3K/AKT and mTOR signalling pathways.

BRAF is a RAF family member displaying the highest basal activity and being considered to play an important role in tumorigenesis [13,57] It is implicated in the so-called mitogen-activated protein kinase (MAPK) pathway [39].

Chappé *et al.* [13] found *BRAFV600E* mutation in ca. 30% of DNT. Analysis was performed by a combination of polymerase chain reaction-high resolution melting (PCR-HRM), direct sequencing and immunohistochemistry as a complementary method.
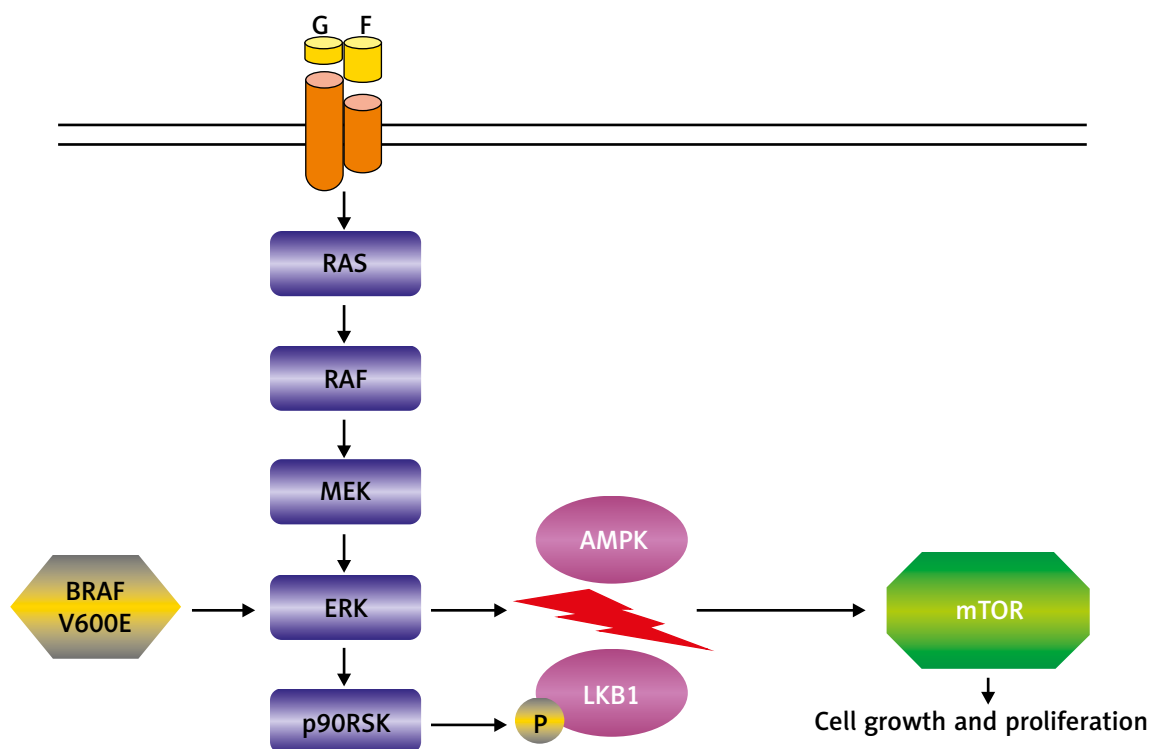
Fig. 5. Diagram illustrating probable mechanism leading to mammalian target of rapamycin (mTOR) activation. Activation of RAS/mitogen activated protein kinase (ERK) – p90 ribosomal six kinase (p90RSK) pathway as well as activating mutation of *BRAFV600E* may impact on separation of liver kinase B1 (LKB1) from AMP-activated protein kinase (AMPK), what leads to mTOR activation. However, the mechanism seems to be independent of phosphorylation of LKB1 by p90RSK.

High occurrence of *BRAFV600E* mutations (51%) was detected in a study performed on a group of 51 DNT cases [34]. Furthermore, the authors have found that mutations were significantly more frequent in tumours with extratemporal location.

In another direct sequencing study performed on 77 samples of DNT, frequent *BRAFV600E* mutation was shown in approximately 30% of cases [47]. Intriguingly, the authors did not find *BRAFV600E* mutation in the simple form of DNT. They also reported immunohistochemical co-localization of BRAF V600E-mutated protein with phosphorylated ribosomal S6 protein (pS6) and phosphorylated liver kinase B1 (pLKB1), as well as they found a significant correlation between presence of *BRAFV600E*

mutations and pS6 expression in dysplastic neurons in DNTs. The pS6 is a marker of mTOR activation. Thus, a mutation in *BRAF* might indirectly activate mTOR by the LKB1/AMP-activated protein kinase (AMPK) pathway (Fig. 5). LKB1 with its downstream effector AMPK may act as a tumour suppressor by downregulation of mTOR activity [26]. The crosstalk LKB1/AMPK with RAS/ERK/p90RSK pathway was previously described in melanoma cell cultures [25]. BRAF copy number gain was reported for the first time in DNT tumours by Kakkar *et al.* [32]. Alterations in the *BRAF* gene, and activation of mTOR and MAPK signalling pathways are suggested to play an important role in pathogenesis of DNT, and may be considered as a target for future treatment.
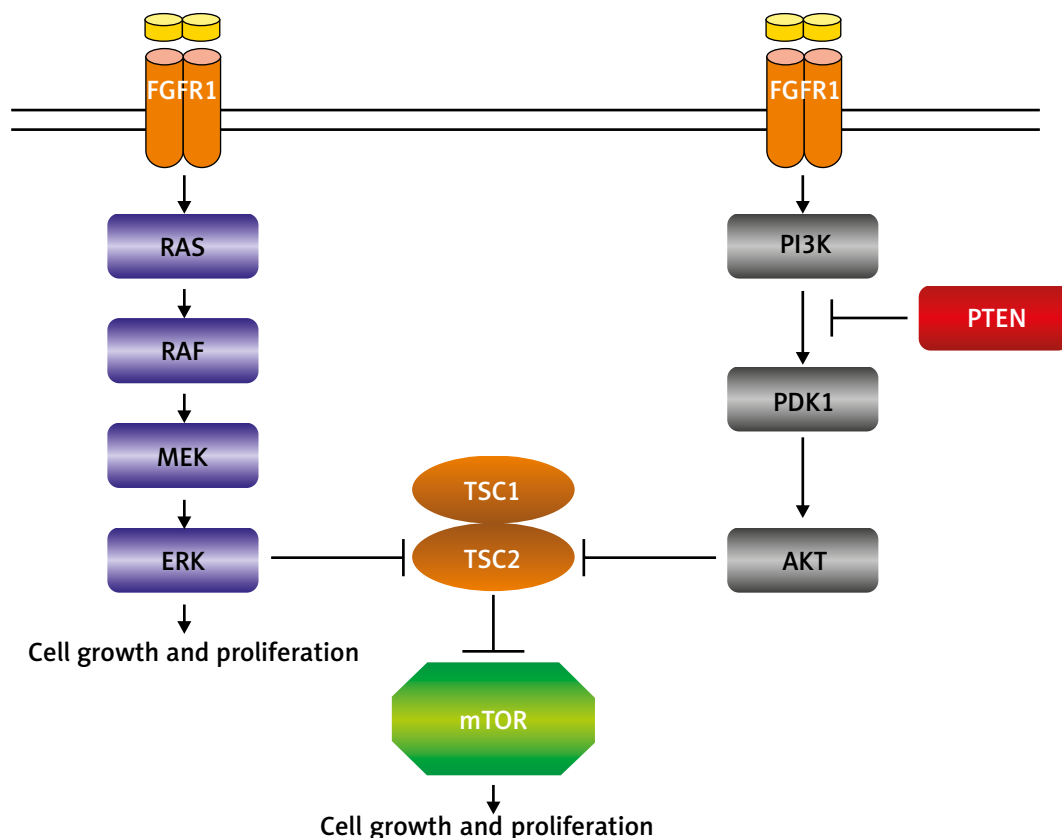
Fig. 6. Diagram illustrating activation of signalling pathways, which activation was examined in dysembryoplastic neuroepithelial tumour (DNT). Activation of the receptor, i.e. fibroblast growth factor receptor 1 (FGFR1) leads to RAS activation and consequently to phosphorylation of mitogen activated protein kinase (ERK) through cascade of protein kinases: RAF and mitogen activated protein kinase (MEK). Phosphorylated ERK may activate transcription factors as well as impact on tuberous sclerosis complex 2 (TSC2) – an inhibitor of mammalian target of rapamycin (mTOR). Lack of mTOR suppression implies cell growth and proliferation. Similarly to ERK, also phosphorylation of AKT by 3-phosphoinositide-dependent kinase 1 (PDK1) leads to mTOR activation. Phosphatase and tensin homolog (PTEN) might reverse phosphatidylinositol-3-kinase (PI3K) phosphorylation and inhibit activation of downstream proteins of the pathway.

The targeted therapies might be especially useful in patients with incomplete surgical resection and persistent seizures.

On the contrary, the study of Boer *et al.* [9] showed that activation of the mTOR pathway is similar to the control human brain. However, it should be stressed that this study was performed on nine samples of the simple DNT type, which may explain lack of active mTOR. Immunocytochemical analysis of activation of the PI3K/AKT pathway also revealed no differences as compared to the control brain.

Pathogenesis of DNT may also include phosphatase and tensin homolog (PTEN), a tumour suppressor protein, which is involved in regulation of the PI3K/AKT pathway [28] (Fig. 6). However, mutations of the *PTEN* gene were not detected using single strand conformation polymorphism (SSCP) analysis and direct sequencing in a sample of DNT [21]. Furthermore, it must be stressed that this investigation was performed on one DNT sample only.

The possible way of RAS/ERK, as well as PI3K/AKT activation, is phosphorylation of fibroblast growth factor receptor 1 (FGFR1). Investigations by Zhang *et al.* [69] on paediatric low grade gliomas showed duplication of the tyrosine kinase domain of *FGFR1*. It leads to autophosphorylation of the receptor and consequently RAS/ERK and PI3K/AKT upregulation.

Recent studies have shown genetic alterations of *FGFR1* in 82% of examined DNTs, where dominant types of alterations were tyrosine kinase domain duplications and single nucleotide variations [53].

Furthermore, high frequency of *FGFR1* mutations was presented by Rivera *et al.* [56]. Interestingly, they distinguished two groups of tumours from collected samples, which were primarily diagnosed as DNTs. Histopathological revision using current WHO diagnostic criteria distinguished the group of typical DNTs with characteristic glioneuronal elements. The non-DNT group was composed of the other tumours whose histopathological view and clinical features might correspond to the non-specific type of DNT. Mutations of *FGFR1* were more frequent in specific DNT (58%) in comparison to the non-DNT group (19%). The main type of alteration in the specific DNT group was tyrosine kinase domain duplication. Moreover, mutation of *BRAFV600E* was observed in 22.6% of non-DNTs, while it was not detected in specific DNT.

In addition, the authors described germline *FGFR1* mutation in the three familial cases with multino-dular DNTs. It was localized in the region coding tyrosine kinase domain. The tumours, which were resected from proband's children, shared somatic "hot spot" mutations [56].

Prabowo *et al.* [48] studied chromosomal copy number aberrations in DNTs and gangliogliomas. Using whole genome sequencing, they found a wide spectrum of copy number aberrations with chromosome 5 and 7 being the most often changed ones. Furthermore, FISH analysis performed on five samples of DNT showed that copy number gain on chromosome 7 is detected in cells with glial morphology, but not in cells with neuronal morphology.

The involvement of the local microenvironment in tumour development

It is plausible that the development of DNT may be also affected by brain parenchyma and elements, which constitute environment of the tumour.

Aronica *et al.* [3] have found that the amount of cells of the microglia/macrophage lineage in DNTs and gangliogliomas was much higher compared to the control brain. In the majority of samples there was a diffuse distribution of HLA-DR immunoreactivity. The positive cells revealed morphology of activated microglia.

Another study performed on samples of epilepsy-associated lesions DNTs, gangliogliomas and focal cortical dysplasias, has shown positive immunostaining for interleukin 1β (IL-1β) and IL-1 receptor type I (IL-1RI) in neurons as well as in astrocytes and microglial cells. Noteworthy, immunoreactivity of interleukin 1 receptor antagonist (IL-1Ra), which may act as an inhibitory control of IL-1β, was lower than immunoreactivity of IL-1β and IL-1RI in examined samples and its extension was negatively related to the duration of seizures [55].

Differential diagnosis

The diagnosis of DNT requires consideration of clinical, neuroradiological and pathological data. In cases with incomplete resection and limited tissue samples the correct diagnosis might be doubtful. Moreover, the particular forms of DNT, especially the non-specific and diffuse form can be mistakenly identified as diffuse gliomas. However, in the differential diagnosis of DNT, first of all, the oligodendroglioma and diffuse astrocytoma should be considered.

Immunohistochemical staining with specific marker as S-100, synaptophysin, CD34 or BRAF protein and analysis of genetic aberrations might be helpful to differentiate DNT from other brain tumours.

Evaluation of 1p/19q status as well as mutation of the *IDH1* gene in codon 132 (R132H) may be useful to distinguish DNT from oligodendroglioma. Both, loss of heterozygosity for 1p, 17p and 19q [31, 49] and *IDH1* gene mutation [10] are not identified in DNTs and their presence excludes the diagnosis of DNT lesion. Also, the *IDH1* and *TP53* mutation is helpful in identification of diffuse astrocytomas and distinguish them from DNT. Moreover, strong GFAP immunopositivity of neoplastic cells is related with astrocytic differentiation in pure astroglial tumours. The low proliferative index Ki67 might indicate the benign DNT tumour rather than diffuse gliomas.

Treatment and outcome

The predominant and the most effective treatment in DNT symptomatic cases is a total tumour resection. It leads to a seizure-free outcome even in more than 80% of patients during at least a one-year observation [12]. Even better results may be obtained by the complete resection of the tumour together with the epileptogenic zone [15]. Thus, it is believed that the majority of DNT lesions are surgically curable.

However, the cases of DNT with recurrences and malignant transformations of initially recognized benign tumours have been sporadically reported [1,27,68]. The malignant transformation of DNT seems to be unique, however it argues the possibility of more aggressive behaviour of this originally described benign lesion [6]. Time of recurrence after the initial resection may ranges between several months to several years. Occasionally, another brain tumour with higher malignancy has been detected after DNT resection, including atypical teratoid rhabdoid tumour (AT/RT), a highly aggressive embryonal brain tumour [43]. This emphasizes the importance of the prolonged period of clinical and neuroimaging follow-up of DNT resected lesions.

Prognosis

Most commonly, the DNT resection results in stabilization of the clinical course, even after subtotal resection. The meta-analysis conducted on 910 patients with DNT or ganglioglioma showed that the seizure outcome depends on the duration and type of epilepsy, and extensiveness of resection [24]. Secondarily generalized seizures, longer than one-year epilepsy and subtotal lesionectomy were connected with a worse seizure outcome. It was documented that there were no significant differences in the seizure outcome between DNT and ganglioglioma.

Another analysis conducted on data of 78 patients operated on for DNT confirmed a statistically significant correlation between a shorter duration of epilepsy before the surgery and a more favourable outcome [14].

Furthermore, a study on paediatric patients with glioneuronal tumours (ganglioglioma and DNT) showed that a shorter duration of seizures was connected with a better cognitive functioning [54]. It might indicate a negative effect of epilepsy as well as antiepileptic drugs on cognitive development.

Another study revealed the presence of cells of the microglial/macrophage cell system and indicated a significant functional correlation between HLA-DR positive cells and the duration of epilepsy and also a preoperative seizure frequency in glioneuronal tumours (gangliogliomas and DNTs) [3]. Moreover, the connection between the presence of microglial cells and the seizure outcome after surgery was found. The presence of microglial cells was connected with an inflammatory process that might have a negative effect on the disease process. The authors pointed out that the duration of epilepsy had an impact on the occurrence of microglial cells and probably also on the inflammation, which developed during the neoplasm growth.

Final considerations

The theory that DNTs are only glial tumours, whereas the neuronal component consists of entrapped normal neurons, demands further investigations on a larger group, which will contain also the non-specific and diffuse type. On the one hand, the occurrence of copy number aberrations only in the cells with glial morphology is in accordance with the mentioned theory. But, on the other hand, the mutations in *BRAF* were found in neuronal cells. Moreover, the FISH analysis of copy number aberrations should be performed on a higher number of cases to ensure it.

Differences in immunophenotype of distinct types of DNT may suggest a distinct origin of the non-specific and diffuse type or might indicate that it is an earlier form of DNT, which might progress

into the simple or complex form. The diagnosis of non-specific and diffuse variant of DNT is still not obvious. Moreover, the changes in classification of tumours associated with long-term epilepsy are postulated. The idea is to categorize all three types of DNT into different groups of tumours [7]. The proposed classification is based on histopathological features as well as immunohistochemical labelling (CD34, MAP2) and testing for *IDH1* mutations.

Histological categorization might be supported by differences in molecular mechanisms involved in pathogenesis. *BRAFV600E* mutations seem to be implicated mainly in non-specific and diffuse types of DNT, while *FGFR1* mutations were observed mostly in specific DNTs.

Moreover, the microglia cells and released cytokines seem to be implicated in the DNT pathological process and they are related to the clinical presentation. Probably, the role of microglia is associated with IL-1β release and induction of the inflammatory process, which causes seizures.

Summarizing, DNT is a benign tumour lesion of a distinct clinical and neuroimaging picture but heterogonous, often confusing morphology, uncertain histogenesis and not fully defined molecular background.

Disclosure

Authors report no conflict of interest.

References

1. Aggarwal A, Salunke P, Sodhi HB, Vasishta RK, Gowda KK. Dysembryoplastic neuroepithelial tumor transforming into malignancy: a case report. Neurol India 2014; 62: 323-325.
2. Altinors N, Calisaneller T, Gulsen S, Ozen O, Onguru O. Intraventricular dysembryoplastic neuroepithelial tumor: case report. Neurosurgery 2007; 61: E1332-1333; discussion E1333.
3. Aronica E, Gorter JA, Redeker S, Ramkema M, Spliet WG, van Rijen PC, Leenstra S, Troost D. Distribution, characterization and clinical significance of microglia in glioneuronal tumours from patients with chronic intractable epilepsy. Neuropathol Appl Neurobiol 2005; 31: 280-291.
4. Baimbridge KG, Celio MR, Rogers JH. Calcium-binding proteins in the nervous system. Trends Neurosci 1992; 15: 303-308.
5. Bilginer B, Yalnizoglu D, Soylemezoglu F, Turanli G, Cila A, Topcu M, Akalan N. Surgery for epilepsy in children with dysembryoplastic neuroepithelial tumor: clinical spectrum, seizure outcome, neuroradiology, and pathology. Childs Nerv Syst 2009; 25: 485-491.
6. Blümcke I, Thom M, Aronica E, Armstrong DD, Vinters HV, Palmini A, Jacques TS, Avanzini G, Barkovich AJ, Battaglia G, Becker A, Cepeda C, Cendes F, Colombo N, Crino P, Cross JH, Delalande O, Dubeau F, Duncan J, Guerrini R, Kahane P, Mathern G, Najm I, Ozkara C, Raybaud C, Represa A, Roper SN, Salamon N, Schulze-Bonhage A, Tassi L, Vezzani A, Spreafico R. The clinicopathologic spectrum of focal cortical dysplasias: a consensus classification proposed by an ad hoc Task Force of the ILAE Diagnostic Methods Commission. Epilepsia 2011; 52: 158-174.
7. Blumcke I, Aronica E, Urbach H, Alexopoulos A, Gonzalez-Martinez JA. A neuropathology-based approach to epilepsy surgery in brain tumors and proposal for a new terminology use for long-term epilepsy-associated brain tumors. Acta Neuropathol 2014; 128: 39-54.
8. Bodi I, Selway R, Bannister P, Doey L, Mullatti N, Elwes R, Honavar M. Diffuse form of dysembryoplastic neuroepithelial tumour: the histological and immunohistochemical features of a distinct entity showing transition to dysembryoplastic neuroepithelial tumour and ganglioglioma. Neuropathol Appl Neurobiol 2012; 38: 411-425.
9. Boer K, Troost D, Timmermans W, van Rijen PC, Spliet WG, Aronica E. Pi3K-mTOR signaling and AMOG expression in epilepsy-associated glioneuronal tumors. Brain Pathol 2010; 20: 234-244.
10. Capper D, Reuss D, Schittenhelm J, Hartmann C, Bremer J, Sahm F, Harter PN, Jeibmann A, von Deimling A. Mutation-specific IDH1 antibody differentiates oligodendrogliomas and oligoastrocytomas from other brain tumors with oligodendroglioma-like morphology. Acta Neuropathol 2011; 121: 241-252.
11. Cataltepe O, Marshall P, Smith TW. Dysembryoplastic neuroepithelial tumor located in pericallosal and intraventricular area in a child. Case report. J Neurosurg Pediatr 2009; 3: 456-460.
12. Chang EF, Christie C, Sullivan JE, Garcia PA, Tihan T, Gupta N, Berger MS, Barbaro NM. Seizure control outcomes after resection of dysembryoplastic neuroepithelial tumor in 50 patients. J Neurosurg Pediatr 2010; 5: 123-130.
13. Chappe C, Padovani L, Scavarda D, Forest F, Nanni-Metellus I, Loundou A, Mercurio S, Fina F, Lena G, Colin C, Figarella-Branger D. Dysembryoplastic neuroepithelial tumors share with pleomorphic xanthoastrocytomas and gangliogliomas BRAF(V600E) mutation and expression. Brain Pathol 2013; 23: 574-583.
14. Chassoux F, Rodrigo S, Mellerio C, Landre E, Miquel C, Turak B, Laschet J, Meder JF, Roux FX, Daumas-Duport C, Devaux B. Dysembryoplastic neuroepithelial tumors: an MRI-based scheme for epilepsy surgery. Neurology 2012; 79: 1699-1707.
15. Chassoux F, Landre E, Mellerio C, Laschet J, Devaux B, Daumas-Duport C. Dysembryoplastic neuroepithelial tumors: epileptogenicity related to histologic subtypes. Clin Neurophysiol 2013; 124: 1068-1078.
16. Daghistani R, Miller E, Kulkarni AV, Widjaja E. Atypical characteristics and behavior of dysembryoplastic neuroepithelial tumors. Neuroradiology 2013; 55: 217-224.
17. Daumas-Duport C, Scheithauer BW, Chodkiewicz JP, Laws ER, Jr, Vedrenne C. Dysembryoplastic neuroepithelial tumor: a surgically curable tumor of young patients with intractable partial seizures. Report of thirty-nine cases. Neurosurgery 1988; 23: 545-556.
18. Daumas-Duport C. Dysembryoplastic neuroepithelial tumours. Brain Pathol 1993; 3: 283-295.

19. Daumas-Duport C, Varlet P, Bacha S, Beuvon F, Cervera-Pierot P, Chodkiewicz JP. Dysembryoplastic neuroepithelial tumors: non-specific histological forms – a study of 40 cases. J Neurooncol 1999; 41: 267-280.

20. Daumas-Duport C PT, Lantos PL. Dysembryoplastic neuroepithelial tumor. In: Pathology and genetics of tumors of the central nervous system. Kleihus P, Cavenee WK (eds.). IARC Press, Lyon 2000; pp. 103-104.

21. Duerr EM, Rollbrocker B, Hayashi Y, Peters N, Meyer-Puttlitz B, Louis DN, Schramm J, Wiestler OD, Parsons R, Eng C, von Deimling A. PTEN mutations in gliomas and glioneuronal tumors. Oncogene 1998; 16: 2259-2264.

22. Duggal N, Taylor R, Zou GY, Hammond RR. Dysembryoplastic neuroepithelial tumours: clinical, proliferative and apoptotic features. J Clin Pathol 2008; 61: 127-131.

23. Emmez H, Kale A, Egemen E, Eser P, Kaymaz M, Pasaoglu A. Intraventricular dysembryoplastic neuroepithelial tumour: case report. Neurol Neurochir Pol 2012; 46: 192-195.

24. Englot DJ, Berger MS, Barbaro NM, Chang EF. Factors associated with seizure freedom in the surgical resection of glioneuronal tumors. Epilepsia 2012; 53: 51-57.

25. Esteve-Puig R, Canals F, Colome N, Merlino G, Recio JA. Uncoupling of the LKB1-AMPKalpha energy sensor pathway by growth factors and oncogenic BRAF. PLoS One 2009; 4: e4771.

26. Faubert B, Vincent EE, Poffenberger MC, Jones RG. The AMP-activated protein kinase (AMPK) and cancer: many faces of a metabolic regulator. Cancer Lett 2015; 356: 165-170.

27. Hammond RR, Duggal N, Woulfe JM, Girvin JP. Malignant transformation of a dysembryoplastic neuroepithelial tumor. Case report. J Neurosurg 2000; 92: 722-725.

28. Hers I, Vincent EE, Tavare JM. Akt signalling in health and disease. Cell Signal 2011; 23: 1515-1527.

29. Honavar M, Janota I, Polkey CE. Histological heterogeneity of dysembryoplastic neuroepithelial tumour: identification and differential diagnosis in a series of 74 cases. Histopathology 1999; 34: 342-356.

30. Ishizawa K, Terao S, Kobayashi K, Yoshida K, Hirose T. A neuroepithelial tumor showing combined histological features of dysembryoplastic neuroepithelial tumor and pleomorphic xanthoastrocytoma – a case report and review of the literature. Clin Neuropathol 2007; 26: 169-175.

31. Johnson MD, Vnencak-Jones CL, Toms SA, Moots PM, Weil R. Allelic losses in oligodendroglial and oligodendroglioma-like neoplasms: analysis using microsatellite repeats and polymerase chain reaction. Arch Pathol Lab Med 2003; 127: 1573-1579.

32. Kakkar A, Majumdar A, Kumar A, Tripathi M, Pathak P, Sharma MC, Suri V, Tandon V, Chandra SP, Sarkar C. Alterations in BRAF gene, and enhanced mTOR and MAPK signaling in dysembryoplastic neuroepithelial tumors (DNTs). Epilepsy Res 2016; 127: 141-151.

33. Komori T, Arai N. Dysembryoplastic neuroepithelial tumor, a pure glial tumor? Immunohistochemical and morphometric studies. Neuropathology 2013; 33: 459-468.

34. Lee D, Cho YH, Kang SY, Yoon N, Sung CO, Suh YL. BRAF V600E mutations are frequent in dysembryoplastic neuroepithelial tumors and subependymal giant cell astrocytomas. J Surg Oncol 2015; 111: 359-364.

35. Lee DY, Chung CK, Hwang YS, Choe G, Chi JG, Kim HJ, Cho BK. Dysembryoplastic neuroepithelial tumor: radiological findings (including PET, SPECT, and MRS) and surgical strategy. J Neurooncol 2000; 47: 167-174.

36. Lee J, Lee BL, Joo EY, Seo DW, Hong SB, Hong SC, Suh YL, Lee M. Dysembryoplastic neuroepithelial tumors in pediatric patients. Brain Dev 2009; 31: 671-681.

37. Louis DN, Ohgaki H, Wiestler OD, Cavenee WK, Burger PC, Jouvet A, Scheithauer BW, Kleihues P. The 2007 WHO classification of tumours of the central nervous system. Acta Neuropathol 2007; 114: 97-109.

38. Matyja E, Grajkowska W, Kunert P, Marchel A. A peculiar histopathological form of dysembryoplastic neuroepithelial tumor with separated pilocytic astrocytoma and rosette-forming glioneuronal tumor components. Neuropathology 2014; 34: 491-498.

39. Mendoza MC, Er EE, Blenis J. The Ras-ERK and PI3K-mTOR pathways: cross-talk and compensation. Trends Biochem Sci 2011; 36: 320-328.

40. Michalczyk K, Ziman M. Nestin structure and predicted function in cellular cytoskeletal organisation. Histol Histopathol 2005; 20: 665-671.

41. Minkin K, Klein O, Mancini J, Lena G. Surgical strategies and seizure control in pediatric patients with dysembryoplastic neuroepithelial tumors: a single-institution experience. J Neurosurg Pediatr 2008; 1: 206-210.

42. Mizuguchi R, Sugimori M, Takebayashi H, Kosako H, Nagao M, Yoshida S, Nabeshima Y, Shimamura K, Nakafuku M. Combinatorial roles of olig2 and neurogenin2 in the coordinated induction of pan-neuronal and subtype-specific properties of motoneurons. Neuron 2001; 31: 757-771.

43. Nadi M, Ahmad T, Huang A, Hawkins C, Bouffet E, Kulkarni AV. Atypical Teratoid Rhabdoid Tumor Diagnosis after Partial Resection of Dysembryoplastic Neuroepithelial Tumor: Case Report and Review of the Literature. Pediatr Neurosurg 2016; 51: 191-198.

44. Nasit JG, Shah P, Zalawadia H. Coexistent dysembryoplastic neuroepithelial tumour and pilocytic astrocytoma. Asian J Neurosurg 2016; 11: 451.

45. Nielsen JS, McNagny KM. Novel functions of the CD34 family. J Cell Sci 2008; 121: 3683-3692.

46. Pietsch T HC, Varlet P, Blumcke I, Hirose T. Dysembryoplastic neuroepithelial tumour. In: WHO Classification of Tumors of the Central Nervous System. Louis DN, Oghaki H, Wiesttler OD, Cavenee WK, Elison DW (eds.). Revised 4th Edition. IARC Press, Lyon 2016; pp. 132-135.

47. Prabowo AS, Iyer AM, Veersema TJ, Anink JJ, Schouten-van Meeteren AY, Spliet WG, van Rijen PC, Ferrier CH, Capper D, Thom M, Aronica E. BRAF V600E mutation is associated with mTOR signaling activation in glioneuronal tumors. Brain Pathol 2014; 24: 52-66.

48. Prabowo AS, van Thuijl HF, Scheinin I, Sie D, van Essen HF, Iyer AM, Spliet WG, Ferrier CH, van Rijen PC, Veersema TJ, Thom M, Schouten-van Meeteren AY, Reijneveld JC, Ylstra B, Wesseling P, Aronica E. Landscape of chromosomal copy number aberrations in gangliogliomas and dysembryoplastic neuroepithelial tumours. Neuropathol Appl Neurobiol 2015; 41: 743-755.

49. Prayson RA, Castilla EA, Hartke M, Pettay J, Tubbs RR, Barnett GH. Chromosome 1p allelic loss by fluorescence in situ hybridization is not observed in dysembryoplastic neuroepithelial tumors. Am J Clin Pathol 2002; 118: 512-517.

50. Prayson RA, Fong J, Najm I. Coexistent pathology in chronic epilepsy patients with neoplasms. Mod Pathol 2010; 23: 1097-1103.

51. Prayson RA, Napekoski KM. Composite ganglioglioma/dysembryoplastic neuroepithelial tumor: a clinicopathologic study of 8 cases. Hum Pathol 2012; 43: 1113-1118.

52. Preusser M, Budka H, Rossler K, Hainfellner JA. OLIG2 is a useful immunohistochemical marker in differential diagnosis of clear cell primary CNS neoplasms. Histopathology 2007; 50: 365-370.

53. Qaddoumi I, Orisme W, Wen J, Santiago T, Gupta K, Dalton JD, Tang B, Haupfear K, Punchihewa C, Easton J, Mulder H, Boggs K, Shao Y, Rusch M, Becksfort J, Gupta P, Wang S, Lee RP, Brat D, Peter Collins V, Dahiya S, George D, Konomos W, Kurian KM, McFadden K, Serafini LN, Nickols H, Perry A, Shurtleff S, Gajjar A, Boop FA, Klimo PD Jr, Mardis ER, Wilson RK, Baker SJ, Zhang J, Wu G, Downing JR, Tatevossian RG, Ellison DW. Genetic alterations in uncommon low-grade neuroepithelial tumors: BRAF, FGFR1, and MYB mutations occur at high frequency and align with morphology. Acta Neuropathol 2016; 131: 833-845.

54. Ramantani G, Kadish NE, Anastasopoulos C, Brandt A, Wagner K, Strobl K, Mayer H, Schubert-Bast S, Stathi A, Korinthenberg R, Feuerstein TJ, Mader I, van Velthoven V, Zentner J, Schulze-Bonhage A, Bast T. Epilepsy surgery for glioneuronal tumors in childhood: avoid loss of time. Neurosurgery 2014; 74: 648-657; discussion 657.

55. Ravizza T, Boer K, Redeker S, Spliet WG, van Rijen PC, Troost D, Vezzani A, Aronica E. The IL-1beta system in epilepsy-associated malformations of cortical development. Neurobiol Dis 2006; 24: 128-143.

56. Rivera B, Gayden T, Carrot-Zhang J, Nadaf J, Boshari T, Faury D, Zeinieh M, Blanc R, Burk DL, Fahiminiya S, Bareke E, Schüller U, Monoranu CM, Sträter R, Kerl K, Niederstadt T, Kurlemann G, Ellezam B, Michalak Z, Thom M, Lockhart PJ, Leventer RJ, Ohm M, MacGregor D, Jones D, Karamchandani J, Greenwood CM, Berghuis AM, Bens S, Siebert R, Zakrzewska M, Liberski PP, Zakrzewski K, Sisodiya SM, Paulus W, Albrecht S, Hasselblatt M, Jabado N, Foulkes WD, Majewski J. Germline and somatic FGFR1 abnormalities in dysembryoplastic neuroepithelial tumors. Acta Neuropathol 2016; 131: 847-863.

57. Roskoski R Jr. RAF protein-serine/threonine kinases: structure and regulation. Biochem Biophys Res Commun 2010; 399: 313-317.

58. Sanchez C, Diaz-Nido J, Avila J. Phosphorylation of microtubule-associated protein 2 (MAP2) and its relevance for the regulation of the neuronal cytoskeleton function. Prog Neurobiol 2000; 61: 133-168.

59. Sharma MC, Jain D, Gupta A, Sarkar C, Suri V, Garg A, Gaikwad SB, Chandra PS. Dysembryoplastic neuroepithelial tumor: a clinicopathological study of 32 cases. Neurosurg Rev 2009; 32: 161-169; discussion 169-170.

60. Spalice A, Ruggieri M, Grosso S, Verrotti A, Polizzi A, Magro G, Caltabiano R, Pavone P, Del Balzo F, Platania N, Iannetti P. Dysembryoplastic neuroepithelial tumors: a prospective clinicopathologic and outcome study of 13 children. Pediatr Neurol 2010; 43: 395-402.

61. Sung CO, Suh YL. Different pattern of expression of nestin in the non-specific form of dysembryoplastic neuroepithelial tumors compared to the simple and complex forms. J Neurooncol 2009; 92: 7-13.

62. Sung CO, Suh YL, Hong SC. CD34 and microtubule-associated protein 2 expression in dysembryoplastic neuroepithelial tumours with an emphasis on dual expression in non-specific types. Histopathology 2011; 59: 308-317.

63. Takahashi A, Hong SC, Seo DW, Hong SB, Lee M, Suh YL. Frequent association of cortical dysplasia in dysembryoplastic neuroepithelial tumor treated by epilepsy surgery. Surg Neurol 2005; 64: 419-427.

64. Teng J, Takei Y, Harada A, Nakata T, Chen J, Hirokawa N. Synergistic effects of MAP2 and MAP1B knockout in neuronal migration, dendritic outgrowth, and microtubule organization. J Cell Biol 2001; 155: 65-76.

65. Thom M, Toma A, An S, Martinian L, Hadjivassiliou G, Ratilal B, Dean A, McEvoy A, Sisodiya SM, Brandner S. One hundred and one dysembryoplastic neuroepithelial tumors: an adult epilepsy series with immunohistochemical, molecular genetic, and clinical correlations and a review of the literature. J Neuropathol Exp Neurol 2011; 70: 859-878.

66. Wang F, Qiao G, Li X, Gui Q. A dysembryoplastic neuroepithelial tumor in the area of the caudate nucleus in a 57-year-old woman: case report. Neurosurgery 2007; 61: E420; discussion E420.

67. Yu AH, Chen L, Li YJ, Zhang GJ, Li KC, Wang YP. Dysembryoplastic neuroepithelial tumors: magnetic resonance imaging and magnetic resonance spectroscopy evaluation. Chin Med J (Engl) 2009; 122: 2433-2437.

68. Zakrzewski K, Biernat W, Liberski PP, Polis L, Nowoslawska E. Pilocytic astrocytoma as a predominant component of a recurrent complex type DNT. Folia Neuropathol 2009; 47: 284-288.

69. Zhang J, Wu G, Miller CP, Tatevossian RG, Dalton JD, Tang B, Orisme W, Punchihewa C, Parker M, Qaddoumi I, Boop FA, Lu C, Kandoth C, Ding L, Lee R, Huether R, Chen X, Hedlund E, Nagahawatte P, Rusch M, Boggs K, Cheng J, Becksfort J, Ma J, Song G, Li Y, Wei L, Wang J, Shurtleff S, Easton J, Zhao D, Fulton RS, Fulton LL, Dooling DJ, Vadodaria B, Mulder HL, Tang C, Ochoa K, Mullighan CG, Gajjar A, Kriwacki R, Sheer D, Gilbertson RJ, Mardis ER, Wilson RK, Downing JR, Baker SJ, Ellison DW; St. Jude Children's Research Hospital–Washington University Pediatric Cancer Genome Project. Whole-genome sequencing identifies genetic alterations in pediatric low-grade gliomas. Nat Genet 2013; 45: 602-612.

70. Zhou Q, Wang S, Anderson DJ. Identification of a novel family of oligodendrocyte lineage-specific basic helix-loop-helix transcription factors. Neuron 2000; 25: 331-343.

Folia
Neuropathologica

Mesenchymal/proangiogenic factor YKL-40 related to glioblastomas and its relationship with the subventricular zone

Kelvin M. Piña Batista[1], Sayoa Alvarez de Eulate-Beramendi[1], Kenia Y. Álvarez Reyes de Piña[2],

Pedro Reimunde Figueira[1], Adan Fernandez Canal[1], Josué M. Avecillas Chasin[3], Ángela Meilan[1], Rodrigo Ugalde[1],

Ivan Fernandez Vega[1]

[1]Department of Neurosurgery, Hospital Universitario Central de Asturias, Asturias, [2]Hospital Vital Alvarez Buylla, Asturias,
[3]Hospital Universitario Joan XXIII, Tarragona, Spain

Abstract

Glioblastoma is the most common primary brain tumor. Despite multimodality therapy with aggressive microsurgical resection and adjuvant chemotherapy and radiotherapy, the median survival is below 15 months. Glioblastomas are heterogeneous tumors with high resistance to most chemotherapeutic drugs. According to reliable evidence, YKL-40, one of the best investigated chitinase-like protein, may facilitate invasion, migration and angiogenesis, and could be also responsible for temozolomide resistance in glioblastoma, thus conferring a dismal prognosis. Previous studies have demonstrated that glioblastoma stem cells give rise to endothelial cells through an YKL-40 influence. Such factor is closely related to the subventricular zone. This review focuses on the most recent theories involving the possible relationship between topographic gliomagenesis related to the subventricular zone and YKL-40.

***Key words:** glioblastoma, subventricular zone, YKL-40, glioblastoma stem cells.*

Introduction

Glioblastoma (GB) is the most common primary malignant brain tumor in adults [6,86], accounting for more than 45% of primary malignant brain tumors. Glioblastoma has an incidence that increases with age and peaks between 75 and 84 years old, being more common in white males, according to the most recent Central Brain Tumor Registry of the United States (CBTRUS) statistical report. The median survival for patients diagnosed with GB using the current standard of care is only 12 to 15 months [8,52,77,81] despite multimodality treatment with aggressive microsurgical resection, combined radiation and chemotherapy, and adjuvant chemotherapy [81]. GB cells are diffusely infiltrative and motile; consequently, GB renders them incurable by surgery alone [24,78,79]. Thus, a novel therapeutic approach is urgently needed to control recurrence and overcome resistance to treatment.

Over the last few decades, it has become clear that GBs are characterized by an extreme degree of phenotypic, cellular, genetic, epigenetic, and radiological heterogeneity, as implied by the older term "multiforme" [37,73], which challenges our ability

Communicating author:
Kelvin M. Piña Batista, MD, MSc, MBA, PhD, Department of Neurosurgery, Hospital Universitario Central de Asturias,
Av. de Las Segadas 22, 4a 33006 Oviedo, Spain, phone: +34 693 86 24 81, e-mail: pineappledr@gmail.com

to understand or treat it. There have been several studies that seek to determine which factors can be prognostic or predictive to impact on overall survival and progression free survival [3,19,33,41,46,53,55].

Although currently more research is needed, biomarkers must be taken into account when deciding which treatment modality is most appropriate for the individual patient. We review the evidence and theories involving the possible relationship between topographic gliomagenesis related to the subventricular zone (SVZ) and YKL-40, in an attempt to reveal either cellular mechanisms or molecular factors associated with ubiquitous GB stem-like cells (GSCs) support and motility. The following aspects are summarized: subventricular zone, mesenchymal factor YKL-40, radial glia and the perivascular tumor cells.

Levels of circulating, subgranular or subventricular YKL-40 (chitinase 3-like 1 or cartilage glycoprotein-39), have the potential to be used in the optimization of glioblastoma therapies. Elevated serum levels of YKL-40 were found in 55-75% of patients with GB with shorter OS [6,7,29,31].

One of the most recent and attractive evidence included YKL-40 as the most predictive and prognostic marker in patients with GB [15,87], and it has been shown directly associated with tumor radioresistance, invasiveness, migration, recurrence, chromosome 10 loss [6,29,54], hypoxia-induced mesenchymal transition [36], and poor clinical outcome prognosis. Recently, Akiyama *et al.* using a TMZ-resistant (TMZ-R) U87 GB cell *in vitro* and *in vivo* identified that YKL-40 could be also responsible for temozolomide resistance in GB and suggested that therapies targeting YKL-40 may be potentially beneficial in GB treatment [2].

Glioblastoma stem cells and YKL-40

Glioblastoma is composed of cancer cells and surrounding stromal cells with diverse genetic/epigenetic backgrounds. Increasing evidence suggests that the tumorigenic process in GB is apparently initiated and maintained by a rare and special subpopulation of slow-cycling clonogenic cells referred to as GSCs [28,62,66,67]. It has been assumed that overall survival heterogeneity [33,45,46] in patients with GB might be related to GSCs variability and brain microenvironment [58]. Presently, it is not clear what the origin of GSCs is, but presumably it may

arise from SVZ stem cells. Based on *in vivo* evidence, GSCs are responsible for tumor growth, recurrence, and resistance to therapies [15,48,59] and endowed with unregulated self-renewal, robust proliferative potential, high motility, diversity of progeny association with blood vessels and white matter tracts, multi-lineage differentiation capacities, invasiveness [22,63], and relatively resistant to radio- and chemotherapies [56,80], which express markers of both undifferentiated and differentiated cells [73], with a similar behavior to neural stem cells (NSCs) [5], which are present during the early development of the brain [7]. Nevertheless, the specific intrinsic factors that govern such characteristics are not well understood [27,66,83].

Mounting evidence shows that GSCs are largely dependent on distinctive and specialized vascular, perivascular or perinecrotic microenvironment called "niche" [11,30,63,64,66,68,76]. Furthermore, some investigators observe that GSCs give rise to endothelial cells (ECs)60, as shown in Figure 1, and induce changes in vascular niches, characterized by the sprouting of new blood vessels, consisting of an abundant, leaky and highly disorganized "glomeruloid" vascular network through the cooperative secretion of pro-angiogenic factors [1,61,67], such as VEGF, IL-8 and YKL-40 [2,29,56], highly different in patients with the same tumor [42,56,60,82]. YKL-40, also known as chitinase-like protein 1 or human cartilage glycoprotein-39 [6], is a highly conserved glycoprotein that belongs to the glycosyl hydrolase family 18 with no chitinolytic activity [7,84], included as a mesenchymal marker overexpressed in GB and postulated as one of the most promising predictive serum markers since it was found to have elevated levels in the serum of patients with GB [6,29,31,32,35].

So far, YKL-40 has been found to induce tight interplay between the membrane receptors syndecan-1 and an adjacent membrane-associated protein integrin $\alpha v\beta 5$ [21] on endothelial cells [70,71], and triggered a signaling cascade through pFAK [8,61] to MAP kinase ERK-1 and ERK-2 by regulating VEGF expression and inducing angiogenesis as an independent angiogenic factor under hypoxic conditions.

However, these vascular formations usually lack basement membrane and pericyte coverage. In addition, recent studies [1,44,66] support that vasculogenesis [34,56] by GSCs may occur directly via
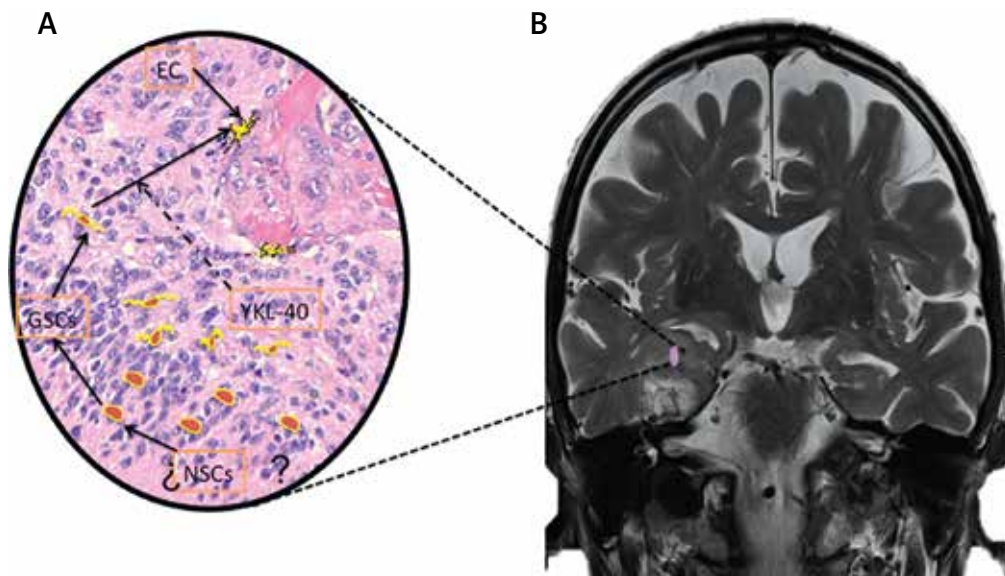
Kelvin M. Piña Batista, Sayoa Alvarez de Eulate-Beramendi, Kenia Y. Álvarez Reyes de Piña, Pedro Reimunde Figueira, Adan Fernandez Canal, Josué M. Avecillas Chasin, Ángela Meilan, Rodrigo Ugalde, Ivan Fernandez Vega

Fig. 1. Model depicting the glioblastoma stem-like cells (GSCs) transdifferentiation into Ecs. YKL-40 acts as an angiogenic factor to trigger tumor vascular development. **B)** Magnetic resonance image of a glioblastoma tumor, and **(A)** tissue sample from the same tumor illustrating tumor microenvironment.

differentiation of cells that participate in vasculo-genesis, tumor growth, or indirectly via cytokines and chemokines production stimulated by hypoxia, which are known to activate endothelial cells. Interestingly, through a three dimensional reconstruction, Calabrese *et al.* demonstrated that brain GSCs are preferentially located in close contact to tumor microvasculature and that endothelial cells release trophic factors that maintain these cells in a self-renewing and undifferentiated state [12].

As a well-recognized component of the tumor microenvironment, intratumoral low oxygen concentration upregulates the expression of multiple factors such as hypoxia-inducible factors (HIFs), members of a subfamily of basic helix-loop helix transcription factor that regulates different aspects of cell biogenesis such as metabolism, migration, proliferation, differentiation, apoptosis, angiogenesis, resistance to chemotherapy, and stem cell maintenance [13,14,28,44,50]. Importantly, recent findings indicate that GSCs are the origin of tumor recurrence in glioblastoma [13,62,83]. Indeed, it has been demonstrated through a genetically-engineered mouse model that after arrest of tumor cell proliferation with temozolomide, the first cell population to undergo proliferation and lead to tumor regrowth is the nestin-positive (a marker also for neural stem cells) GSC population [13].

Growing evidence indicates that nuclear accumulation of HIF results in transcriptional activation of the vascular endothelial growth factor (VEGF) whose pathway is modulated by reactive oxygen species (ROS), and demonstrating VEGF downregulation following HIF1a gene deletion and that HIF1/2 determined VEGF levels [4,28,44]. Francescone *et al.* identified that YKL-40 (CHI3L1) closely upregulates VEGF expression, and YKL-40-induced tumor vasculogenesis is at least partially dependent on VEGF [21].

Adult stem cells, human subventricular zone and YKL-40 expression in glioblastoma

In the adult human brain, astrocytes are the largest glial population, and provide structural, metabolic, and trophic support for neurons. Astrocytes can also support proliferation of adult NSCs lining the SVZ. Adult neurogenesis is a lifetime process, which has been isolated from two specific neurogenic regions: the dentate gyrus of the hippocampus, and the subventricular zone of the lateral ventricles. In both regions, NSCs are identified as a subpopulation of astrocytes that are able to produce undifferentiated neuronal and glial precursors [13,18,40,67].

The adult SVZ, most pronounced in the dorso-lateral wall of the lateral ventricle, is the main

source of new neurons in the adult brain, and contains a subset of astrocytes which behave as stem cells both *in vivo* and *in vitro* [18,25,30,43,45,68], and derive from radial glia (RG) cells [17,39]. In fact, RG cells also act as NSCs and source of neurogenesis, and probably give rise to astrocytes in the cerebral cortex [17,23,64,74]. In the adult human brain, the cellular composition and cytoarchitecture of the SVZ is organized into four distinct layers: layer I is found adjacent to the lateral ventricle, and represents a single layer of multi-cialiated ependymal cells; layer II, also known as a hypocellular layer [64], consisting of a diffuse network of a large number of astrocytic, ependymal and neuronal processes, but a few cell bodies; layer III, a strip of astrocytic bodies, and externally, layer IV, adjacent to the brain parenchyma, we find a transition zone composed of many myelin tracts and neuronal bodies (Fig. 2) [25,26,30,38,57].

Interestingly, NSCs, identified as a subpopulation of astrocytes called B1 astrocytes, give rise to actively proliferating transit amplifying progenitors (type C cells), which in turn differentiate into neuroblasts (type A cells) that differentiate into interneurons and eventually migrate toward the olfactory bulb (OB) circuitry, via the rostral migratory stream (RMS), preferentially located in the ventral anterior SVZ of the adult hu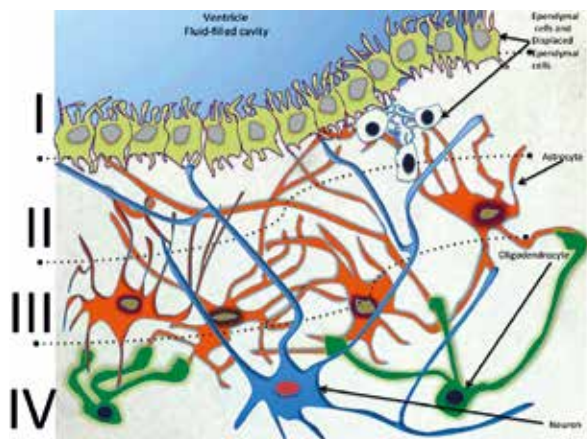man brain (Fig. 3). In the adult human brain, there are a small number of migratory neuroblasts in the SVZ and RMS. Nevertheless, so far there has been no consensus about the exact mechanisms underlying such neural migration toward OB in the adult human SVZ, and also whether there is an RMS [16,57,65]. Although the cytoarchitecture of the adult human SVZ have been characterized, a transcriptional analysis has not been fully established and understood. Interestingly, a recent transcriptional analysis [51] distinguished human SVZ astrocytes from parenchymal astrocytes based on gene expression, suggesting that SVZ astrocytes (type B) maintain the stemness in the adult human brain. Alternatively, it was found that *in vitro* CSCs have a tropism toward normal vasculature.

A putative source of glioma cells is the SVZ, the largest area of neurogenesis in the adult human brain. NSCs line the lateral ventricles in the SVZ, and recruitment of these progenitor cells may play a role in the aggressive behavior encountered in GB. In animal studies, the SVZ demonstrated increased susceptibility to tumorigenesis compared with cortical regions. Experiments and clinical findings provide evidence that neuronal progenitor cells in the SVZ with a high migratory potential are involved in the aggressive GB subtype. Recently, the SVZ has been identified as the source cells of malignant gliomas [55,63-66,68].

Fig. 2. A diagrammatic sectional view of the human subventricular zone. Lateral ventricle illustrating the cellular composition and cytoarchitecture of subventricular zone (SVZ), consisting of four layers: layer I – ependymal cells, layer II – hypocellular gap, layer III – a strip of astrocyte bodies, and layer IV – transitional zone.

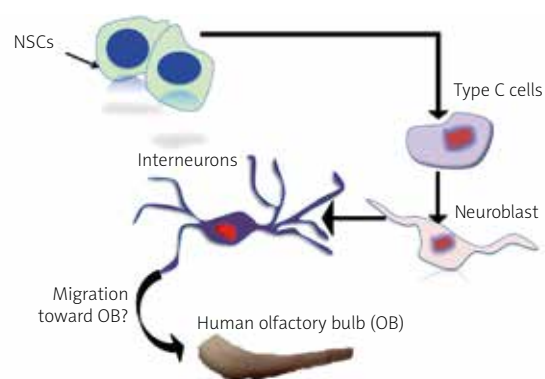**Fig. 3.** Cell types and anatomy of the subventricular zone (SVZ) niche. Neural stem cells in the human brain, which generate the type C cells. These transit amplifying cells, type C cells, mature into type A cells, or neuroblasts that differentiate into interneurons and eventually migrate toward the olfactory bulb circuitry, preferentially located in the ventral anterior SVZ of the adult human brain.

Kelvin M. Piña Batista, Sayoa Alvarez de Eulate-Beramendi, Kenia Y. Álvarez Reyes de Piña, Pedro Reimunde Figueira, Adan Fernandez Canal, Josué M. Avecillas Chasin, Ángela Meilan, Rodrigo Ugalde, Ivan Fernandez Vega

Based on cancer stem cell theory, and images of GB, SVZ was classified according to one of these categories: type I – tumor in which the contrast-enhancing lesion contacts both the SVZ and the cortex; type II – tumor contacts the SVZ but not the cortex; type III – tumor contacts the cortex but not the SVZ, and type IV – tumor contacts neither the SVZ nor the cortex [46]. Regarding the multifocal and/or multicentric GBs there are many theories, but supported by few studies [46,69], showing an association with group I given the findings consistent with high migratory and invasiveness of cells, according to Willis' theory. Although relevant data suggest that GSCs may be important in gliomagenesis originating from SVZ, recent research has differed from this argument, hypothesizing through a combination of clinical observations and mathematical modeling that GBs may arise from cells distributed throughout the white matter and not limited to the region of the SVZ [9].

In a novel and interesting study on the YKL-40 expression in developing human embryonic and fetal tissues conducted by Bjornbak [7], YKL-40 was found to be associated with tissues undergoing morphogenetic changes. In this research, YKL-40 was found significantly marked in GB, as compared with normal human brain SVZ. By using immunohistochemical, double-labeling immunofluorescence and mRNA analysis through brain development (from 6th to 21st week post-conception), the authors pointed out that YKL-40 may be implicated in controlling angiogenesis and access of peripheral cells to the forebrain.

On the cellular lever, Bjornbak also suggested that YKL-40 plays a role in the developing brain barriers as well as is possibly involved in the differentiation of a particular astrocytic lineage. Consistent with our previous findings [55], in this study there was a decreased YKL-40 immunoreactivity in proximity to the cortex and ECs of the pia mater were not positive for YKL-40. Additionally, YKL-40 immunoreactivity was found also to be produced by the choroid plexus epithelium and secreted into the ventricular system and either detected in both neuroepithelial cells and radial glial end feet. Strikingly, Antonelly et al. [3] reported on 22 children with GBs who underwent tumor resection and immunohistochemistry was performed on tumor tissue for YKL-40 immunoexpression, showing less expression and better OS. However, such disagreement with recent data may be due to a small sample size, as stated by the authors.

Recent studies with gene expression profiles have established that cells expressing increased mesenchymal properties have a tendency to display self-renewal capacity. Interestingly, mesenchymal signature genes such as YKL-40 (shown in the early stage of development and probably related to neural stem cells) and oncostatin M – which belongs to interleukin 6 group of cytokines – receptor are associated with highly invasive feature and worse prognosis in GB patients [49,72].

Current data provide several useful insights [47,71]. First, YKL-40-positive cells may be responsible for the aggressive and invasive pattern seen in GSC. What are the properties of the microenvironment that permit widespread invasion? The previous phenomenon probably could be mediated by NSCs cues or by direct response of YKL-40 over ECs. Since most GBs tumors occur late in life and recently it was suggested a relationship between YKL-40 and SVZ, we can estimate that GBs could be initiated either by unknown trigger factors over preformed pathways. As regards YKL-40 immunoexpression, is there a special association between SVZ regionalization and GB formation? Under this topic, further studies in large series are needed to evaluate how YKL-40 measurements and pathways change throughout life. Furthermore, currently we are conducting a study that seeks to determine the factors causing tumor YKL-40 overexpression and whether such factors are expressed in both SVZ in close relationship to GB and in SVZ without a close relationship with GB in the same brain patients.

The role of YKL-40, glial cells and perivascular scaffold in migration and invasion

The existence of possible anatomical scaffolds allowing motility and migration of neuronal precursors toward the olfactory bulb along the vessels was first suggested and reported by Bovetti et al. [11] based on experimental analysis of olfactory bulb (OB) in rodents. Ontogenically, RG cells have been described as the first glia to appear, developing probably from the neuroepithelial youngest cells [17].

Although RG cells maintain a close contact with the SVZ in humans throughout adulthood, its apical processes are shortened by a probable retractable

mechanism with posterior acquisition of ependymal characteristics, suggesting that RG cells turn into astrocytes, carried out by a mechanism not well understood [10,75], although the factors responsible for radial glia and their maintenance are lost during development.

Even though the existence of neuronal migration along RG during development is patent, in the mammalian adulthood such phenomenon is not experimentally demonstrated. Based on the latter findings, recent research suggests that heterotopic RG cells progeny spread at early postnatal stages with local proliferation [17].

We hypothesize that GB tumors regionalization in adult human brain could be explained by the fact that residual RG-tumor promoter could be 'lost' in different brain pathways, but given the technical difficulty following stem cells along the extension of the RG cells and to determine the microanatomic localization of perivascular glioma cells, the invasive and motility pattern of gliomas may be explained nowadays by the understanding of branching blood vessel architecture. The study of all mechanisms that control and modulate the migration and invasion of GSCs and progeny is a crucial step for the design of therapies against GB.

Baker *et al.* [4] studied the requirement for neoangiogenesis in perivascular glioma by treating animals with angiogenesis inhibitors bevacizumab and DC101. In their work, the authors explained that perivascular invasion give rise to neoangiogenesis by digesting normal brain tissue in a VEGF-independent way that leads to tumor invasion. In line with a vascular-guided GSCs migration pattern during GB progression, Shao *et al.*, reviewed how the mesenchymal marker YKL-40 acts on GSCs to lead to the formation of angiogenesis. They explained that YKL-40 maintains vascular integrity. This fact is of paramount relevance as the microanatomic vascular scaffold was long thought to be non-neoplastic and that the relationship between tumor cells and ECs are independent [20].

Conclusions

Glioblastoma with SVZ infiltration showed decreased PFS and OS rates, probably due to GSCs and its aggressive mesenchymal growth pattern. YKL-40 seems to play a key role in the motility and migrating patterns of GSCs and their transdifferentiation into ECs. These findings may be associated with the location of GSCs in the SVZ and the occurrence of a more invasive and migratory GB subtype. Furthermore, GSCs can be the source for inter-tumoral heterogeneity with an impact on clinical outcome.

Although tumor development is highly dependent of several molecular factors, angiogenesis may be the key to developing novel therapeutic agents able to inhibit molecular pathways responsible for GB.

Disclosure

Authors report no conflict of interest.

References

1. Abraham S, Hu N, Jensen R. Hypoxia-inducible factor-1-regulated protein expression and oligodendroglioma patient outcome: comparison with established biomarkers and preoperative UCSF low-grade scoring system. J Neurooncol 2012; 108: 459-468.
2. Akiyama Y, Ashizawa T, Komiyama M, Miyata H, Oshita C, Omiya M, Iizuka A, Kume A, Sugino T, Hayashi N, Mitsuya K, Nakasu Y, Yamaguchi K. YKL-40 downregulation is a key factor to overcome temozolomide resistance in a glioblastoma cell line. Oncol Rep 2014; 32: 159-166.
3. Antonelli M, Buttarelli FR, Arcella A, Nobusawa S, Donofrio V, Oghaki H, Giangaspero F. Prognostic significance of histological grading, p53 status, YKL-40 expression, and IDH1 mutations in pediatric high-grade gliomas. J Neurooncol 2010; 99: 209-215.
4. Baker GJ, Yadav VN, Motsch S, Koschmann C, Calinescu AA, Mineharu Y, Camelo-Piragua SI, Orringer D, Bannykh S, Nichols WS, deCarvalho AC, Mikkelsen T, Castro MG, Lowenstein PR. Mechanisms of glioma formation: iterative perivascular glioma growth and invasion leads to tumor progression, VEGF-independent vascularization, and resistance to antiangiogenic therapy. Neoplasia 2014; 16: 543-561.
5. Barami K, Sloan AE, Rojiani A, Schell MJ, Staller A, Brem S. Relationship of gliomas to the ventricular walls. J Clin Neurosci 2009; 16: 195-201.
6. Barciszewska AM. MicroRNAs as efficient biomarkers in high-grade gliomas. Folia Neuropathol 2016; 54: 351-359.
7. Bernardi D, Padoan A, Ballin A, Sartori M, Manara R, Scienza R, Plebani M, Della Puppa A. Serum YKL-40 following resection for cerebral glioblastoma. J Neurooncol 2011; 107: 299-305.
8. Bjornbak C, Brochner CB, Larsen LA, Johansen JS, Mollgard K. Brain barriers and a subpopulation of astroglial progenitors of developing human forebrain are immunostained for the glycoprotein YKL-40. J Histochem Cytochem 2014; 62: 369-388.
9. Bleeker FE, Molenaar RJ, Leenstra S. Recent advances in the molecular understanding of glioblastoma. Journal Neurooncol 2012; 108: 11-27.
10. Bohman LE, Swanson KR, Moore JL, Rockne R, Mandigo C, Hankinson T, Assanah M, Canoll P, Bruce JN. Magnetic Resonance Imaging Characteristics of Glioblastoma Multiforme: Implications for Understanding Glioma Ontogeny. Neurosurgery 2010; 67: 1319-1328.

Kelvin M. Piña Batista, Sayoa Alvarez de Eulate-Beramendi, Kenia Y. Álvarez Reyes de Piña, Pedro Reimunde Figueira, Adan Fernandez Canal, Josué M. Avecillas Chasin, Ángela Meilan, Rodrigo Ugalde, Ivan Fernandez Vega

11. Bovetti S, Hsieh YC, Bovolin P, Perroteau I, Kazunori T, Puche AC. Blood vessels form a scaffold for neuroblast migration in the adult olfactory bulb. J Neurosci 2007; 27: 5976-5980.

12. Brooks MD, Sengupta R, Snyder SC, Rubin JB. Hitting Them Where They Live: Targeting the Glioblastoma Perivascular Stem Cell Niche. Curr Pathobiol Rep 2013; 1: 101-110.

13. Calabrese C, Poppleton H, Kocak M, Hogg TL, Fuller C, Hamner B, Oh EY, Gaber MW, Finklestein D, Allen M, Frank A, Bayazitov IT, Zakharenko SS, Gajjar A, Davidoff A, Gilbertson RJ. A perivascular niche for brain tumor stem cells. Cancer Cell 2007; 11: 69-82.

14. Chen J, Li Y, Yu TS, McKay RM, Burns DK, Kernie SG, Parada LF. A restricted cell population propagates glioblastoma growth after chemotherapy. Nature 2012; 488: 522-526.

15. Cheng L, Bao S, Rich JN. Potential therapeutic implications of cancer stem cells in glioblastoma. Biochem Pharmacol 2010; 80: 654-665.

16. Colman H, Zhang L, Sulman EP, McDonald JM, Shooshtari NL, Rivera A, Popoff S, Nutt CL, Louis DN, Cairncross JG, Gilbert MR, Phillips HS, Mehta MP, Chakravarti A, Pelloski CE, Bhat K, Feuerstein BG, Jenkins RB, Aldape K. A multigene predictor of outcome in glioblastoma. Neurooncol 2010; 12: 49-57.

17. Curtis MA, Kam M, Nannmark U, Anderson MF, Axell MZ, Wikkelso C, Holtås S, van Roon-Mom WM, Björk-Eriksson T, Nordborg C, Frisén J, Dragunow M, Faull RL, Eriksson PS. Human neuroblasts migrate to the olfactory bulb via a lateral ventricular extension. Science 2007; 315: 1243-1249.

18. Dimou L, Gotz M. Glial cells as progenitors and stem cells: new roles in the healthy and diseased brain. Physiol Rev 2014; 94: 709-737.

19. Doetsch F, Caillé I, Lim DA, García-Verdugo JMG, Alvarez-Buylla A. Subventricular zone astrocytes are neural stem cells in the adult mammalian brain. Cell 1999; 97: 703-716.

20. Ellison DW, Steart PV, Bateman AC, Pickering RM, Palmer J, Weller RO. Prognostic indicators in a range of astrocytic tumours: an immunohistochemical study with Ki-67 and p53 antibodies. J Neurol Neurosurg Psychiatry 1995; 59: 413-419.

21. Folkman J, Merler E, Abernathy C, Williams G. Isolation of a tumor factor responsible for angiogenesis. J Exp Med 1971; 133: 275-288.

22. Francescone RA, Scully S, Faibish M, Taylor SL, Oh D, Moral L, Yan W, Bentley B, Shao R. Role of YKL-40 in the angiogenesis, radioresistance, and progression of glioblastoma. J Biol Chem 2011; 286: 15332-15343.

23. Galli R, Binda E, Orfanelli U, Cipelletti B, Gritti A, De Vitis S, Fiocco R, Foroni C, Dimeco F, Vescovi A. Isolation and characterization of tumorigenic, stem-like neural precursors from human glioblastoma. Cancer Res 2004; 64: 7011-7021.

24. Ge WP, Jia JM. Local production of astrocytes in the cerebral cortex. Neuroscience 2016; 323: 1-7.

25. Ghazi SO, Stark M, Zhao Z, Mobley BC, Munden A, Hover L, Abel TW. Cell of origin determines tumor phenotype in an oncogenic Ras/p53 knockout transgenic model of high-grade glioma. J Neuropathol Exp Neurol 2012; 71: 729-740.

26. Gonzalez-Perez O, Garcia-Verdugo JM, Quinones-Hinojosa A, Luquin S, Gudino-Cabrera G, Gonzalez-Castaneda RE. Neural stem cells in the adult brain: from benchside to clinic. Stem Cells Int 2012; 2012: 378356.

27. Gonzalez-Perez O. Neural stem cells in the adult human brain. Biol Biomed Rep 2012; 2: 59-69.

28. Gursel DB, Beyene RT, Hofstetter C, Greenfield JP, Souweidane MM, Kaplitt M, Arango-Lievano M, Howard B, Boockvar JA. Optimization of glioblastoma multiforme stem cell isolation, transfection, and transduction. J Neurooncol 2011; 104: 509-522.

29. Heddleston JM, Li Z, Hjelmeland AB, Rich JN. The hypoxic microenvironment maintains glioblastoma stem cells and promotes reprogramming towards a cancer stem cell phenotype. Cell Cycle 2009; 20: 3274-3284.

30. Hormigo A, Gu B, Karimi S, Riedel E, Panageas KS, Edgar MA, Tanwar MK, Rao JS, Fleisher M, DeAngelis LM, Holland EC. YKL-40 and matrix metalloproteinase-9 as potential serum biomarkers for patients with high-grade gliomas. Clin Cancer Res 2006; 12: 5698-5704.

31. Ihrie RA, Alvarez-buylla A. Lake-front property: a unique germinal niche by the lateral ventricles of the adult brain. Neuron 2011; 70: 674-686.

32. Iwamoto FM, Hormigo A. Unveiling YKL-40, from serum marker to target therapy in glioblastoma. Front Oncol 2014; 4: 90.

33. Iwamoto FM, Hottinger AF, Karimi S, Riedel E, Dantis J, Jahdi M, Panageas KS, Lassman AB, Abrey LE, Fleisher M, DeAngelis LM, Holland EC, Hormigo A. Serum YKL-40 is a marker of prognosis and disease status in high-grade gliomas. Neurooncol 2011; 13: 1244-1251.

34. Jafri NF, Clarke JL, Weinberg V, Barani IJ, Cha S. Relationship of glioblatoma multiforme to the subventricular zone is associated with survival. Neurooncol 2013; 15: 91-96.

35. Jhaveri N, Chen TC, Hofman FM. Tumor vasculature and glioma stem cells: contributions to glioma progression. Cancer Lett 2016; 380: 545-551.

36. Johansen JS, Cintin C, Jørgensen M, Kamby C, Price PA. Serum YKL-40: a new potential marker of prognosis and location of metastases of patients with recurrent breast cancer. Eur J Cancer 1995; 31: 1437-1442.

37. Joseph JV, Conroy S, Pavlov K, Sontakke P, Tomar T, Eggens-Meijer E, Balasubramaniyan V, Wagemakers M, den Dunnen WF, Kruyt FA. Hypoxia enhances migration and invasion in glioblastoma by promoting a mesenchymal shift mediated by the HIF1α-ZEB1 axis. Cancer Lett 2015; 359: 107-116.

38. Kimura M, Lee Y, Miller R, Castillo M. Glioblastoma multiforme: relationship to subventricular zone and recurrence. Neuroradiol J 2013; 26: 542-547.

39. Kotagiri P, Chance SA, Szele FG, Esiri MM. Subventricular zone cytoarchitecture changes in Autism. Dev Neurobiol 2013; 74: 25-41.

40. Kriegstein A, Alvarez-Buylla A. The glial nature of embryonic and adult neural stem cells. Annu Rev Neurosci 2009; 32: 149-184.

41. Lacar B, Herman P, Platel JC, Kubera C, Hyder F, Bordey A. Neural Progenitor Cells Regulate Capillary Blood Flow in the Postnatal Subventricular Zone. J Neurosci 2012; 32: 16435-16448.

42. Lamborn KR. Prognostic factors for survival of patients with glioblastoma: Recursive partitioning analysis. Neurooncol 2004; 6: 227-235.

43. Lathia JD, Mack SC, Mulkearns-Hubert EE, Valentim CL, Rich JN. Cancer stem cells in glioblastoma. Genes Dev 2015; 29: 1203-1217.

44. Laywell ED, Rakic P, Kukekov VG, Holland EC, Steindler DA. Identification of a multipotent astrocytic stem cell in the imma-

ture and adult mouse brain. Proc Natl Acad Sci USA 2000; 97: 13883-13888.

45. Li L, Candelario KM, Thomas K, Wang R, Wright K, Messier A, Cunningham LA. Hypoxia Inducible Factor-1 (HIF-1) Is Required for Neural Stem Cell Maintenance and Vascular Stability in the Adult Mouse SVZ. J Neurosci 2014; 34: 16713-16719.

46. Lim DA, Alvarez-Buylla A. Adult neural stem cells stake their ground. Trends Neurosci 2014; 37: 563-571.

47. Lim DA, Cha S, Mayo MC, Chen MH, Keles E, VandenBerg S, Berger MS. Relationship of glioblastoma multiforme to neural stem cell regions predicts invasive and multifocal tumor phenotype. Neuro Oncol 2007; 9: 424-429.

48. Liu Y, Ye F, Yamada K, Tso JL, Zhang Y, Nguyen DH, Dong Q, Soto H, Choe J, Dembo A, Wheeler H, Eskin A, Schmid I, Yong WH, Mischel PS, Cloughesy TF, Kornblum HI, Nelson SF, Liau LM, Tso CL. Autocrine endothelin-3/endothelin receptor B signaling maintains cellular and molecular properties of glioblastoma stem cells. Mol Cancer Res 2011; 9: 1668-1685.

49. Michaelsen SR, Christensen IJ, Grunnet K, Stockhausen M-TRS, Broholm H, Kosteljanetz M, Poulsen HS. Clinical variables serve as prognostic factors in a model for survival from glioblastoma multiforme: an observational study of a cohort of consecutive non-selected patients from a single institution. BMC Cancer 2013; 13: 402.

50. Natesh K, Bhosale D, Desai A, Chandrika G, Pujari R, Jagtap J, Chugh A, Ranade D, Shastry P. Oncostatin-M differentially regulates mesenchymal and proneural signature genes in gliomas via STAT3 signaling. Neoplasia 2015; 17: 225-237.

51. Nduom EK, Hadjipanayis CG, Van Meir EG. Glioblastoma cancer stem-like cells: implications for pathogenesis and treatment. Cancer J 2012; 18: 100-106.

52. Oldham MC, Konopka G, Iwamoto K, Langfelder P, Kato T, Horvath S, Geschwind DH. Functional organization of the transcriptome in human brain. Nat Neurosci 2008; 11: 1271-1282.

53. Ostrom QT, Gittleman H, Liao P, Rouse C, Chen Y, Dowling J, Wolinsky Y, Kruchko C, Barnholtz-Sloan J. CBTRUS statistical report: primary brain and central nervous system tumors diagnosed in the United States in 2007-2011. Neuro Oncol 2014; 16 Suppl 4: iv1-iv63.

54. Pelloski CE, Lin E, Zhang L, Yung WKA, Colman H, Liu JL, Woo SY, Heimberger AB, Suki D, Prados M, Chang S, Barker FG 3rd, Fuller GN, Aldape KD. Prognostic associations of activated mitogen-activated protein kinase and Akt pathways in glioblastoma. Clin Cancer Res 2006; 12: 3935-3941.

55. Pelloski CE, Mahajan A, Maor M, Chang EL, Woo S, Gilbert M Colman H, Liu JL, Woo SY, Heimberger AB, Suki D, Prados M, Chang S, Barker FG 3rd, Fuller GN, Aldape KD. YKL-40 expression is associated with poorer response to radiation and shorter overall survival in glioblastoma. Clin Cancer Res 2005; 11: 3326-3334.

56. Piña Batista KM, Fernandez Vega I, Alvarez de Eulate-Beramendi S, Gutierrez Morales JC, Kurbanov A, Asnel D, Meilan A, Astudillo A. Prognostic significance of the markers IDH1 and YKL40 related to the subventricular zone. Folia Neuropathol 2015; 53: 52-59.

57. Piña Batista KM, Lourenco Costa BA, Cuervo-Arango Herreros I, Fernandez Vega I, Gutierrez Morales JC, Vallina Álvarez A, Mar-

ron PI, Meilán A, Astudillo A, Alvarez KY. Analysis of Olig2 and YKL-40 expression: a clinicopathological/immunohistochemical study for the distinction between subventricular zone II and III glioblastomas. Folia Neuropathol 2016; 54: 31-39.

58. Ping YF, Zhang X, Bian XW. Cancer stem cells and their vascular niche: Do they benefit from each other? Cancer Lett 2016; 380: 561-567.

59. Quinones-Hinojosa A, Sanai N, Soriano-Navarro M, Gonzalez-Perez O, Mirzadeh Z, Gil-Perotin S, Romero-Rodriguez R, Berger MS, Garcia-Verdugo JM, Alvarez-Buylla A. Cellular composition and cytoarchitecture of the adult human subventricular zone: a niche of neural stem cells. J Comp Neurol 2006; 494: 415-434.

60. Rath BH, Fair JM, Jamal M, Camphausen K, Tofilon PJ. Astrocytes enhance the invasion potential of glioblastoma stem-like cells. PLoS One 2013; 8: e54752.

61. Reardon DA, Wen PY, Desjardins A, Batchelor TT, Vredenburgh JJ. Glioblastoma multiforme: an emerging paradigm of anti-VEGF therapy. Expert Opin Biol Ther 2008; 8: 541-553.

62. Ricci-Vitiani L, Pallini R, Biffoni M, Todaro M, Invernici G, Cenci T, Maira G, Parati EA, Stassi G, Larocca LM, De Maria R. Tumour vascularization via endothelial differentiation of glioblastoma stem-like cells. Nature 2010; 468: 824-828.

63. Rodriguez FJ, Orr BA, Ligon KL, Eberhart CG. Neoplastic cells are a rare component in human glioblastoma microvasculature. Oncotarget 2012; 3: 98-106.

64. Safa AR, Saadatzadeh MR, Cohen-Gadol AA, Pollok KE, Bijangi-Vishehsaraei K. Glioblastoma stem cells (GSCs) epigenetic plasticity and interconversion between differentiated non-GSCs and GSCs. Genes Dis 2015; 2: 152-163.

65. Sanai N, Alvarez-buylla A, Berger MS. Neural stem cells and the origin of gliomas. N Engl J Med 2005; 353: 811-822.

66. Sanai N, Nguyen T, Ihrie RA, Mirzadeh Z, Tsai HH, Wong M, Gupta N, Berger MS, Huang E, Garcia-Verdugo JM, Rowitch DH, Alvarez-Buylla A. Corridors of migrating neurons in the human brain and their decline during infancy. Nature 2012; 478: 382-386.

67. Sanai N, Tramontin AD, Quinones-Hinojosa A, Barbaro NM, Gupta N, Kunwar S, Lawton MT, McDermott MW, Parsa AT, Manuel-García Verdugo J, Berger MS, Alvarez-Buylla A. Unique astrocyte ribbon in adult human brain contains neural stem cells but lacks chain migration. Nature 2004; 427: 740-744.

68. Schiffer D, Mellai M, Annovazzi L, Caldera V, Piazzi A, Denysenko T, Melcarne A. Stem cell niches in glioblastoma: a neuropathological view. Biomed Res Int 2014; 2014: 725921.

69. Segarra M, Kirchmaier BC, Acker-Palmer A. A vascular perspective on neuronal migration. Mech Dev 2015; 138 Pt 1: 17-25.

70. Sequerra EB. Subventricular zone progenitors in time and space: generating neuronal diversity. Front Cell Neurosci 2014; 8: 434.

71. Shakur SF, Bit-Ivan E, Watkin WG, Merrell RT, Farhat HI. Multifocal and multicentric glioblastoma with leptomeningeal gliomatosis: a case report and review of the literature. Case Rep Med 2013; 2013: 132679.

72. Shao R, Francescone RA, Ngernyuang N, Bentley B, Taylor SL, Moral L, Yan W. Anti-YKL-40 antibody and ionizing irradiation synergistically inhibit tumor vascularization and malignancy in glioblastoma. Carcinogenesis 2014; 35: 373-382.

Kelvin M. Piña Batista, Sayoa Alvarez de Eulate-Beramendi, Kenia Y. Álvarez Reyes de Piña, Pedro Reimunde Figueira, Adan Fernandez Canal, Josué M. Avecillas Chasin, Ángela Meilan, Rodrigo Ugalde, Ivan Fernandez Vega

73. Shao R, Taylor SL, Oh DS, Schwartz LM. Vascular heterogeneity and targeting: the role of YKL-40 in glioblastoma vascularization. Oncotarget 2015; 6: 40507-40518.

74. Singh SK, Bhardwaj R, Wilczynska KM, Dumur CI, Kordula T. A complex of nuclear factor I-X3 and STAT3 regulates astrocyte and glioma migration through the secreted glycoprotein YKL-40. J Biol Chem 2011; 286: 39893-39903.

75. Soeda A, Hara A, Kunisada T, Yoshimura SI, Iwama T, Park DM. The evidence of glioblastoma heterogeneity. Sci Rep 2015; 5: 9630.

76. Spalding KL, Bergmann O, Alkass K, Bernard S, Salehpour M, Huttner HB, Bostrom E, Westerlund I, Vial C, Buchholz BA, Possnert G, Mash DC, Druid H, Frisen J. Dynamics of hippocampal neurogenesis in adult humans. Cell 2013; 6: 1219-1227.

77. Spassky N, Merkle FT, Flames N, Tramontin AD, Garcia-Verdugo JM, Alvarez-Buylla A. Adult ependymal cells are postmitotic and are derived from radial glial cells during embryogenesis. J Neurosci 2005; 25: 10-18.

78. Stiles CD, Rowitch DH. Glioma stem cells: a midterm exam. Neuron 2008; 58: 832-846.

79. Stupp R, Pavlidis N, Jelic S; ESMO Guidelines Task Force. ESMO Minimum Clinical Recommendations for diagnosis, treatment and follow-up of malignant glioma. Ann Oncol 2005; 16 Suppl 1: i64-65.

80. Thomas RP, Xu LW, Lober RM, Li G, Nagpal S. The incidence and significance of multiple lesions in glioblastoma. J Neurooncol 2013; 112: 91-97.

81. Tran B, Rosenthal MA. Survival comparison between glioblastoma multiforme and other incurable cancers. J Clin Neurosci 2010; 17: 417-421.

82. Tso JL, Yang S, Menjivar JC, Yamada K, Zhang Y, Hong I, Bui Y, Stream A, McBride WH, Liau LM, Nelson SF, Cloughesy TF, Yong WH, Lai A, Tso CL. Bone morphogenetic protein 7 sensitizes O6-methylguanine methyltransferase expressing-glioblastoma stem cells to clinically relevant dose of temozolomide. Mol Cancer 2015; 14: 189.

83. Van Meir EG, Hadjipanayis CG, Norden AD, Shu HK, Wen PY, Olson JJ. Exciting new advances in neuro-oncology: the avenue to a cure for malignant glioma. Cancer J Clin 2010; 60: 166-193.

84. Wang R, Chadalavada K, Wilshire J, Kowalik U, Hovinga KE, Geber A, Fligelman B, Leversha M, Brennan C, Tabar V. Glioblastoma stem-like cells give rise to tumour endothelium. Nature 2010; 468: 829-833.

85. Yan K, Yang K, Rich JN. The evolving landscape of glioblastoma stem cells. Curr Opin Neurol 2013; 26: 701-707.

86. Zhang S, Lai N, Liao K, Sun J, Lin Y. MicroRNA-210 regulates cell proliferation and apoptosis by targeting regulator of differentiation 1 in glioblastoma cells. Folia Neuropathol 2015; 53: 236-244.

87. Zhang W, Kawanishi M, Miyake K, Kagawa M, Kawai N, Murao K, Nishiyama A, Fei Z, Zhang X, Tamiya T. Association between YKL-40 and adult primary astrocytoma. Cancer 2010; 116: 2688-2697.

Evidence from spatial pattern analysis for the anatomical spread of α-synuclein pathology in Parkinson's disease dementia

Richard A. Armstrong

Vision Sciences, Aston University, Birmingham, United Kingdom

Abstract

The objective of this study was to determine whether there is evidence from quantitative morphometry and spatial pattern analysis to support the hypothesis of anatomical spread of α-synuclein in Parkinson's disease dementia (PDD). Hence, clustering of α-synuclein-immunoreactive Lewy bodies (LB), Lewy neurites (LN), and Lewy grains (LG) was studied in α-synuclein-immunolabeled sections of cortical and limbic regions in 12 cases of PDD. The data suggested that: (1) LB, LN, and LG occurred in clusters which in 63% of regions were regularly distributed parallel to the tissue boundary, (2) in approximately 30% of cortical regions, the estimated cluster size of LB, LN, and LG was within the size range of cellular columns associated with the cortico-cortical pathways, (3) regularly distributed clusters were present in anatomically connected regions, and (4) the clustering pattern was similar to that of prion protein (PrP^sc) deposits in Creutzfeldt-Jacob disease (CJD). The clustering patterns of LB, LN, and LG were similar to those exhibited by cellular inclusions in other synucleinopathies and by PrP^sc deposits in prion disease and therefore, anatomical spread of pathogenic α-synuclein could be involved in the pathogenesis of PDD.

Key words: *Parkinson disease dementia (PDD), synucleinopathy, Lewy body (LB), Lewy neurite (LN), Lewy grain (LG), spatial pattern, anatomical spread.*

Introduction

The 'synucleinopathies', viz. Parkinson's disease dementia (PDD), dementia with Lewy bodies (DLB), and multiple system atrophy (MSA) are characterized by the formation of cellular inclusions containing pathological forms of the pre-synaptic protein α-synuclein. These pathologies include Lewy bodies (LB), Lewy neurites (LN), and Lewy grains (LG) in PDD and DLB [33] and glial cytoplasmic inclusions (GCI) in MSA [31]. α-Synuclein is a small molecular weight protein which regulates the functioning of dopamine transporter and tyrosine hydroxylase [27]. In normal brain, monomers of α-synuclein are unfolded soluble proteins, the oligomeric and fibrillar species existing in equilibrium. In the synucleinopathies, however, aggregation of α-synuclein occurs to form β-sheet configurations rich in amyloid [34] resulting in the formation of pathogenic inclusions such as LB.

Pathogenic α-synuclein may be secreted from cells, enter other cells, and seed small intracellular aggregates to form larger inclusions [23,35,37]. Hence, in PDD, pathological α-synuclein may exhibit 'prion-like' behaviour and propagate through the brain via anatomical connections. In the prion dis-

Communicating author:

Dr Phil. Richard A. Armstrong, Vision Sciences, Aston University, Birmingham B4 7ET, United Kingdom, phone: 0121-204-4102, fax: 0121-204-4048, e-mail: R.A.Armstrong@aston.ac.uk

ease, Creutzfeldt-Jakob disease (CJD), in which propagation of prion protein (PrP^{sc}) along anatomical pathways is well established [12,13], PrP^{sc} deposits are clustered in the cerebral cortex, the clusters often being regularly distributed parallel to the pia mater [7,9]. Clustering could therefore be a consequence of PrP^{sc} spreading among regions via anatomical pathways [7]. To determine whether similar clustering of α-synuclein pathology occurs in PDD, the spatial patterns of LB, LN, and LG were studied in cortical and limbic regions in twelve cases of PDD.

Material and methods

Cases

Parkinson's disease dementia cases ($n = 12$, details in Table I) were consecutive cases meeting the diagnostic criteria for Parkinson's disease (PD) and PDD and were obtained from the Movement Disorders Center at Washington University School of Medicine in St. Louis [11,26]. Initial diagnosis of PD was based on modified United Kingdom Parkinson Disease Society Brain Bank (UKPDSBB) clinical diagnostic criteria [24]: (1) bradykinesia was present in association with at least one of the following, viz. rigidity, 4-6 Hz rest tremor, or postural instability, (2) three supporting criteria were also present such

as unilateral onset, rest tremor, a progressive disorder, persistent asymmetry, a clinical condition present for more than 10 years, or excellent response to levodopa, and (3) the various exclusion criteria were applied such as the absence of stroke, persistent head injury, definite encephalitis, oculogyric crisis, family history of the disease, sustained remission, unilateral features after three years, progressive supranuclear palsy (PSP), early severe autonomic involvement, early signs of dementia, Babinski sign, cerebral tumor, exposure to MPTP, and negative response to levodopa [24]. Age of PD onset was determined by chart review and defined by onset of motor symptoms. Dementia in PD was determined by clinical assessment including the presence of impairment of attention, memory, executive, and visuo-spatial function together with behavioural disturbance, hallucinations and apathy [20]. The main pathological correlate of PDD is the presence of Lewy-body type degeneration in the cerebral cortex and limbic regions [20]. In addition, PDD cases are frequently associated with Alzheimer's disease neuropathologic change (ADNC) and the degree of ADNC was assessed using National Institute on Aging-Alzheimer's (NIA-AA) association guidelines 'ABC' [25]. This system uses four-point scales to assess the abundance of β-amyloid (Aβ) deposits

Table I. Demographic features, duration of disease, and disease stage of the twelve cases of Parkinson disease dementia (PDD). Lewy body (LB) stage was assessed using a PD staging scale (range: 0, 1-6) and the McKeith *et al.* staging scale (McKeith *et al.* 1996, 2005). Alzheimer's disease neuropathological change (ADNC) was rated using the National Institute on Aging-Alzheimer's (NIA-AA) association guidelines: A stage indicating β-amyloid (Aβ) deposition, B stage frequency of tau-immunoreactive neurofibrillary tangles (NFT), and C stage frequency of neuritic plaques (NP)

Case	Sex	Age	Dur. (PD)	Dur. (DM)	LB stage	ADNC			Level of AD
						A	B	C	
A	F	82	12	9	6	0	2	0	N
B	M	80	18	7	6	3	2	1	I
C	M	78	12	1	6	1	3	0	L
D	M	79	19	6	6	1	1	0	L
E	M	71	8	7	6	3	2	1	I
F	M	78	22	6	6	3	3	2	I
G	M	76	12	6	6	1	1	0	L
H	M	67	11	4	6	3	1	1	L
I	M	67	34	7	6	3	1	1	L
J	F	73	8	1	6	0	1	0	N
K	M	76	18	11	6	3	3	1	I
L	M	77	14	13	6	1	1	1	L

Dur. – duration, M – male, F – female, Aβ – amyloid-β, PD – Parkinson disease, DM – dementia, N – not AD, L – low level of AD, I – intermediate level of AD

('A' score), neurofibrillary tangles (NFT) ('B' score), and neuritic plaques (NP) ('C' score), the distribution of the three scores equating to four levels of ADNC, viz. 'not', 'low', 'intermediate', and 'high'. The 12 PDD cases in the present study equated to levels of ADNC from 'not' to 'intermediate' levels of AD.

Tissue preparation

After death, the consent of next-of-kin was obtained for brain removal, following local Institutional Review Board procedures and the 1995 Declaration of Helsinki (as modified in Edinburgh, 2000). Brains were fixed in 10% neutral buffered formalin for two weeks, paraffin-embedded, and sections cut at 6 mm. Blocks were taken from frontal and temporal lobes, the latter including the amygdala, hippocampus (HC), and dentate gyrus (DG). Histologic stains included hematoxylin and eosin and modified Bielschowsky silver impregnation. Immunohistochemistry was performed using the following antibodies: Aβ (10D5, 1 : 100,000; Elan Pharmaceuticals, San Francisco, CA), phosphorylated tau (PHF-1, 1 : 500; supplied by Dr. Peter Davies, Albert Einstein Medical School, Bronx, NY), ubiquitin (Dako, Glostrup, Denmark) and phosphorylated α-synuclein (1 : 10,000; Wako Chemicals USA Inc., Richmond, VA), and phosphorylated TDP-43 (pTDP-43, 1 : 40,000; Cosmo Bio Inc., Carlsbad, CA). Lewy bodies stage was assessed using a PD staging scale (range: 0, 1-6) [15,16] and the McKeith *et al.* staging scale [28,29].

Morphological methods

In the superior frontal gyrus (SFG) (BA 8,6), cingulate gyrus (CG) (BA 24), and entorhinal cortex (EC) (BA 28), the densities of LB, LN, and LG were counted along strips of tissue orientated parallel to the pia mater, using 250 x 50 μm sample fields arranged contiguously [3]. The sample fields were located both in the upper and lower (laminae V/VI) cortex (minimum $n = 32$ sample fields in each region), the short edge of the sample field orientated parallel with the pia mater and aligned with guidelines marked on the slide. In the HC, densities of inclusions were measured in sectors CA1 and CA2 ($n = 32$ fields in total), the short dimension of the sample field being aligned with the edge of the alveus. In the DG ($n = 32$ fields), the sample fields were aligned to study the molecular and granule cell layers. In the amygdala ($n = 16$ fields), the fields were arranged across

the maximum diameter of the basolateral nucleus, a region with severe α-synuclein pathology in PDD [11]. All distinct α-synuclein-immunoreactive rounded inclusions were counted as LB, LN were thread-like structures often contorted in shape, and small circular dot-like structures were identified as LG [11].

Data analysis

To determine patterns of clustering of the LB, LN, and LG, the data were analyzed by spatial pattern analysis [1-3] which was carried out on all brain regions with sufficient density of the pathology, i.e., at least 20 lesions were present along the strip of tissue analyzed. Departure from a random distribution can be measured by calculating the variance/ mean (V/M) ratio of the counts of a pathology in contiguous sample fields. If individuals of a pathology are randomly distributed, the number of samples containing 0, 1, 2, 3 … n, inclusions should correspond to a Poisson distribution and the V/M ratio should approximate to unity. A V/M ratio less than unity indicates a regular or uniform distribution of individual lesions and greater than unity a clumped or clustered distribution. If a pathology exhibits clustering along the strip of tissue examined, the mean size and distribution of the clusters can be estimated from counts in adjacent sample fields added together successively to provide data for increasing field sizes, e.g., 50 × 250 μm, 100 × 250 μm, 200 × 250 μm etc., up to a size limited by the total length of strip sampled. The V/M ratio is plotted against field size. A V/M peak estimates the presence of regularly-spaced clusters and location of the peak indicates mean cluster size, statistical significance of a V/M peak being tested using the 't' distribution [2,3]. Mean cluster sizes of the LB, LN, and LG were compared among brain regions using a one-way analysis of variance (ANOVA). Relationships between spatial pattern, α-synuclein pathology, and brain region were tested using chi-square (χ^2) contingency table tests. Correlations between cluster size of the LB, LN, and LG and patient age, disease duration, and ADNC 'ABC' stages were tested using Pearson's correlation coefficient ('r'). As the number of analyses performed was large and without pre-planned hypotheses, p values were adjusted using the Bonferroni correction which suggested that a p value of 0.001 should be used as the critical level to judge significance [5].

Results

Figure 1 shows the typical α-synuclein-immuno-reactive pathology in the EC of a case of PDD. Lewy bodies typically occur in small clusters whereas LN and LG are more widespread often developing in larger clusters.

Examples of the spatial pattern analysis are shown in Figure 2. In the upper laminae of the EC (Case A), LB exhibited a V/M peak at a field size of 100 mm suggesting a regular distribution of clusters of LB, 100 mm in diameter, distributed parallel to the pia mater. In the lower laminae of the CG (Case A), LN exhibited a V/M peak at a field size of 400 mm suggesting a regular distribution of clusters 400 mm in diameter, distributed parallel to the pia mater. In the upper laminae of the CG (Case A), there was an increase in V/M of the LG with field size without reaching a peak, suggesting a large cluster of LG of at least 800 mm in diameter.

The frequency of the different spatial patterns exhibited by the LB, LN, and LG in all regions and cases are summarized in Table II. In the majority of regions, the LB, LN, and LG were clustered and most frequently, the clusters were regularly distributed parallel to the tissue boundary. In addition, in a proportion of regions, the LB, LN, and LG were randomly distribute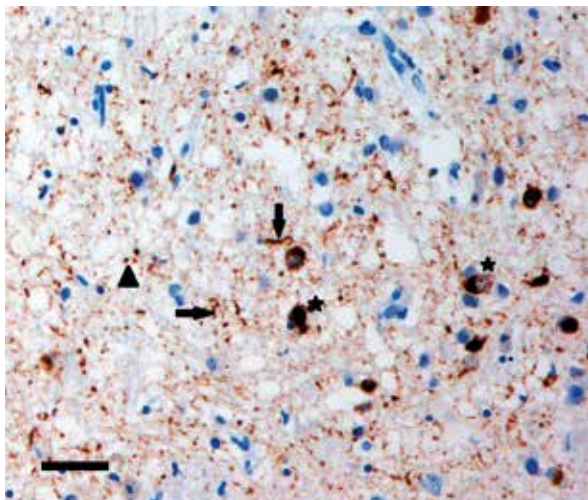d or present in large, non-regularly distributed clusters > 800 mm in diameter. The LB and LN exhibited a similar range of spatial patterns ($\chi^2 = 6.11$, $p > 0.05$) but the LG were more frequently present in large, non-regularly distributed clusters than the LB ($\chi^2 = 21.04$, $p < 0.001$) or the LN ($\chi^2 = 9.51$, $p < 0.05$). No significant differences in the frequencies of spatial patterns were observed in upper compared with lower cortical laminae or in cortical regions compared with CA1/CA2, the dentate gyrus, and basolateral amygdala.

The frequency distribution of cluster sizes of the LB, LN, and LG in cortical regions, viz., SFG, CG, and EC is shown in Table III. The majority of clusters were in the size range of 100-800 mm, significantly fewer gyri having cluster sizes as small as 50 mm or as large as 800 mm. Mean cluster size of the LB, LN, and LG in each brain region is shown in Figure 3. ANOVA suggested that mean cluster size of the LB was significantly less than that of the LN and LG ($F = 7.19$, $p < 0.001$). There were no statistically significant differences in cluster size among regions.

Correlations among cluster size of the LB, LN, LG and patient age, disease duration, and NIA-AA 'ABC' stage are shown in Table IV. Several correlations were present but after Bonferroni adjustment only cluster size of the LN was positively correlated with NFT ('B') stage in the lower laminae of the EC ($r = 0.99$, $p < 0.001$).

Fig. 1. The α-synuclein pathology of a case of Parkinson disease dementia (PDD) showing Lewy bodies (LB) (star), Lewy neurites (LN) (arrow), and Lewy grains (LG) (arrowhead) in the entorhinal cortex (α-synuclein immunohistochemistry, hematoxylin, bar = 50 mm).
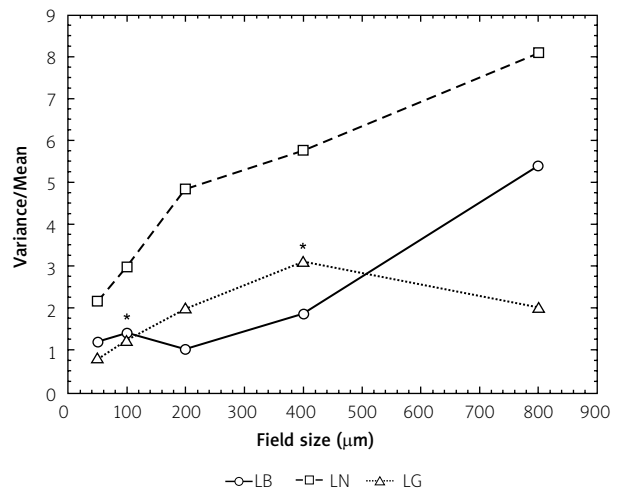

Fig. 2. Examples of the spatial patterns exhibited by Lewy bodies (LB), Lewy neurites (LN), and Lewy grains (LG) in a case of Parkinson disease dementia (PDD) (Case A). *Significant variance/mean peaks.

Table II. Frequency of different spatial patterns of the α-synuclein pathology in twelve cases of Parkinson disease dementia (PDD)

		Frequency of spatial pattern				
Region	Lesion	*N*	*R*	Reg	Regular clusters	Large clusters
SFG-U	LB	5	1	1	2	1
	LN	8	0	3	3	2
	LG	10	0	1	5	4
SFG-L	LB	4	2	0	2	0
	LN	9	0	2	3	4
	LG	11	1	1	6	3
CG-U	LB	6	3	0	3	0
	LN	11	2	2	5	2
	LG	12	2	3	4	3
CG-L	LB	10	2	0	8	0
	LN	12	2	0	8	2
	LG	12	0	1	6	5
EC-U	LB	9	1	0	7	1
	LN	12	3	0	6	3
	LG	11	1	0	5	5
EC-L	LB	7	0	1	6	0
	LN	11	5	1	3	2
	LG	11	0	1	7	3
AM	LB	10	6	1	2	1
	LN	10	2	1	6	1
	LG	10	2	0	3	5
CA1/2	LB	7	1	0	5	1
	LN	10	2	0	5	3
	LG	12	0	3	6	3
DG (ML)	LB	3	1	1	1	1
	LN	1	0	0	1	0
	LG	8	2	0	4	2
DG (GCL)	LN	4	2	0	2	0
	LG	8	0	0	6	2

LB – Lewy bodies, LN – Lewy neurites, LG – Lewy grains, SFG – superior frontal gyrus, CG – cingulate gyrus, EC – entorhinal cortex, U – upper cortex, L – lower cortex, AM – amygdala, CA1/2 – sectors of the hippocampus, DG – dentate gyrus, ML – molecular layer, GCL – granule cell layer, N – number of regions studied, R – random distribution, Reg – regular or uniform distribution of individual lesions
Statistical analysis: Comparison of frequencies (Chi-square (χ^2) contingency table tests totaled over regions): Comparison of different α-synuclein pathologies $\chi^2 = 22.72$ (6DF, $p < 0.001$), LN vs. LG $\chi^2 = 9.51$ (3DF, $p < 0.05$), LB vs. LN $\chi^2 = 6.11$ (3DF, $p > 0.05$), LB vs. LG $\chi^2 = 21.04$ (3DF, $p < 0.001$). Comparison of upper and lower cortex LB $\chi^2 = 3.69$ (3DF, $p > 0.05$), LN $\chi^2 = 0.45$ (3DF, $p > 0.05$), LG $\chi^2 = 3.29$ (3DF, $p > 0.05$). Comparison of cortical areas and HC/amygdala LB $\chi^2 = 3.57$ (3DF, $p > 0.05$), LN $\chi^2 = 1.60$ (3DF, $p > 0.05$), LG $\chi^2 = 1.89$ (3DF, $p > 0.05$).

Discussion

In cortical regions in PDD, the LB, LN, and LG were most frequently clustered and in a significant proportion of regions the clusters exhibited a regular distribution parallel to the pia mater. Similar clustering patterns were observed in sectors CA1/CA2 of the HC, DG, and basolateral amygdala. Hence, clustering of the α-synuclein pathology in PDD is similar to that reported previously in various neurodegenerative dis-

orders including the synucleinopathies DLB and MSA [8,10]. Clustering patterns of the α-synuclein pathology in PDD are also similar to that of PrP^{sc} deposits in CJD [7,9] in which propagation of PrP^{sc} among brain regions is particularly well documented [12,13].

A number of features of the data suggest that α-synuclein may have spread among brain regions via anatomical connections. First, in approximately 60% of cortical gyri, the LB, LN, and LG occurred in

Table III. Frequency distribution of cluster size of α-synuclein pathology (% of totals in parentheses) in cortical regions of twelve cases of Parkinson disease dementia (PDD)

		Cluster size (mm)			
Inclusion	N	50	100-200	400-800	> 800
Lewy bodies	31	8(26)	17 (55)	6 (19)	0
Lewy neurites	43	8 (19)	15 (35)	13 (30)	7 (16)
Lewy grains	48	9 (19)	15 (31)	16 (33)	8 (17)

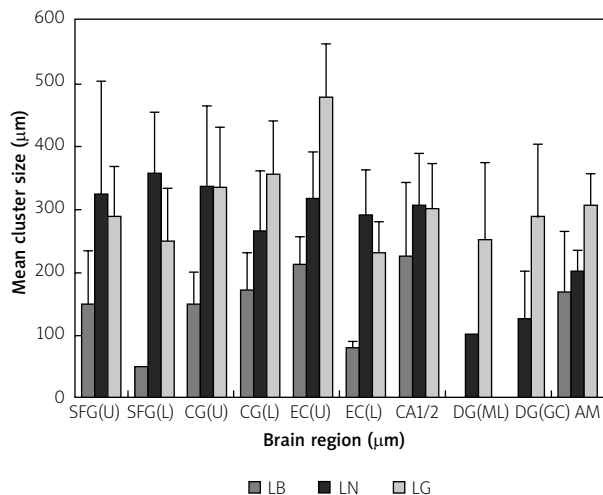*N – number of brain regions studied*

Fig. 3. Mean cluster sizes (bars = SE of mean) of the Lewy bodies (LB), Lewy neurites (LN), and Lewy grains (LG) in various brain regions (SFG – superior frontal cortex, CG – cingulate gyrus, EC – entorhinal cortex, CA1/2 – sectors of the hippocampus, DG – dentate gyrus, ML – molecular layer, GC – granule cell layer, AM – amygdala, U – upper cortex, L – lower cortex) in fifteen cases of Parkinson disease dementia (PDD). Analysis of variance (one-way ANOVA): among lesions F = 7.19 (p < 0.001); among regions: LB, F = 0.70 (p > 0.05), LN, F = 0.29 (p > 0.05), LG, F = 1.12 (p > 0.05).

either small regularly distributed clusters 50-200 mm in diameter or in larger regularly distributed clusters 400-800 mm in diameter. The smaller clusters could reflect an association between the pathology and columns of cells originating either from the midbrain or brain stem nuclei which repeat at 30-40 mm intervals or the commissural and ipsilateral association fibers, which terminate in vertically oriented columns 200-500 mm in width [30]. The larger regularly distributed clusters 400-800 mm in diameter, however, are within the size range of the columns of

cells associated with the cortico-cortical pathways [19,22,32]. These cells are themselves clustered and occur in bands regularly distributed along the cortex parallel to the pia mater [19,22]. Individual bands of cells have a mean dimension of approximately 500-1000 mm in width depending on the region, and traverse the laminae in columns; a similar size to the clusters of the LB, LN, and LG is observed in 30% of gyri in PDD. Second, positive correlations between cluster size, disease duration, and NIA-AA 'A' or 'B' stage in some regions in a region over time or with developing ADNC co-pathology consistent with spread and recruitment of α-synuclein. However, only the correlation between LN and NFT 'B' stage in the EC remained significant after Bonferroni adjustment suggesting less convincing evidence for an increasing burden of the pathology as the disease develops. Third, anatomically connected regions exhibited similar regularly distributed clusters, e.g. across the basolateral amygdala and in the CG and EC [17] and in dentate gyrus granule cells and EC ('perforant path') [6].

The data suggest a close relationship in PDD between the developing pathology and anatomical pathways which could have resulted from the spread of pathogenic α-synuclein in PDD [14,18,35]. This raises the possibility, first proposed by Braak *et al.* [21], that a pathogenic agent introduced via ingestion or inhalation, may transfer along axons to basal areas of the brain, the brain stem, and then to the cerebral cortex. α-Synuclein may be the target of this unknown agent causing protein misfolding and subsequent spread of α-synuclein via connecting cells. Hence, olfactory deficits are an early non-motor feature of PD and the pathology could potentially spread via the olfactory bulb and vagal system to the substantia nigra [36]. Further spread into cortical and limbic areas could then occur with subsequent propagation of the pathology among cortical regions

Table IV. Significant correlations (Pearson's 'r') between the cluster sizes of α-synuclein pathology and patient age (years), duration of disease (years), and Alzheimer's disease stage of twelve cases of Parkinson disease dementia (PDD)

Region	Lesion	Correlation				
		Age	Duration (PD)	Duration (Dem)	A-stage	B-stage
SFG (U)	LB	−0.06	−0.18	−0.92*	0	0.67
SFG (L)	LN	0.76*	0.59	−0.25	0.27	0.78*
	LG	0.23	0.89*	0	0.33	0.31
CG (U)	LN	0.58*	−0.32	−0.22	0.40	0.15
CG (L)	LN	0.15	0.16	−0.13	0.72**	0.48
EC (L)	LN	−0.69	0.16	0.50	0.44	0.97***
	LG	0.69*	0.27	−0.10	0.26	0.55
CA1/2	LB	0.47	−0.23	0.46	0.70*	0.28
	LG	0.27	0.01	0.35	0.74*	−0.08

LB – Lewy bodies, LN – Lewy neurites, LG – Lewy grains, SFG – superior frontal gyrus, CG – cingulate gyrus, EC – entorhinal cortex, CA1/2 – sectors of the hippocampus, U – upper cortical laminae, L – lower cortical laminae
*p < 0.05, **p < 0.01, ***p < 0.001. After Bonferroni adjustment only the correlation in bold remained significant.

via the cortico-cortical projections. Such a spread could therefore be an important factor in the development of dementia in PDD.

In conclusion, several features of the spatial patterns of the LB, LN, and LG suggest the anatomical spread of α-synuclein pathology in PDD: (1) the pathology occurred in clusters which were regularly distributed parallel to the tissue boundary, (2) in several regions the estimated cluster size of the LB, LN, and LG was within the size range of cellular columns associated with the cortico-cortical pathways, (3) regularly distributed clusters were present in anatomically connected regions, and (4) the clustering pattern was similar to that of PrP^{sc} deposits in CJD. If this hypothesis is correct, the presence of regularly distributed clusters of the pathology could be a useful indicator of this spread in both human patients and in animal models of the disease.

Acknowledgements

Disclosure

Author reports no conflicts of interest.

References

1. Armstrong RA. The usefulness of spatial pattern analysis in understanding the pathogenesis of neurodegenerative disorders, with particular reference to plaque formation in Alzheimer's disease. Neurodegeneration 1993; 2: 73-80.
2. Armstrong RA. Analysis of spatial patterns in histological sections of brain tissue. J Neurosci Meth 1997; 73: 141-147.
3. Armstrong RA. Quantifying the pathology of neurodegenerative disorders: quantitative measurements, sampling strategies and data analysis. Histopathology 2003; 42: 521-529.
4. Armstrong RA. Methods of studying the planar distribution of objects in histological sections of brain tissue. J Microscopy 2006; 221: 153-158.
5. Armstrong RA. When to use the Bonferoni correction. Ophthal Physiol Opt 2014; 34: 502-508.
6. Armstrong RA, Cairns NJ, Lantos PL. Clustering of Pick bodies in the dentate gyrus in Pick's disease. Neuropathology 2000; 20: 170-175.
7. Armstrong RA, Lantos PL, Cairns NJ. The spatial pattern of prion protein deposits in patients with sporadic Creutzfeldt-Jacob disease. Neuropathology 2001; 21: 19-24.
8. Armstrong RA, Lantos PL, Cairns NJ. What does the study of spatial patterns of pathological lesions tell us about the pathogenesis of neurodegenerative disease? Neuropathology 2001; 21: 1-12.
9. Armstrong RA, Cairns NJ, Ironside JW, Lantos PL. The spatial patterns of prion protein deposits in cases of variant Creutzfeldt-Jakob disease. Acta Neuropathol 2002; 104: 665-669.
10. Armstrong RA, Cairns NJ. Different molecular pathologies result in similar spatial patterns of cellular inclusions in neurodegenerative disease: a comparative study of eight disorders. J Neural Transm 2012; 119: 1551-1560.
11. Armstrong RA, Kotzbauer PT, Perlmutter JS, Campbell MC, Hurth KM, Schmidt RE, Cairns NJ. A quantitative study of α-synu-

clein pathology in fifteen cases of dementia associated with Parkinson disease. J Neural Transm 2014; 121: 171-181.

12. Beekes M, McBride, PA, Baldauf E. Cerebral targeting indicates vagal spread of infection in hamsters fed with scrapie. J Gen Virol 1998; 79: 601-607.

13. Beekes M, McBride PA. Early accumulation of pathological prion protein in the enteric nervous system and gut-associated lymphoid tissue of hamsters orally infected with scrapie. Neurosci Lett 2000; 278: 181-184.

14. Beekes M, Thomzig A, Schultz-Schaeffer W, Burger R. Is there a risk of prion-like transmission by Alzheimer- or Parkinson-associated protein particles. Acta Neuropathol 2014; 128: 463-476.

15. Braak H, del Tredici K, Rub U, de Vos RAI, Steur ENHJ, Braak E. Staging of brain pathology related to sporadic Parkinson's disease. Neurobiol Aging 2003; 24: 197-211.

16. Braak H, Ghebremedhin E, Rub U, Bratzke H, Del Tredici K. Stages in the development of Parkinson disease-related pathology. Cell Tissue Res 2004; 318: 121-134

17. Brodal A. Neurological anatomy. 3rd ed. Oxford University Press, New York and Oxford, 1981.

18. Cooper JM, Wiklander PBO, Nordin JZ, Al-Shawi R, Wood MJ, Vithiani M, Scapira AHV, Simons JP, El-Andaloussi S, Alvarez-Erviti L. Systemic exosomal siRNA delivery reduced alpha-synuclein aggregates in brains of transgenic mice. Mov Disord 2014; 29: 1476-1485.

19. De Lacoste M, White CL. The role of cortical connectivity in Alzheimer's disease pathogenesis: a review and model system. Neurobiol Aging 1993; 14: 1-16.

20. Emre M, Aarsland D, Brown R, Burn DJ, Duyckaerts C, Mizuno Y, Broe GA, Cummings J, Dickson DW, Gauthier S, Goldman J, Goetz C, Korczyn A, Lees A, Levy R, Litvan I, McKeith I, Olanow W, Poewe W, Quinn N, Sampaio C, Tolosa E, Dubois B. Clinical diagnostic criteria for dementia associated with Parkinson's disease. Mov Disord 2007; 15: 1680-1707.

21. Hawkes CH, Del Tredici K, Braak H. Parkinson disease: a dual hit hypothesis. Neuropathol Appl Neurobiol 2007; 33: 599-614.

22. Hiorns RW, Neal JW, Pearson RCA, Powell TPS. Clustering of ipsilateral cortico-cortical projection neurons to area 7 in the rhesus monkey. Proc Roy Soc (Lond) 1991; 246: 1-9.

23. Holmes BB, Devos SL, Kfoury N, Li M, Jacks R, Yanamandra K, Ouidja MO, Brodsky FM, Marasa J, Bagchi DP, Kotzbauer PT, Miller TM, Papy-Garcia D, Diamond MI. Heparan sulfate proteoglycans mediate internalization and propagation of specific proteopathic seeds. Proc Natl Acad Sci USA 2013; 110: E3138-E3147.

24. Hughes AJ, Daniel SE, Kilford L, Lees AJ. Accuracy of clinical diagnosis of idiopathic Parkinson disease: a clinic-pathological study of 100 cases. J Neurol Neurosurg Pyschiatr 1992; 55: 181-184.

25. Hyman BT, Phelps CH, Beach TG, Bigio EH, Cairns NJ, Carrillo MC, Dickson DW, Duyckaerts C, Frosch MP, Masliah E, Mirra SS, Nelson PT, Schneider JA, Thal DR, Thies B, Trojanowski JQ, Vinters HV, Montine TJ. National Institute on Aging-Alzheimer's Association guidelines for the neuropathologic assessment of Alzheimer's disease. Alz & Dement 2012; 8, 1-13.

26. Kotzbauer PT, Cairns NJ, Campbell MC, Racette BA, Tabbal SD, Perlmutter JS. Pathological accumulation of α-synuclein and Aβ in Parkinson disease patients with dementia. Arch Neurol 2012; 23: 1-6.

27. Kovacs GG, Milenkovic IJ, Preusser M, Budka H. Nigral burden of alpha-synuclein correlates with striatal dopamine deficit. Mov Disord 2008; 23: 1608-1612.

28. McKeith IG, Galasko D, Kosaka K, Perry EK, Dickson DW, Hansen LA, Salmon DP, Lowe J, Mirra SS, Byrne EJ, Lennox G, Quinn NP, Edwardson JA, Ince PG, Bergeron C, Burns A, Miller BL, Lovestone S, Collerton D, Jansen ENH, Ballard C, de Vos RAI, Wilcock GK, Jellinger KA, Perry RH. Consensus guidelines for the clinical and pathologic diagnosis of dementia with Lewy bodies (DLB): report of the consortium on DLB international workshop. Neurology 1996; 47: 1113-1124

29. McKeith IG, Dickson DW, Lowe J, Emre M, O'Brien JT, Feldman H, Cummings J, Duda JE, Lippa C, Perry EK, Aarsland D, Arai H, Ballard CG, Boeve B, Burn DJ, Costa D, Del Ser T, Dubois B, Galasko D, Gauthier S, Goetz CG,Gomez-Tortusa E, Holliday G, Hansen LA, hardy J, Iwatsubo T, Kalaria RN, Kaufer D, Kenny RA, Korczun A, Kosaka K, Lee VMY, Lees A, Litvan I, Londos E, Lopez OL, Minoshima S, Mijano Y, Molina JA, Mukaetova-Landinska EB, Pasquier F, Perry RH, Schultz JB, Trojanowski JQ, Yamada M. Diagnosis and management of dementia with Lewy bodies: third report of the DLB Consortium. Neurology 2005; 65: 1863-1872.

30. Mountcastle VB. An organizing principle for cerebral function: The unit module and the distributed system. In: The Neurosciences. 4th Study Program. Schmitt FO, Worden FG (eds.). 1979; 21-42.

31. Papp MI, Lantos PL. The distribution of oligodendroglial inclusions in multiple system atrophy and its relevance to clinical symptomology. Brain 1994; 117: 235-243.

32. Pearson RCA, Esiri MM, Hiorns RW, Wilcock GK, Powell TPS. Anatomical correlates of the distribution of the pathological changes in the neocortex in Alzheimer's disease. Proc Natl Acad Sci 1985; 82: 4531-4534.

33. Saito Y, Ruberu NN, Sawabe M, Arai T, Tanaka N, Kakuta Y, Yamanouchi H, Marayama S. Staging of argyrophilic grains: an age-associated tauopathy. J Neuropathol Exp Neurol 2004; 63: 911-918.

34. Spillantini MG, Crowther RA, Jakes R, Cairns NJ, Lantos PL, Goedert M. Filamentous alpha-synuclein inclusions link multiple system atrophy with Parkinson disease and dementia with Lewy bodies. Neurosci Lett 1998; 251: 205-208.

35. Steiner JA, Angot E, Brunden P. A deadly spread: cellular mechanisms of α-synuclein transfer. Cell Death and Differentiation 2011; 18:1425-1433.

36. Ubeda-Bannon I, Saiz-Sanchez D, De la Rosa-Prieto, Martinez-Marcos A. Alpha-synuclein in the olfactory system in Parkinson's disease: role of neural connections on spreading pathology. Brain Struc Funct 2014; 219: 1513-1526.

37. Voipicelli-Daley LA, Luk KC, Patel TP, Tanik SA, Eiddle DM, Stieber A, Meaney DF, Trojanowski JQ, Lee VMY. Exogenous alpha-synuclein fibrils induce Lewy body pathology leading to synaptic dysfunction and neuron death. Neuron 2011; 72: 57-71.

Folia
Neuropathologica

Frequency and topography of small cerebrovascular lesions in vascular and in mixed dementia: a post-mortem 7-tesla magnetic resonance imaging study with neuropathological correlates

Jacques De Reuck, Florent Auger, Nicolas Durieux, Vincent Deramecourt, Claude-Alain Maurage,
Charlotte Cordonnier, Florence Pasquier, Didier Leys, Regis Bordet

Centre Hospitalier Régional Universitaire de Lille (CHRU), Lille, France

Abstract

Introduction: Mixed dementia (MixD) refers to a combination of definite Alzheimer's disease (AD) and vascular encephalopathy. The existence of a "pure" type of vascular dementia (VaD) is controversial. There is a need to find magnetic resonance imaging (MRI) characteristics allowing the distinction between VaD and MixD. The present post-mortem 7.0-tesla MRI compares the frequency or severity and the topography of the small cerebrovascular lesions in brains of patients with VaD and with MixD.

Material and methods: Based on neuropathological criteria, 14 brains were classified as VaD, 24 as MixD and 11 as controls. Three coronal sections of a cerebral hemisphere and a horizontal section of a cerebellar hemisphere underwent T2 and T2* 7.0-tesla MRI examination. The mean values and topographic distribution of white matter changes (WMCs), lacunar infarcts (LIs), cortical microbleeds (CoMBs) and cortical microinfarcts (CoMIs) were determined and compared between the different groups.

Results: Compared to the controls, both VaD and MixD brains had significantly more severe WMCs and increased numbers of CoMBs and CoMIs. Lacunar infarcts predominated only in the VaD cases. On mutual comparison of VaD and MixD brains, CoMBs and CoMIs predominated in the frontal lobe and the cerebellum of VaD, while were mainly present in the occipital lobe of MixD. White matter changes predominated in the temporal lobe of MixD cases. Lacunar infarcts were significantly increased in the corona radiata and putamen of VaD patients.

Conclusions: The present post-mortem MRI study shows clear differences in the distribution and the types of cerebrovascular lesions on high-field MRI, confirming that VaD and MixD are different diseases.

Key words: post-mortem 7.0-tesla MRI, vascular dementia, mixed dementia, topographic distribution of small cerebrovascular lesions, cortical microbleeds, cortical microinfarcts, white matter changes, lacunar infarcts.

Communicating author:
Prof. Jacques De Reuck, CHRU Lille, EA 1046, Leopold II Laan 96, 9000 Ghent, Belgium, phone: 32 9 2218844, 32 9 2215668,
e-mail: dereuck.j@gmail.com

Introduction

Mixed dementia (MixD) refers to a combination of definite Alzheimer's disease (AD) and vascular encephalopathy. The distinction between MixD and "pure" vascular dementia is controversial [15,23]. In demented patients vascular lesions on structural magnetic resonance imaging (MRI) are often misdiagnosed as probable vascular dementia (VaD) as compared to autopsy-confirmed diagnosis [20]. Also the utility of their detection for the individual diagnosis of VaD or MixD is limited [28]. Major vascular lesions differ between VaD and MixD [17].

An important obstacle in the standardization of diagnosis is the fact that vascular brain lesions are a large group comprising heterogeneous changes that have different pathogenesis [14]. Our previous post-mortem study showed that the lesion pattern in VaD and MixD is different: while the global severity of the white matter changes is more or less similar, lacunes in the corona radiata predominate in the former and cerebral amyloid angiopathy-related lesions in the latter [9].

So there is a need to quantify and determine the topography of the different types of cerebrovascular lesions in VaD and MixD. Post-mortem MRI is an additional complement of the neuropathological assessment of these lesions [21]. 7-tesla MRI is the most suitable technique to detect small cerebrovascular lesions in post-mortem brains [26].

The present post-mortem 7.0-tesla MRI study with neuropathological correlates investigates whether there are differences in severity and topography of small cerebrovascular lesions between VaD and MixD brains in order to find neuroimaging criteria that allow the distinction between both disease entities.

Material and methods

Out of a series of 162 consecutive autopsied patients, followed up at the Lille University Hospital, who underwent a MRI examination, according to the neuropathological criteria [2,4], 14 with a diagnosis of VaD, 24 of MixD and 11 control brains, without a history of dementia or stroke, were selected.

They all underwent a post-mortem 7.0-tesla MRI examination of 3 coronal sections of a cerebral hemisphere and one horizontal section of a cerebellar hemisphere, followed by an extensive histological examination of the brain samples.

Previously obtained informed consent of the patients or from the nearest family allowed an autopsy for diagnostic and scientific purposes. The brain tissue samples were acquired from the Lille Neuro-Bank of the Lille University that is a part of the "Centres des Resources Biologiques" and acts as an institutional review board.

One fresh cerebral hemisphere was frozen for biochemical examination. The remaining hemisphere, the brainstem, and most of the cerebellum were fixed in formalin for three weeks.

Neuropathological examination

The disease diagnosis was made according a standard procedure and examination of a large number of samples. In addition to the detection of macroscopic visible lesions such as haematomas, territorial and lacunar infarcts (LIs), a whole coronal section of a cerebral hemisphere, at the level of the mammillary body and a horizontal section of a cerebellar hemisphere were taken for the semi-quantitative evaluation of the small cerebrovascular lesions such as white matter changes (WMCs), cortical microbleeds (CoMBs), and cortical microinfarcts (CoMIs).

The mean values for WMCs were the average of the ranking scores: no change (R0), a few isolated (R1), frequent scattered in the corona radiata (R2) and forming confluent lesions (R3) of myelin and axonal loss. For the other cerebrovascular lesions, their mean values corresponded to their percentage number [6].

The diagnosis of cerebral angiopathy (CAA) was made when a majority of β-amyloid stained vessels were present in at least three of the four examined samples and as not-CAA, β when absent or scarce, in case of a few stained vessels in one or two slides [13].

Magnetic resonance imaging examination

Three coronal sections of a cerebral hemisphere were submitted to T2 and T2* MRI: a frontal one at the level of the head of the caudate nucleus, a central one at the level of the mammillary body and one at the level of the parietal and occipital lobes. In addition, one horizontal section of a cerebellar hemisphere was also examined.

A 7.0-tesla MRI Bruker BioSpin SA with an issuer-receiver cylinder coil of 72 mm inner diameter

(Ettlingen, Germany) was used, according to a previous described method [7].

The ranking scores of severity of the WMCs were evaluated separately in the different brain sections as done on the neuropathological section. Lacunar infarcts were defined as small-rounded lesions with a diameter between 3 and 15 mm in the corona radiata, internal capsule, caudate nucleus, putamen, globus pallidus, thalamus and cerebellar white matter [27]. The number and the location of the small cerebrovascular lesions were determined by consensus evaluation of three observers (JDR, FA, ND), blinded to the neuropathological diagnosis. The inter-rater reliability resulted in an interclass correlation coefficient of 0.82.

Statistical analysis

Univariate comparisons of unpaired groups were performed with the Fisher's exact test for categorical data. The non-parametric Mann-Whitney U-test was used to compare continuous variables. The significance level, two-tailed, was set at ≤ 0.01 for significant and ≤ 0.001 for highly significant. Values set at ≤ 0.05 but more than > 0.01 were considered as marginal significant and not included as relevant due to the relative small sample sizes.

Results

The average age at death was not significantly different between the groups: 75 (± 10) years in the VaD patients, 76 (± 11) in the MixD and 71 (± 9) in the control group (p = 0.16). Also the gender distribution was similar with 80% males in VaD, 54% in MixD and 73% in the control groups, respectively (p = 0.62).

Arterial hypertension and the use of antithrombotic agents were the only more frequently found clinical vascular risk factors in the VaD and MixD patients compared to the controls (Table I).

On neuropathological examination, the semi-quantitative evaluation of the degree of severity showed a significant increase in WMCs and higher incidence of CoMIs and CoMBs in VaD as MixD compared to controls. On the other hand, LIs and territorial infarcts were only more frequent in the VaD group, while CAA related lesions were more observed in the MixD group (Table II).

Table I. Comparison of vascular risk factors between normal controls (C) and patients with vascular dementia (VaD) and mixed dementia (MixD)

Vascular risk factors	C	VaD	MixD
	(n = 11)	(n =14)	(n = 24)
Arterial hypertension	18%	86%**	75%*
Diabetes	0%	43%	33%
Hypercholesterolemia	27%	50%	46%
Smoking	18%	21%	13%
Antithrombotic use	18%	93%**	83%**

*p ≤ 0.01; **p ≤ 0.001

Table II. Mean values (standard deviations) of the neuropathological lesions in normal controls (C) compared to those in vascular dementia (VaD) and mixed dementia (MixD) brains

Cerebrovascular lesions	C	VaD	MixD
	(n = 11)	(n = 14)	(n = 24)
White matter changes	0.4 (0.7)	1.7 (1.3)*	1.4 (1.2)*
Cerebral amyloid angiopathy	0.0 (0.0)	0.5 (0.8)	2.7 (0.5)**
Lacunar infarct	0.0 (0.0)	2.5 (0.9)**	0.2 (0.5)
Territorial infarct	0.0 (0.0)	2.0 (1.4)**	0.1 (0.4)
Haematoma	0.0 (0.0)	0.9 (1.2)	0.4 (0.7)
Cortical microinfarcts	0.2 (0.4)	2.2 (1.3)**	3.4 (1.0)**
Cortical microbleeds	0.3 (0.5)	1.7 (0.9)**	2.0 (1.3)**

*p ≤ 0.01; **p ≤ 0.001

The same findings were observed on the post-mortem MRI, concerning WMCs, LIs, CoMBs and CoMIs (Table III).

On mutual comparison of the VaD and the MixD brain CoMBs, predominated in the frontal lobe and in the cerebellum of the former, while increased in the temporal and the occipital lobes in the latter group (Fig. 1). Cortical microinfarcts predominated in the frontal lobe and the cerebellum of the VaD group, while increased in the occipital lobe of the MixD group (Fig. 2). White matter changes predominated only in the temporal lobe of the MixD group (Fig. 3). As to LIs they were significantly increased in the corona radiata and the putamen in the VaD group (Fig. 4, Table IV).

Discussion

The present study shows a difference in the distribution and types of the small cerebrovascular lesions in patients with VaD compared to those with MixD. Their heterogeneity was already previously suspected [16,22,25]. Our previous neuropathological study demonstrated that LIs due to arteriosclerotic angiopathy are the most common lesions in VaD, while CAA related lesions are more frequent in MixD, suggesting that the latter represent the natural end-stage evolution of Alzheimer's disease [9]. There is a strong correlation between CAA and age [17,19]. However, in contrast to a previous neuropathological study [1], more territorial infarcts are observed in VaD than in MixD brains. This is probably due to more additional large-vessel disease in the former group [18].

Cortical microinfarcts predominate in the frontal lobe and in the cerebellum of VaD as cerebral arteriosclerosis is their main cause [8,18], while according to the validated Boston criteria for CAA, they predominate in the occipital lobe in MixD [10]. The same is also observed for CoMBs, although also

Table III. Mean values (standard deviations) of the MRI lesions in normal controls (C) compared to those in vascular dementia (VaD) and mixed dementia (MixD) brains.

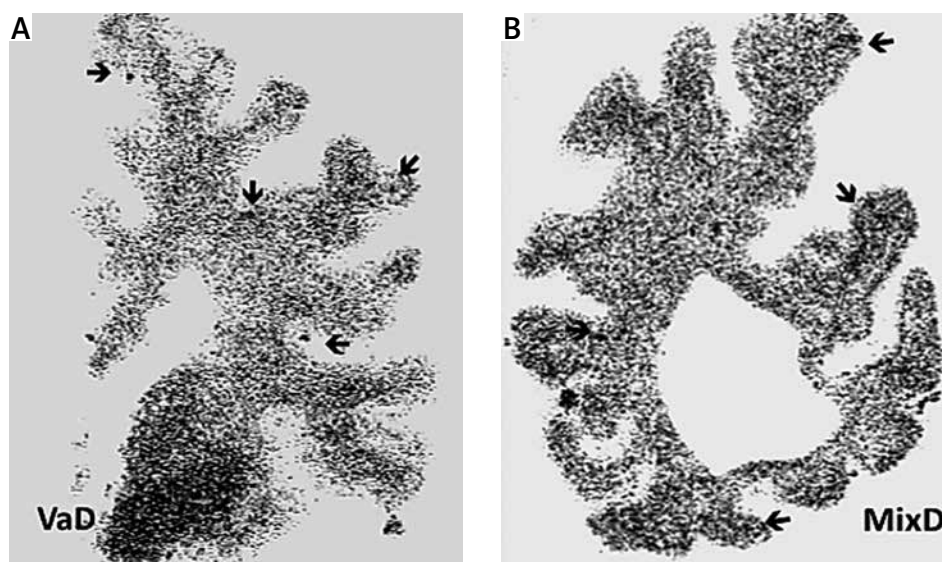| MRI lesions	C	VaD	MixD
	($n = 11$)	($n = 14$)	($n = 24$)
White matter changes	0.2 (0.4)	1.4 (0.6)**	1.5 (0.6)**
Lacunar infarct	2.8 (1.0)	14.4 (1.9)**	3.3 (2.2)
Cortical microinfarcts	0.2 (0.4)	5.2 (1.4)**	4.9 (0.8)**
Cortical microbleeds	3.3 (1.1)	10.4 (1.6)**	9.8 (2.0)**

*$p \leq 0.01$; **$p \leq 0.001$*

Fig. 1. T2* MRI demonstrating the presence of cortical microbleeds (arrows) on a coronal section of the frontal lobe in a patient with vascular dementia **(A)** and of the occipital lobe in a patient with mixed dementia **(B)**.
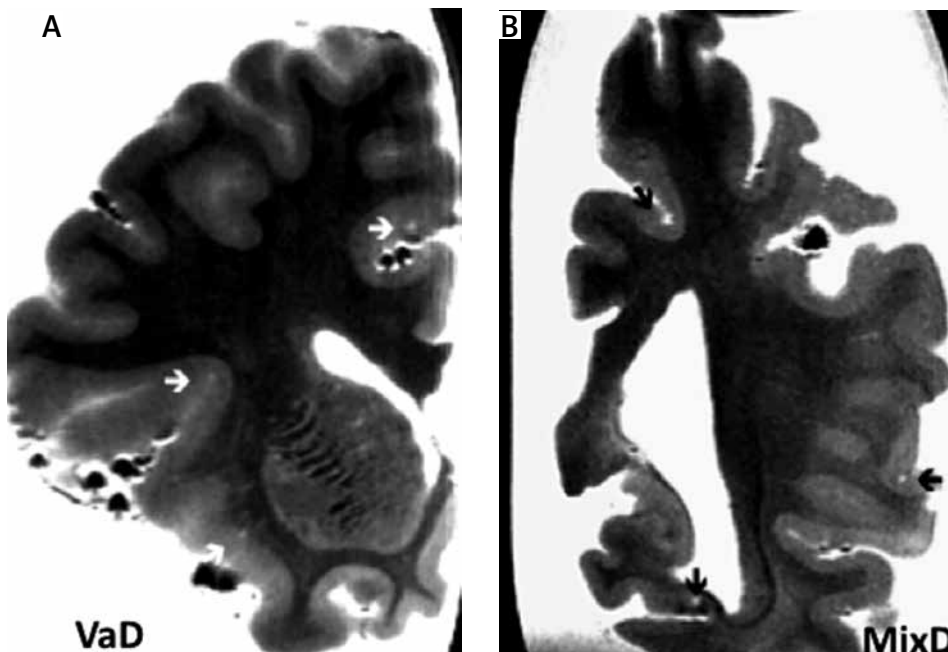
Fig. 2. T2 MRI demonstrating the presence of cortical microinfarcts (arrows) on a coronal section of the frontal lobe in a patient with vascular dementia **(A)** and of the occipital lobe in a patient with mixed dementia **(B)**.
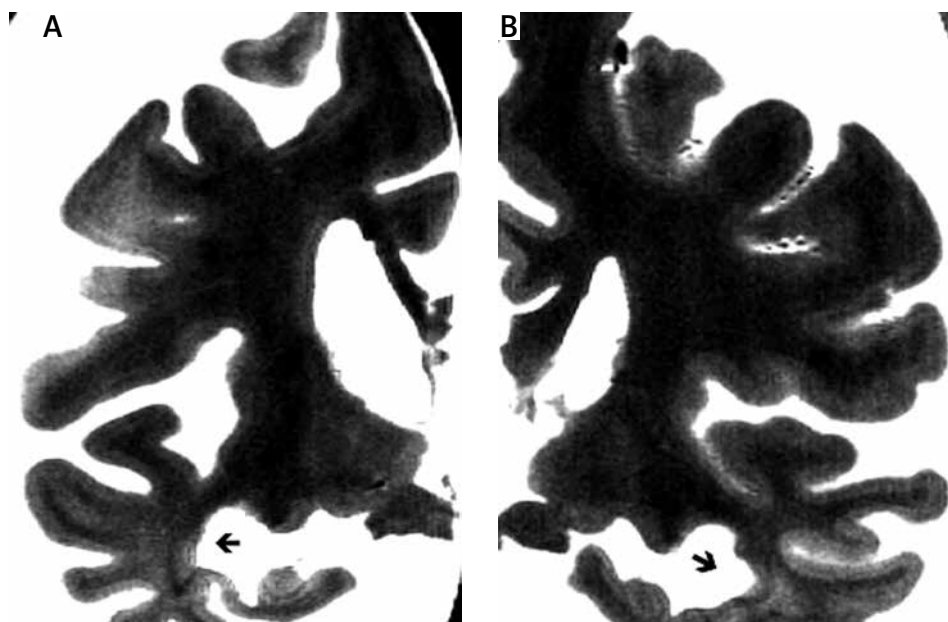

Fig. 3. T2 MRI of a central coronal section of a mixed dementia brain showing, in addition to the enlargement of the temporal horn, more selective temporal white matter changes.

highly present in the temporal lobe of MixD brains. The latter can be explained by the fact that CoMBs are not only due to micro-vascular lesions, but also to the severity of the neurodegenerative changes themselves in AD [6].

White matter changes are, as a whole, as severe in VaD as in MixD [9]. The present study shows a predominance in the temporal lobe of MixD brains associated to the temporal lobe atrophy, due to the underlying severity of the Alzheimer lesions [3].

Table IV. Comparison of the mean values (standard deviations) of the topography of the small cerebrovascular lesions on magnetic resonance imaging between brains with vascular dementia (VaD) and mixed dementia (MixD)

Cerebrovascular lesions	VaD (n = 14)	MixD (n = 24)
Cortical microbleeds		
Frontal lobe	4.1 (0.8)**	2.1 (1.0)
Temporal lobe	1.5 (0.9)	2.6 (1.0)**
Parietal lobe	1.4 (0.6)	1.6 (1.1)
Occipital lobe	1.5 (0.9)	3.4 (1.0)**
Cerebellum	2.7 (1.1)**	0.8 (1.1)
Cortical microinfarcts		
Frontal lobe	1.6 (0.8)*	0.8 (0.8)
Temporal lobe	0.4 (0.6)	0.9 (0.8)
Parietal lobe	1.3 (1.1)	1.6 (0.6)
Occipital lobe	0.5 (0.3)	1.4 (0.8)**
Cerebellum	1.9 (0.7)**	0.4 (0.6)
White matter changes		
Frontal lobe	1.6 (0.6)	1.1 (0.8)
Temporal lobe	0.3 (0.6)	1.3 (0.9)**
Parietal lobe	0.9 (0.8)	1.7 (0.9)
Occipital lobe	0.9 (0.9)	1.3 (0.9)
Cerebellum	0.8 (0.8)	0.3 (0.7)
Lacunar infarcts		
Corona radiata	7.0 (0.5)**	0.6 (0.8)
Caudate nucleus	1.1 (0.8)	0.4 (0.7)
Internal capsule	1.1 (0.6)	0.6 (0.8)
Putamen	3.2 (0.8)**	0.9 (0.9)
Globus pallidus	1.3 (0.9)	0.3 (0.4)
Thalamus	0.7 (0.7)	0.3 (0.4)
Cerebellum	0.2 (0.4)	0.0 (0.0)

*$p \leq 0.01$; **$p \leq 0.001$

Although in our previous study, only LIs in the corona radiata were found in VaD compared to MixD [12], our present study also shows an additional increase in the putamen. Their topography corresponds to the vascular territory of the lenticulostriate arteries [5]. These findings correlate well with "in vivo" measurements of lenticulostriate arteries using 7-tesla MRI that show fewer side-branches in VaD [24].

The present post-mortem MRI study shows clear differences in the distribution and the types of cerebrovascular lesions, confirming that VaD and MixD are different diseases.
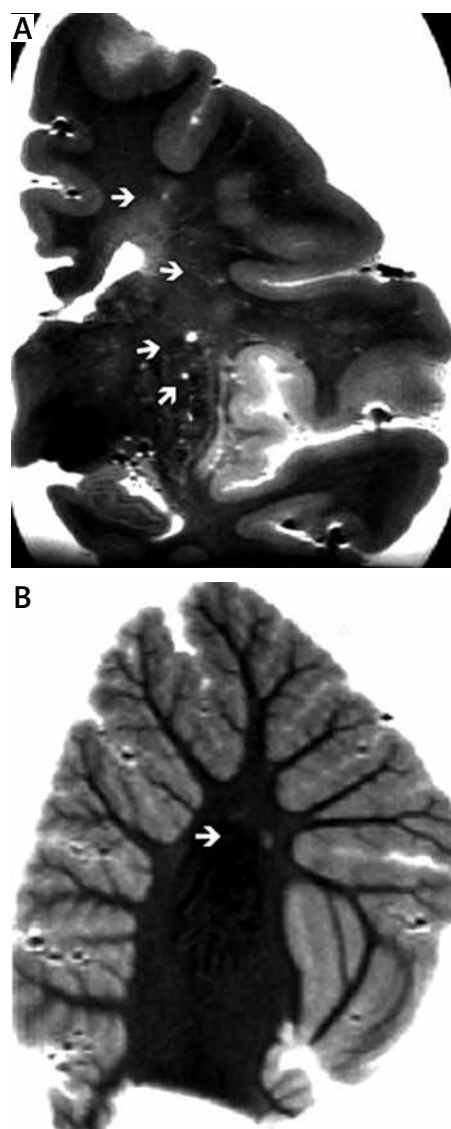

Fig. 4. T2 MRI showing on a central coronal section in addition to diffuse white matter changes also several lacunar infarcts in the corona radiata and putamen (arrows) in a patient with vascular dementia **(A)**. A lacunar infarct is also observed in the cerebellar white matter of the same patient **(B)**.

Disclosure

Authors report no conflict of interest.

References

1. Attems J, Jellinger KA. The overlap between vascular disease and Alzheimer's disease – lessons from pathology. BMC Med 2014; 12: 206.

2. Braak H, Braak E. Evolution of neuronal changes in the course of Alzheimer's disease. Acta Neuropathol 1991; 82: 239-259.

3. Bombois S, Debette S, Bruander A, Delbeuck X, Delmaire C, Leys D, Pasquier F. Vascular subcortical hyperintensities predict conversion to vascular and mixed dementia in MCI patients. Stroke 2008; 39: 2046-2051.

4. Deramecourt V, Slade JY, Oakley AE, Perry RH, Ince PG, Maurage CA, Kalaria RH. Staging and natural history of cerebrovasular pathology in dementia. Neurology 2012; 78: 1043-1050.

5. De Reuck J. The human periventricular arterial blood supply and the anatomy of cerebral infarctions. Eur Neurol 1971; 5: 321-334.

6. De Reuck J, Deramecourt V, Cordonnier C, Leys D, Pasquier F, Maurage CA. Prevalence of small cerebral bleeds in patients with a neurodegenerative dementia: A neuropathological study. J Neurol Sci 2011; 300: 63-66.

7. De Reuck J, Auger F, Cordonnier C, Deramecourt V, Durieux N, Pasquier F, Bordet R, Maurage CA, Leys D. Comparison of 7.0-T T2*-magnetic resonance imaging of cerebral bleeds in post-mortem brain sections of Alzheimer patients with their neuropathological correlates. Cerebrovasc Dis 2011; 31: 511-517.

8. De Reuck JL, Deramecourt V, Durieux N, Cordonnier C, Devos D, Defebvre L, Moreau C, Capparos-Lefebvre D, Pasquier F, Leys D, Maurage CA, Bordet R. The significance of cortical cerebellar microbleeds and microinfarcts in neurodegenerative and cerebrovascular diseases. A post-mortem 7.0-tesla magnetic resonance study with neuropathological correlates. Cerebrovasc Dis 2015; 39: 138-143.

9. De Reuck J, Deramecourt V, Cordonnier C, Pasquier F, Leys D, Maurage CA, Bordet R. Incidence of post-mortem neurodegenerative and cerebrovascular pathology in mixed dementia. J Neurol Sci 2016; 366: 164-166.

10. De Reuck j, Cordonnier C, Deramecourt V, Auger F, Durieux N, Leys D, Pasquier F, Maurage CA. Lobar intracerebral haematoma. Neuropathological and 7.0-tesla magnetic resonance imaging evaluation. J Neurol Sci 2016; 369: 121-125.

11. De Reuck J, Auger F, Durieux N, Cordonnier C, Deramecourt V, Pasquier F, Maurage CA, Leys D, Bordet R. The topography of cortical microinfarcts in neurodegenerative diseases and vascular dementia: a postmortem 7.0-tesla magnetic resonance imaging study. Eur Neurol 2016; 76: 57-61.

12. De Reuck J, Auger F, Durieux N, Cordonnier C, Deramecourt V, Pasquier F, Maurage CA, Leys D, Bordet R. Topographic distribution of white matter changes and lacunar infarcts in neurodegenerative and vascular dementia syndromes: A post-mortem 7.0-tesla magnetic resonance imaging study. Eur Stroke J 2016; 1: 122-129.

13. Ellis RJ, Olichney JM, Thal LJ, Mirra SS, Morris JC, Beekly D, Heyman A. Cerebral amyloid angiopathy in the brains of patients with Alzheimer's disease: the CERAD experience, Part XV. Neurology 1996; 46: 1592-1596.

14. Grinberg LT, Heinsen H. Toward a pathological definition of vascular dementia. J Neurol Sci 2010; 299: 136-138.

15. Jellinger KA, Attems J. Neuropathological evaluation of mixed dementia. J Neurol Sci 2007; 25: 80-87.

16. Jellinger KA. The pathology of "vascular dementia": a critical update. J Alzheimers Dis 2008; 14: 107-123.

17. Jellinger KA, Attems J. Prevalence and pathology of vascular dementia in the oldest-old. J Alzheimers Dis 2010; 21: 1283-1293.

18. Kitagawa K, Miwa K, Yagita Y, Okazaki S, Sakaguchi M, Mochizuki H. Association between carotid stenosis or lacunar infarction and incident dementia in patients with vascular risk factors. Eur J Neurol 2015; 22: 187-192.

19. Kovari E, Herrmann FR, Hof PR, Bouras C. The relation between cerebral amyloid angiopathy and cortical microinfarcts in brain ageing and Alzheimer's disease. Neuropathol Appl Neurobiol 2013; 39: 498-509.

20. Niemantsverdriet E, Feyen BF, Le Bastard N, Martin JJ, Goeman J, De Deyn PP, Engelborghs S. Overdiagnosing vascular dementia using structural brain imaging for dementia work-up. J Alzheimers Dis 2015; 45: 1039-1043.

21. McAleese KE, Firbank M, Hunter D, Sun L, Hall R, Near JW, Mann DM, Esiri M, Jellinger KA, O'Brien JT, Attems J. Magnetic resonance imaging of fixed post mortem brains reliably reflects subcortical vascular pathology of frontal, parietal and occipital white matter. Neuropathol Appl Neurobiol 2013; 39: 485-497.

22. Lo RY, Jagust WJ; Alzheimer's Disease Neuroimaging Initiative. Vascular burden and Alzheimer disease pathological progression. Neurology 2012; 79: 1349-1355.

23. Lopez OL, Kuller LH, Becker JT, Jagust WJ, DeKosky ST, Fitzpatrick A, Breitner J, Lyketsos C, Kawas C, Carlson M. Classification of vascular dementia in the Cardiovascular Health Study Cognition Study. Neurology 2005; 64:1539-1547.

24. Seo SW, Kang CK, Kim SH, Yoon DS, Liao W, Worz S, Rohr K, Kim YB, Na DL, Cho ZH. Measurements of lenticulostriate arteries using 7T MRI: new imaging markers for subcortical vascular dementia. J Neurol Sci 2012; 322: 200-205.

25. Staekenborg SS, van Straaten EC, van der Flier WM, Lane R, Barkhof F, Scheltens P. Small vessel versus large vessel vascular dementia: risk factors and MRI findings. J Neurol 2008; 255:1644-1651.

26. Trattnig S, Bogner W, Gruber S, Szomolanyi P, Juras V, Robinson S, Zbyn S, Haneder S. Clinical applications at ultrahigh field (7 T). Where does it make the difference? NMR Biomed 2015; 29: 1316-1334.

27. Wang X, Valdés Hernandez MD, Doubal F, Chappell FM, Piper RJ, Deary IJ, Wardlaw JM. Development and initial evaluation of a semi-automatic approach to assess perivascular spaces on conventional magnetic resonance images. J Neurosci Methods 2015; 257: 34-44.

28. Yassi N, Desmond PM, Masters CL. Magnetic resonance imaging of vascular contributions to cognitive impairment and dementia. J Mol Neurosci 2016; 60: 349-353.

Status of the brain antioxidant system at different growing periods after prenatal stress and *N*-acetyl cysteine administration

Liegelin Kavitha Bernhardt[1], Sampath Madhyastha[2], Lakshminarayana Bairy[3], Anoop Kishore[4]

[1]Department of Physiology, Melaka Manipal Medical College, Manipal University, Manipal, India, [2]Department of Anatomy, Faculty of Medicine, Kuwait University, Kuwait, [3]Department of Pharmacology, Kasturba Medical College, Manipal University, Manipal, India, [4]Department of Pharmacology, MCOPS, Manipal University, Manipal, India

Abstract

Prenatal stress-induced neurobehavioral deficits observed in offspring are multifactorial, including oxidative stress in the developing brain. The time by which the developing brain acquires self-defense against oxidative stress is not clear. Hence in the present study we aimed to evaluate the brain antioxidant status during different developing periods. Further the study also evaluates the role of the glutathione precursor, N-acetyl cysteine (NAC) on the brain antioxidant status. Pregnant rats were subjected to restraint stress during an early or late gestational period. Another set of rats received NAC during the entire gestational period along with early or late gestational stress. The study parameters included several antioxidant studies directly from rat brain homogenate on postnatal day 24 or 48. Early or late gestational stress has caused severe oxidative stress in the developing brain on postnatal day 24 in all the parameters studied. However, brain reduced glutathione (GSH), superoxide dismutase (SOD) and total antioxidant activity (TAO) were not affected by either early or late gestational stress on postnatal day 48, but the brain malondialdehyde (MDA) level remained high and brain glutathione reductase (GSS-Rd) level remained low on postnatal day 48. Prenatal NAC treatment has reversed the oxidative damage in all the parameters on postnatal day 24 and also the brain MDA level and GSS-Rd level on postnatal day 48. This study confirms that the growing brain acquires antioxidant capacity over time but during early postnatal development it is vulnerable to oxidative stress and related neurological consequences. N-acetyl cysteine treatment during the prenatal period as an antioxidant supplement exerted a beneficiary effect in this study. Hence glutathione supplement in the nutritional source would be an idealistic approach to prenatal stress-induced neurological comorbidities in children.

Key words: brain antioxidant system, brain oxidative stress, N-acetyl cysteine, prenatal stress.

Introduction

It is well known that the prenatal stress adversely affects the brain development with neuronal loss and behavioral dysfunction. Among the various mecha- nisms involved in the developmental toxicity, the altered cellular homeostasis by oxidative damage in the developing brain has gained much attention in recent years. The adult brain is known to be well equipped with defense and repair mechanisms to combat

the oxidative stress, but existence of such defensive mechanisms in the developing brain is obscure [14]. Oxidative stress occurs when free radicals are generated more rapidly than they are buffered by the cellular defense mechanisms [4]. Maintenance of a balance between reactive oxygen species (ROS) production and antioxidant defense is very essential for normal development of organisms. Prenatal stress-induced suppression of neuronal proliferation involving brain antioxidant systems was reported by Kawamura *et al.* [16]. Prenatal stress-induced oxidative damage to mitochondrial DNA and damage to hippocampal neurons in neonates is reported by Zhu *et al.* [43]. Hence the cellular damage in the developing brain could be attributed to overproduction of antioxidants.

Administration of an antioxidant which crosses both the placental and blood brain barrier may be helpful in providing the antioxidant defense system in the growing brain. *N*-acetyl cysteine (NAC), a thiol compound having the formula C5H9O3S is a very good source of sulfhydryl (SH) groups that stimulate the reduced glutathione (GSH) synthesis, help detoxification and directly bring about free radical scavenging [44]. Among the various studies conducted on neuroprotective interventions aiming at ameliorating brain injury, only few have been proved safe for clinical use. *N*-acetyl cysteine is one such antioxidant, which is proved to be safe during pregnancy. The efficacy of NAC as a neuroprotector is largely due to its ability to stimulate the reduced GSH synthesis by acting as a cysteine donor [7], cross the blood-brain barrier [12] and boost brain GSH levels during periods of increased oxidative stress [12,19]. Previous studies have demonstrated that NAC has reduced the oxidative stress in rat brains produced by lead exposure [29], limited maternal lipopolysaccharide (LPS) induced oxidative stress and increased lipid peroxidation in the placenta that led to preterm labor [33], prevented birth-linked oxidative stress in neonates, when pre administered to dams [37]. Lante *et al.* [19] found that prenatal exposure to lipopolysaccharide brought about oxidative stress in fetal hippocampus while pretreatment with NAC protected the offspring from impairment of the spatial memory and synaptic plasticity [19]. *N*-acetyl cysteine has been proven to protect the brain against oxidative stress and neurodevelopmental damage associated with prenatal infection [30]. Hence in the present study, NAC, a well-known antioxidant was considered as a therapeutic

strategy to combat the prenatal stress-induced possible oxidative damage in the developing brain.

Material and methods

Animals

Healthy, in-house bred female and male rats of the albino *Wistar* strain (3-4 months of age) were obtained for the study. The rats were maintained in 12 hours light and dark cycle in temperature- and humidity-controlled environment. The rats were fed with standard food pellet and water ad libitum. The polypropylene cage with paddy husk as bedding materials was used for housing the rats. Breeding and maintenance of the animals were done as per the guidelines of the Government of India for use of laboratory animals and also ARRIVE guidelines. The Institutional Animal Ethics Committee approval was obtained before the conduct of the study and care was taken to handle the rats in a humane manner.

Animal breeding

Female rats were allowed to mate with one fertile sexually active male for four hours per day (separate male rats for each group). At the end of four hours, female rats were separated and vaginal smears taken to detect the presence of sperm for the confirmation of pregnancy and the rats were designated as day 0 of pregnancy for further counting the days. The pregnant rats were housed individually in separate cages with a proper label indicating the day of conception and randomly allocated into six groups of eight each. One male and one female pup from each mother (a total of 16 pups in each group) were considered for antioxidant studies.

Induction of prenatal stress

The pregnant rats were stressed (restraint stress) using a wire mesh restrainer [24] three times daily for 45 min. The wire mesh restrainer had a wooden base and stainless steel wire mesh restrainer hinged to the base. A pad lock and latch helped to secure the rat in the restrainer. The restrainer with dimensions of 11 cm (L) × 6 cm (B) × 6 cm (H) was used for rats with gestation day 1 to 10. The restrainer of 11 cm (L) × 8 cm (B) × 8 cm (H) was used for rats with gestation day 11 to till delivery. This type of restrainer will only restrict the animal movement without any pain, discomfort or suffocation.

Liegelin Kavitha Bernhardt, Sampath Madhyastha, Lakshminarayana Bairy, Anoop Kishore

Animal groups and treatment

Group 1 (Control): The pups belonging to the pregnant rats who received only normal saline in a dose of 10 ml/kg body weight (intraperitoneal) throughout pregnancy.

Group 2 (NAC): The pups belonging to the pregnant rats who received NAC alone in a dose of 10 mg/kg body weight (i.p.) throughout pregnancy.

Group 3 (EGS): The pups belonging to the pregnant rats who received restrain stress from gestation day 1 to 10 and normal saline throughout pregnancy.

Group 4 (LGS): The pups belonging to the pregnant rats who received restrain stress from gestation day 11 to delivery and normal saline throughout pregnancy.

Group 5 (EGS+NAC): The pups belonging to the pregnant rats who received restrain stress from gestation day 1 to 10 and NAC (10 mg/kg body weight, i.p.) throughout pregnancy.

Group 6 (LGS+NAC): The pups belonging to the pregnant rats who received restrain stress from gestation day 11 to delivery and NAC (10 mg/kg body weight, i.p.) throughout pregnancy.

All the mothers delivered at term (21-24th day of gestation). The offspring of the all groups were raised by their biological mothers until weaning (21st day after birth).

N-acetyl cysteine treatment

The dose of NAC was selected based on an earlier study by Basyigit et al. [1] where a 10 mg/kg dose (i.p.) was given continuously for 14 days to pregnant rats. The acute oral toxicity of NAC is low e.g. LD 50 > 10,000 mg/kg body weight in adult rats. In rats administered with 250 mg NAC/kg body weight per day for 20 weeks, all NAC-related effects observed are marginal. Hence in the present study, a 10 mg/kg dose of NAC dissolved in physiological saline was administered intraperitoneally.

For the present study, one male and one female pup from each mother were selected randomly. Pups were divided into two groups: the first group was sacrificed on postnatal day 24 (PND 24) and the other group was sacrificed on postnatal day 48 (PND 48) for antioxidant estimations; to assess both short- and long-term effects of prenatal stress.

We aimed at investigating the effect of prenatal stress during two important phases of life, which are childhood and adolescence. PND 24 in rats appears to correspond to the childhood period in humans.

This is the time period in rats when structural maturation of the brain takes place. A plateau in the volume of most brain structures has been found to occur during this period. PND 48 was selected so as to investigate whether the effects of early and late gestational stress last until the adolescent/early adult period. Many adolescent specific neurobehavioral alterations observed in humans are also seen in rats of comparable age. Adolescence is an age period around the time of sexual maturation when age-specific behavioral and psychopharmacological discontinuities are evident.

Estimation of oxidative stress in brain

Preparation of brain homogenate: Pups were weighed and sacrificed by decapitation after ether anesthesia. The whole brain was removed rapidly and rinsed with 0.1 M/l saline phosphate buffer (pH 7.4). Tissue was weighed and homogenized (1 : 10 w/v) in 0.1 M/l saline phosphate buffer. The homogenate was centrifuged at 10 000 g for 20 min at 4°C and aliquots of supernatant were separated and used for following biochemical estimations.

Estimation of total antioxidants: Brain total antioxidant capacity was assayed according to the method of Koracevic et al. [17]. The method is based on determination of the ability to eliminate added hydrogen peroxide. The remaining H_2O_2 is determined calorimetrically by an enzymatic reaction converting 3, 5-dichloro-2-hydroxyl benzenesulfonate to a colored product that is measured at 532 nm.

Estimation of superoxide dismutase activity: Superoxide dismutase (SOD) activity was determined by the method of Marklund et al. [25]. The reaction was performed in an mixture containing 5.6×10^{-5} M nitro blue tetrazolium (NBT), 1.17×10^{-6} M riboflavin, 1×10^{-2} M methionine in 0.05 M potassium phosphate buffer, pH 7.8 with suitably diluted tissue homogenate in a total volume of 3 ml. Illumination of the solution was carried out in an aluminum lined foil box fitted with a 15v fluorescent lamp. The solution taken in a beaker was kept in the box and illuminated exactly for 10 min. The control without the enzyme source was prepared. The absorbance was measured spectrophotometrically with a Systronic-117 UV-Visible spectrophotometer at 560 nm. SOD activity was expressed as specific activity of the enzyme in units per mg protein (U/mg protein). Protein content was determined by the method of Lowry et al. [21].

Estimation of reduced glutathione: Glutathione in the brain was estimated according to the method described by Ellman [10]. 1 ml supernatant was precipitated with 1 ml of 4% sulfosalicylic acid and cold digested at 41°C for 1 hour. The samples were centrifuged at 1200 g for 15 min at 41°C. To 1 ml of this supernatant, 2.7 ml of phosphate buffer (0.1 mol/l, pH 8) and 0.2 ml of 5, 50-dithio-bis (2-nitrobenzoic acid) were added. The yellow color developed was read immediately at 412 nm by using the UV-1700 spectrophotometer, Shimadzu, Japan. Results were calculated using a molar extinction coefficient of chromophore (1.36×10^4/mol/l/cm) and expressed as nmol per mg protein.

Estimation of glutathione reductase: The GSSG-Rd activity was measured using the method originally described by Moron et al. [27]. The reaction mixture consisted of 1.6 ml of 0.067 M potassium phosphate buffer (pH 6.6), 0.12 ml of 0.06% NADPH, 0.12 ml 1.15% GSSG, 0.1 ml of enzyme source and water in a final volume of 2 ml. All mixtures and solutions were prepared at room temperature. Control cuvettes then received 180 µl of deionized water while sample cuvettes received 60 µl of deionized water and 120 µl of GSSG solution. NADPH oxidation was followed for 5 min and was recorded using a Systronic-117 spectrophotometer. The reduction of GSSG to GSH was determined indirectly by the measurement of the consumption of NADPH, as demonstrated by a decrease in absorbance at 340 nm as a function of time. The enzyme activity was calculated using the extinction coefficient of chromophore (1.36×10^4 (mol/l)$^{-1}$ cm^{-1}) and expressed as nmol NADPH oxidized/min/mg protein. Protein content was determined by the method of Lowry et al. [21] with bovine serum albumin as standard.

Estimation of lipid peroxidation: Measurement of lipid peroxidation was done by the method described by Ohkawa et al. [31]. Tissue lipid peroxidation was measured in whole-brain homogenate for 30 min at 37°C. The incubation was interrupted by adding

Table I. Brain oxidant/antioxidant levels in rat brain at PND 24 and PND 48

		Brain oxidant/antioxidants (PND 24)								
		Total antioxidants (mmol/l)		Superoxide dismutase (U/mg protein)		Reduced glutathione (mg/gm brain tissue)		Glutathione reductase (nmol NADPH oxidized/ min/mg protein)		Lipid peroxidation (ng/gm)	
CON	Male (n = 4)	1.97 ± 0.60	p = 0.83 t = 0.22	1.72 ± 0.25	p = 0.46 t = 0.82	2.52 ± 0.50	p = 0.60 t = 0.57	5.75 ± 0.70	p = 0.12 t = 2.13	6.80 ± 0.80	p = 0.33 t = 1.14
	Female (n = 4)	0.81 ± 0.08		2.25 ± 0.23		2.35 ± 0.70		6.90 ± 0.70		7.40 ± 0.30	
NAC	Male (n = 4)	1.75 ± 0.60	p = 0.90 t = 0.12	1.65 ± 0.19	p = 0.54 t = 0.67	2.52 ± 0.90	p = 0.60 t = 0.57	5.81 ± 0.90	p = 0.29 t = 1.27	7.37 ± 0.40	p = 0.80 t = 0.14
	Female (n = 4)	1.82 ± 0.80		1.99 ± 0.35		2.11 ± 0.90		7.29 ± 1.50		7.25 ± 1.40	
EGS	Male (n = 4)	0.72 ± 0.30	p = 0.31 t = 1.21	0.90 ± 0.59	p = 0.96 t = 0.53	1.29 ± 0.72	p = 0.94 t = 0.07	3.85 ± 0.70	p = 0.71 t = 0.40	8.70 ± 1.01	p = 0.58 t = 0.61
	Female (n = 4)	0.60 ± 0.10		0.87 ± 0.57		1.34 ± 0.60		4.21 ± 1.50		9.15 ± 1.10	
LGS	Male (n = 4)	0.85 ± 0.40	p = 0.62 t = 0.54	0.45 ± 0.69	p = 0.48 t = 0.80	0.96 ± 0.25	p = 0.91 t = 0.11	4.45 ± 0.70	p = 0.43 t = 0.91	8.25 ± 1.18	p = 0.06 t = 2.77
	Female (n = 4)	0.62 ± 0.40		0.83 ± 0.56		1.39 ± 0.49		3.96 ± 0.15		10.50 ± 1.30	
EGS+ NAC	Male (n = 4)	1.70 ± 0.70	p = 0.82 t = 0.24	2.25 ± 1.10	p = 0.30 t = 1.00	2.58 ± 0.57	p = 0.62 t = 0.54	5.88 ± 2.10	p = 0.71 t = 0.40	7.27 ± 0.70	p = 0.66 t = 0.47
	Female (n = 4)	1.80 ± 0.80		1.67 ± 0.23		2.30 ± 0.61		6.19 ± 0.90		7.05 ± 0.20	
LGS+ NAC	Male (n = 4)	1.82 ± 1.21	p = 0.85 t = 0.19	1.70 ± 0.70	p = 0.39 t = 0.98	2.68 ± 0.70	p = 0.28 t = 1.29	5.00 ± 0.60	p = 0.05 t = 3.07	7.45 ± 0.90	p = 0.48 t = 0.80
	Female (n = 4)	1.95 ± 0.88		2.20 ± 0.50		2.01 ± 0.40		7.50 ± 1.00		7.70 ± 1.27	

Table I. Cont.

		Brain oxidant/antioxidants (PND 48)									
		Total antioxidants (mmol/l)		Superoxide dismutase (U/mg protein)		Reduced glutathione (mg/gm brain tissue)		Glutathione reductase (nmol NADPH oxidized/min/mg protein)		Lipid peroxidation (ng/gm)	
CON	Male ($n = 4$)	2.95 ± 0.80	$p = 0.46$ $t = 0.82$	3.80 ± 1.10	$p = 0.81$ $t = 0.24$	3.87 ± 0.70	$p = 0.20$ $t = 1.60$	7.05 ± 1.70	$p = 0.64$ $t = 0.50$	4.07 ± 1.00	$p = 0.45$ $t = 0.86$
	Female ($n = 4$)	2.52 ± 0.70		3.60 ± 1.80		2.92 ± 0.40		6.49 ± 1.40		4.92 ± 2.10	
NAC	Male ($n = 4$)	2.28 ± 1.70	$p = 0.06$ $t = 1.40$	2.67 ± 0.50	$p = 0.21$ $t = 1.56$	2.65 ± 0.40	$p = 0.25$ $t = 1.40$	7.78 ± 2.80	$p = 0.47$ $t = 0.82$	4.80 ± 1.30	$p = 0.64$ $t = 0.51$
	Female ($n = 4$)	2.82 ± 1.40		4.36 ± 1.60		3.20 ± 0.90		6.06 ± 2.00		4.25 ± 1.05	
EGS	Male ($n = 4$)	2.48 ± 1.30	$p = 0.27$ $t = 1.32$	3.00 ± 1.71	$p = 0.91$ $t = 0.11$	2.36 ± 0.80	$p = 0.54$ $t = 0.68$	4.70 ± 1.80	$p = 0.82$ $t = 0.24$	6.72 ± 1.20	$p = 0.98$ $t = 0.02$
	Female ($n = 4$)	1.50 ± 0.90		3.08 ± 2.24		2.83 ± 0.90		5.00 ± 0.90		6.75 ± 1.20	
LGS	Male ($n = 4$)	1.47 ± 1.00	$p = 0.50$ $t = 0.74$	3.02 ± 2.08	$p = 0.35$ $t = 1.10$	2.97 ± 0.54	$p = 0.96$ $t = 0.04$	6.06 ± 2.50	$p = 0.24$ $t = 1.42$	7.10 ± 1.90	$p = 0.52$ $t = 2.71$
	Female ($n = 4$)	1.90 ± 0.50		1.96 ± 0.30		2.99 ± 0.84		3.70 ± 0.70		6.40 ± 0.50	
EGS+NAC	Male ($n = 4$)	1.90 ± 0.50	$p = 0.28$ $t = 1.31$	3.67 ± 2.00	$p = 0.88$ $t = 0.15$	3.08 ± 0.93	$p = 0.55$ $t = 0.67$	7.15 ± 2.40	$p = 0.49$ $t = 0.76$	4.25 ± 1.60	$p = 0.47$ $t = 0.80$
	Female ($n = 4$)	2.14 ± 1.51		3.59 ± 1.40		2.70 ± 0.34		6.16 ± 1.60		4.92 ± 0.90	
LGS+NAC	Male ($n = 4$)	3.35 ± 1.70	$p = 0.25$ $t = 1.40$	3.50 ± 0.60	$p = 0.90$ $t = 0.12$	3.31 ± 0.70	$p = 0.68$ $t = 0.45$	4.20 ± 1.14	$p = 0.67$ $t = 0.45$	4.20 ± 1.10	$p = 0.67$ $t = 0.45$
	Female ($n = 4$)	2.32 ± 1.10		3.40 ± 0.60		3.12 ± 0.92		4.80 ± 1.08		4.80 ± 1.80	

0.1 ml of 10% trichloroacetic acid. After centrifugation (1 ml) supernatant was then mixed with 1 ml of 0.65% thiobarbituric acid. The mixture was then kept in a boiling water bath for 15 min. The malondialdehyde formation was determined by reading absorbance at 535 nm. The amount of TBARS was calculated using a molar extinction coefficient of 1.56×10^5 $(M)^{-1}\,cm^{-1}$.

Statistical analysis

All results represent mean ± S.E.M. The significance of differences among the groups was assessed using the one way analysis of variance (ANOVA) test followed by Bonferroni's multiple comparison test. Comparison of data between male and female groups was assessed by unpaired t test. P values < 0.05 were considered significant.

Results

Brain antioxidant levels: There was no sexually dimorphic effect in all the parameters studied, hence mean values for both male and female rats were combined.

Prenatal stress-induced declined total antioxidant capacity (TAO) is reversed by NAC

Effect of prenatal stress and NAC on total antioxidant capacity at PND 24

A significant ($p < 0.05$) decrease in TAO was observed in the early gestational stress group when compared to the control group. Pups exposed to early gestational stress, treated with NAC (group 5) showed an increase ($p < 0.05$) in TAO when compared to the group that received early gestational stress alone. Total antioxidant capacity significantly decreased in group 4 ($p < 0.05$) whereas in group 6, there was a significant elevation of TAO in brain homogenate. There was no significant difference in the level of TAO in the group that received only NAC when compared to the control group (Fig. 1).

Effect of prenatal stress and NAC on total antioxidant capacity at PND 48

Total antioxidant capacity levels did not significantly differ between any of the comparisons (Fig. 1).

Comparison of total antioxidant capacity between PND24 and PND48

Total antioxidant capacity was seen to have significantly increased in group 3 ($p < 0.01$) and group 4 ($p < 0.01$), but did not show any elevation in group 1, 2, 5 and 6 at PND 48 when compared to PND 24.

Prenatal stress-induced declined SOD activity is reversed by NAC

Effect of prenatal stress and NAC on concentration of SOD at postnatal day 24 (PND 24)

There was a significant decrease ($p < 0.05$) in the level of SOD in offspring who received early ges-

tational stress (group 3) and also late gestational stress ($p < 0.01$) but group 5 ($p < 0.05$) and group 6 ($p < 0.01$) pups showed significantly elevated SOD levels when compared with those of group 3 and group 4, respectively. No significant difference was seen in the SOD level in the group that received NAC alone when compared to control animals (Fig. 2).

Effect of prenatal stress and NAC on concentration of SOD at PND 48

Superoxide dismutase activity was not seen to differ significantly between any of the groups (Fig. 2).

Comparison of the SOD level between PND24 and PND48

There was significant increase in brain SOD levels in all groups at PND 48 (group 1 [p < 0.01], group 2 [p < 0.05], group 3 [p < 0.01], group 4 [p < 0.01], group 5 [p < 0.01]) with respect to its levels at postnatal day 24.

Prenatal stress-induced declined reduced GSH activity is reversed by NAC

Effect of prenatal stress and NAC on concentration of reduced glutathione at PND 24

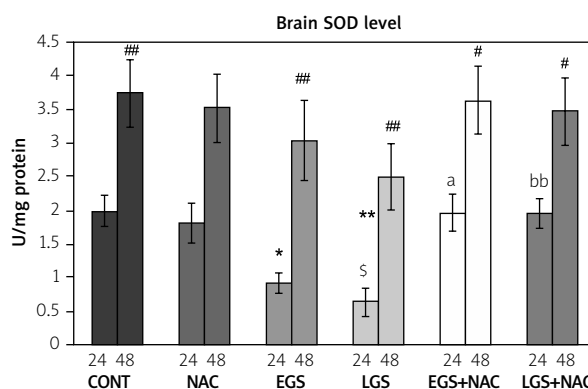Prenatal stress during early gestation (group 3) caused a significant ($p < 0.05$) depletion of the reduc-

Fig. 1. Effect of prenatal stress and *N*-acetyl cysteine (NAC) on brain TAO capacity in 24- and 48-day-old offspring. Abbreviations – CONT: control, EGS: rats received prenatal stress from gestation day 1 to 10, EGS+NAC: rats received stress from gestation day 1 to 10 along with *N* acetyl cysteine during the entire gestation period, LGS: rats received prenatal stress from gestation day 11 until delivery, LGS+NAC: rats received stress from gestation day 11 to delivery along with *N* acetyl cysteine during the entire gestation period, NAC: rats received *N* acetyl cysteine for the entire gestation period. One way ANOVA, Bonferroni's test – CON vs. EGS& LGS, *$p < 0.05$; EGS vs. EGS+NAC, $^{a}p < 0.05$; LGS vs. LGS+NAC, $^{b}p < 0.05$; PND 24 vs. PND 48, $^{##}p < 0.01$.

Fig. 2. Effect of prenatal stress and *N*-acetyl cysteine (NAC) on brain SOD activity in 24- and 48-day-old offspring. Abbreviations – see Fig. 1. One way ANOVA, Bonferroni's test – CON vs. EGS & LGS, *$p < 0.05$, **$p < 0.01$; EGS vs. EGS+NAC, $^{a}p < 0.05$; LGS vs. LGS+NAC, $^{bb}p < 0.01$; NAC vs. LGS, $^{\$}p < 0.05$; PND 24 vs. PND 48, $^{#}p < 0.05$, $^{##}p < 0.01$.

ed glutathione (GSH) level in the brain compared to controls (group 1). Offspring who received early gestational stress and NAC treatment (group 5) showed a significant ($p < 0.05$) increase in the GSH level when compared to offspring of group 3. There was a significant ($p < 0.01$) depletion of GSH concentration in the LGS group but offspring who received late gestational stress and NAC treatment (group 6) showed a significant ($p < 0.01$) increase in the GSH level when compared to offspring who received late prenatal stress. There was no significant difference in the level of GSH in the group that received only NAC when compared to the control group (Fig. 3).

Effect of prenatal stress and NAC on concentration of reduced glutathione at postnatal day 48 (PND 48)

The activity of brain GSSG-Rd did not show a statistically significant difference between any of the groups (Fig. 3).

Comparison of a reduced glutathione concentration between PND24 and PND48

Glutathione levels were significantly increased in group 1 ($p < 0.05$), group 3 ($p < 0.01$), group 4 ($p < 0.001$) and group 6 ($p < 0.05$) at postnatal day 48 in comparison with GSH levels at PND 24.
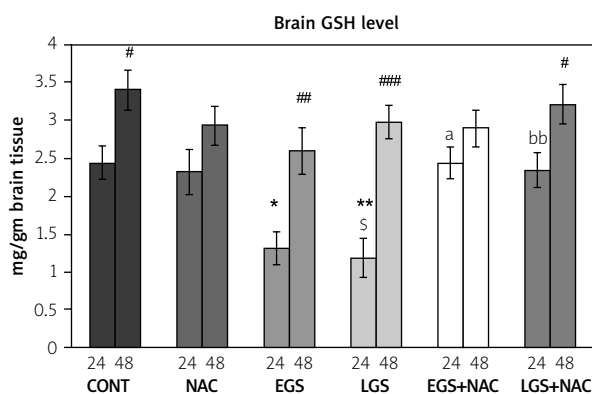
Prenatal stress-induced decline in glutathione reductase (GSHRd) is reversed by NAC

Effect of prenatal stress and NAC on activity of glutathione reductase at PND 24

The activity of glutathione reductase in the brain homogenate of different groups is summarized in Figure 4. GSHRd was significantly ($p < 0.05$) reduced in the offspring that belonged to the early gestational stress group when compared to controls. EGS offspring treated with prenatal NAC showed an elevation in GSSG-Rd, which was quite significant ($p < 0.05$) when compared to the early gestational stress group. It was seen that late gestational stress also significantly ($p < 0.05$) lowered the activity of reduced glutathione in comparison with control pups, whereas this activity was restored in the LGS+NAC group. No significant difference was seen in the GSHRd level in the group that received NAC alone when compared to control animals.

Effect of prenatal stress and NAC on activity of glutathione reductase at PND 48

The activity of brain GSSG-Rd did not show a statistically significant difference between any of the groups (Fig. 4).
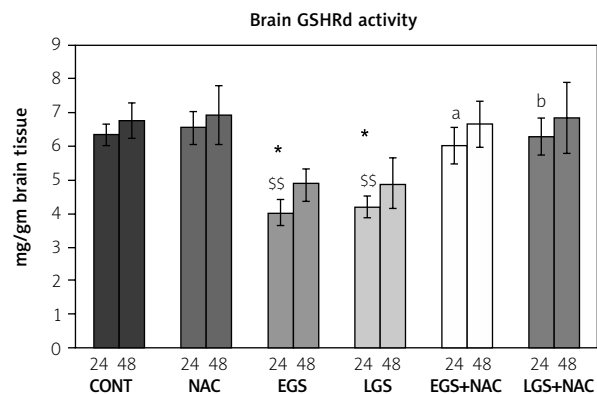

Fig. 3. Effect of prenatal stress and *N*-acetyl cysteine (NAC) on the brain reduced glutathione level in 24- and 48-day-old offspring. Abbreviations – see Fig. 1. One way ANOVA, Tukey-Kramer Multiple Comparisons Test – CON vs. EGS & LGS, *$p < 0.05$, **$p < 0.01$; EGS vs. EGS+NAC, a$p < 0.05$; LGS vs. LGS+NAC, bb$p < 0.01$; NAC vs. LGS, $p < 0.05$; PND 48 vs. PND 24, #$p < 0.05$, ##$p < 0.01$, ###$p < 0.001$.

Fig. 4. Effect of prenatal stress and *N*-acetyl cysteine (NAC) on brain glutathione reductase activity in 24- and 48-day-old offspring. Abbreviations – see Fig. 1. One way ANOVA, Tukey-Kramer Multiple Comparisons Test – CON vs. EGS & LGS, *$p < 0.05$; EGS vs. EGS+NAC, a$p < 0.05$; LGS vs. LGS+NAC, b$p < 0.05$; NAC vs. EGS&LGS, $p < 0.05$, $$p < 0.01$.

Comparison of glutathione reductase activity between PND24 and PND48

As shown in Figure 4, no significant change in brain GSH Rd activity was observed in any of the groups at PND 48, when compared to its levels at PND 24.

Prenatal stress-induced elevated lipid peroxidation is reversed by NAC

Effect of prenatal stress and NAC on lipid peroxidation at postnatal day 24 (PND 24)

The malondialdehyde (MDA) level is a marker of lipid peroxidation. Early gestational stress significantly ($p < 0.05$) increased brain lipid peroxidation in comparison with the control group. A significant ($p < 0.05$) reduction in lipid peroxidation was observed in the early gestational stress group which received NAC (group 5) when compared to group 3. Brain lipid peroxidation was also markedly ($p < 0.001$) increased in the late gestational stress group (group 4) when compared to that of the control group. There was a significant ($p < 0.05$) decrease in the MDA level in the LGS+NAC group as compared with the LGS group. There was no significant difference in the level of MDA in the group that received only NAC when compared to the control group (Fig. 5).

Effect of prenatal stress and NAC on lipid peroxidation at postnatal day 48 (PND 48)

As summarized in Figure 5, a significant ($p < 0.05$) elevation of lipid peroxidation activity in the brain homogenate was observed in the EGS group in comparison with the control group. EGS+NAC showed a significant ($p < 0.05$) decrease in lipid peroxidation when compared to EGS. The MDA level was also elevated significantly ($p < 0.05$) in LGS, whereas in LGS+NAC, a significant ($p < 0.05$) depletion in the MDA level was observed.

Comparison of lipid peroxidation between PND24 and PND48

There was a very significant reduction in brain MDA levels measured at PND 48, in the control group (group 1) ($p < 0.001$), group 3 ($p < 0.001$), group 4 ($p < 0.0001$), group 5 ($p < 0.04$) and group 6 ($p < 0.0002$) when compared to MDA levels measured at PND 24.

Discussion

Oxidative stress has been recognized as one of the earliest factors causing neurodegeneration [3] as
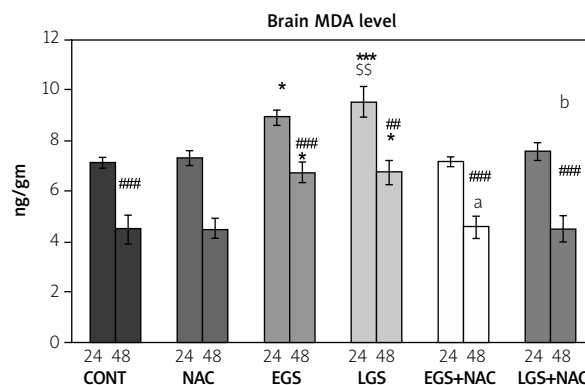

Fig. 5. Effect of prenatal stress and *N*-acetyl cysteine (NAC) on brain lipid peroxidation (MDA level) in 24- and 48-day-old offspring. For all the parameters and legends, data are expressed as mean ± SEM, $n = 8$, and animal groups are abbreviated as in Fig. 1. One way ANOVA, Tukey-Kramer Multiple Comparisons Test – CON vs. EGS&LGS, *$p < 0.05$, ***$p < 0.001$; EGS vs. EGS+NAC, a$p < 0.05$; LGS vs. LGS+NAC, b$p < 0.05$; NAC vs. LGS, SS$p < 0.01$; PND 48 vs. PND 24, ##$p < 0.01$, ###$p < 0.001$.

brain is relatively more vulnerable to oxidative damage due to high levels of oxidizable polyunsaturated fatty acid and redox-active metals, but lower levels of antioxidant molecules [9]. It has previously been shown that oxidative damage produced by prenatal restrain stress resulted in neuronal loss in rat offspring [22C]. Exposure to early as well as late gestational stress brought about brain oxidative damage where decline in SOD, GSH and GSSG-Rd activities [23,39], increase in lipid peroxidation and decrease in total antioxidant capacity were observed [22]. An increase in the content of reactive oxygen species in the hippocampus of prenatally stressed rat offspring was reported by Li *et al.* [20]. In agreement with these studies, we found that early as well as late prenatal stress resulted in brain oxidative stress in 24-day-old offspring as indicated by a decrease in levels of total antioxidants, SOD, GSH and GSH-Rd, as well as an increase in lipid peroxidation. These findings reveal suppressed efficiency of antioxidants to combat the prenatal stress induced ROS in the developing brain.

Super oxide dismutases that form a very important component of antioxidant defenses are a class of metalloenzymes that catalyze dismutation of the superoxide radical into oxygen and H_2O_2 [13]. Our data indicated that prenatal stress has resulted in

significant inhibition of SOD and glutathione reductase activities. This reduction could be a result of increased ROS generation and enhanced lipid peroxidation [5].

Glutathione is required for detoxification of ROS in brain cells [8]. The decrease in GSH concentrations we observed in this study could be due to its increased rate of utilization caused by oxidative stress [36]. Increased levels of free radicals bring about more reduced glutathione (GSH) to convert to its oxidized form (GSSG) [32]. It could also be due to a decreased activity of the enzyme glutathione reductase [6] that is required to restore the GSH level.

Lipid peroxidation is considered as a major source of oxidative damage by stress. The brain being rich in polyunsaturated lipids, and having an elevated rate of oxygen consumption, is highly susceptible to peroxidation by oxygen free radicals [35,15]. Malondialdehyde, a marker of lipid peroxidation, is very reactive and plays a role in cross-linking with DNA and proteins, resulting in mitochondrial dysfunction and cell damage [11]. In the present study, early as well as late prenatal stress has brought about a significant elevation in MDA levels, in 24-day-old offspring, as a possible consequence of decreased antioxidant enzyme activities.

The results of our study demonstrated that prenatal NAC treatment enhanced the activity of the antioxidant defense system in the offspring who received prenatal stress during early as well as late gestation. It prevented the decrease in GSH, GSSG-Rd, SOD and total antioxidant levels and increase in lipid peroxidation in the brain of prenatally stressed offspring, thus proving its neuroprotective role against oxidative damage.

In the present work, we also evaluated the levels of total antioxidant capacity, SOD, GSH, GSSG-Rd and MDA at PND 48 to investigate the long-term effects of early and late gestational stress on the brain antioxidant system; PND 48 in rats corresponds to the early adult period in human subjects. Interestingly, however not expected result suggestive of brain oxidative damage was detected except for a small but significant increase in MDA levels. This shows the possibility of recovery of the brain from gestational stress-induced oxidative damage when the rats reached the early adult stage. Not many studies, to the best of our knowledge, have investigated the long-term effect of gestational restrain stress on oxidative damage in rat whole brain homogenate, although several animal

and human studies have proved long-term effects of different kinds of stress during pregnancy in terms of behavior, physiology, and immunity of the offspring [41,42]. In several studies where long-term effects of prenatal stress were investigated, younger offspring showed higher emotionality levels when compared to older ones [40], higher anxiety and lower locomotion at 1 month, but not at 4 months [2], decrease in dendritic spines in pyramidal neurons of offspring at PND 23 in a study by Murmu *et al.* [28], although no such decrease at PND 100 in response to a similar kind of a repeated prenatal stressor as reported by Michelson *et al.* [26]. In a study by Kraszpulski *et al.*, the decrease in volumes and cell numbers in amygdala resolved after PND 45 [18]. Based on these data and the result of our present study, the response of the offspring brain to prenatal stress appears to at times be short lived and the brain seems to recover from this transient stress effect. Such variation in responses may occur depending on the type, duration, intensity of stress and different strains of animal species. We also compared the brain oxidative status of individual groups between 2 ages where we observed a significant increase in total antioxidant capacity, SOD, GSH, and fall in lipid peroxidation, in all groups at PND 48 when compared to their levels at PND 24. This shows that brain oxidative defense improves with age at early development periods. However oxidative stress during early postnatal development is sufficient enough to adversely affect the neurobehavioral development.

Conclusions

In summary, the present study demonstrated that both early and late gestational stress showed oxidative stress in the developing brain during early postnatal development and this effect did not last until postnatal day 48, which suggests that oxidative stress may be transient and last for a short period of postnatal development. Our data suggest that maternal administration of NAC effectively prevented prenatal stress-induced oxidative changes in the developing brain of the offspring exposed to prenatal stress. Based on the results of this study, we assume that the NAC can be beneficial for preventing the brain oxidative damage and cognitive dysfunction associated with prenatal stress, hence an ideal candidate for clinical trials.

Disclosure

Authors report no conflict of interest.

References

1. Basyigit I, Tugay M, Dilioglugil MO, Yildiz F, Maral H, Sozubir S. Protective effects of N-acetylcysteine on peroxidative changes of the fetal rat lungs whose mothers were exposed to cigarette smoke. Hum Exp Toxicol 2007; 26: 99-103.
2. Batuev AS, Vinogradova EP, Polyakova ON. The effect of prenatal stress on rat offspring anxiety. Zh Vyssh Nerv Deiat Im I P Pavlova 1996; 46: 558-563.
3. Beal MF. Does impairment of energy metabolism result in excitotoxic neuronal death in neurodegenerative illnesses? Ann Neurol 1992; 31: 119-130.
4. Burton GJ, Jauniaux E. Oxidative stress. Best Pract Res Clin Obstet Gynaecol 2011; 25: 287-299.
5. Chaudiere J, Ferrari-Iliou R. Intracellular antioxidants: from chemical to biochemical mechanisms. Food Chem Toxicol 1999; 37: 949-962.
6. Costagliola C. Oxidative state of glutathione in red blood cells and plasma of diabetic patients: in vivo and in vitro study. Clin Physiol Biochem 1989; 8: 204-210.
7. Dringen R, Hamprecht B. N-acetylcysteine, but not methionine or 2-oxothiazolidine-4-carboxylate, serves as cysteine donor for the synthesis of glutathione in cultured neurons derived from embryonal rat brain. Neurosci Lett 1999; 259: 79-82.
8. Dringen R, Hirrlinger J. Glutathione pathways in the brain. Biol Chem 2003; 384: 505-516.
9. Driver AS, Kodavanti PRS, Mundy WR. Age-related changes in reactive oxygen species production in rat brain homogenates. Neurotoxicol Teratol 2000; 22: 175-181.
10. Ellman GL. Tissue sulfhydryl groups. Arch Biochem Biophys 1959; 82: 70-77.
11. Esterbauer H. Cytotoxicity and genotoxicity of lipid-oxidation products. Am J Clin Nutr 1993; 57: 779S-785S.
12. Farr SA, Poon HF, Dogrukol-Ak D, Drake J, Banks WA, Eyerman E, Butterfield DA, Morley JE. The antioxidants α-lipoic acid and N-acetylcysteine reverse memory impairment and brain oxidative stress in aged SAMP8 mice. J Neurochem 2003; 84: 1173-1183.
13. Fridovich I. Superoxide radical and superoxide dismutases. Annu Rev Biochem 1995; 64: 97-112.
14. Garnier Y, Coumans ABC, Jensen A, Hasaart THM, Berger R. Infection-related perinatal brain injury: the pathogenic role of impaired fetal cardiovascular control. J Soc Gynecol Investig 2003; 10: 450-459.
15. Halliwell B. Role of free radicals in the neurodegenerative diseases. Drugs Aging 2001; 18: 685-716.
16. Kawamura T, Chen J, Takahashi T, Ichitani Y, Nakahara D. Prenatal stress suppresses cell proliferation in the early developing brain. Neuroreport 2006; 17: 1515-1518.
17. Koracevic D, Koracevic G, Djordjevic V, Andrejevic S, Cosic V. Method for the measurement of antioxidant activity in human fluids. J Clin Pathol 2001; 54: 356-361.
18. Kraszpulski M, Dickerson PA, Salm AK. Prenatal stress affects the developmental trajectory of the rat amygdala. Stress 2006; 9: 85-95.
19. Lante F, Meunier J, Guiramand J, De Jesus Ferreira M-Cl, Cambonie G, Aimar R, Cohen-Solal C, Maurice T, Vignes M, Barbanel Gr. Late N-acetylcysteine treatment prevents the deficits induced in the offspring of dams exposed to an immune stress during gestation. Hippocampus 2008; 18: 602-609.
20. Li H, Li X, Jia N, Cai Q, Bai Z, Chen R, Song T, Zhu Z, Liu J. NF-kappa B regulates prenatal stress-induced cognitive impairment in offspring rats. Behav Neurosci 2008; 122: 331-339.
21. Lowry OH, Rosebrough NJ, Farr AL, Randall RJ. Protein measurement with the Folin phenol reagent. J Biol Chem 1951; 193: 265-275.
22. Madhyastha S, Sahu SS, Rao G. Resveratrol for prenatal-stress-induced oxidative damage in growing brain and its consequences on survival of neurons. J Basic Clin Physiol Pharmacol 2014; 25: 63-72.
23. Madhyastha S, Sahu SS, Rao GM. Prenatal stress-induced cognitive impairment and neuronal oxidative stress and its amelioration by resveratrol in neonate rats. Res J Pharm Biol Chem Sci 2012; 3: 1387-1399.
24. Madhyastha SK, Prabhu LV, Nayak S, Rai R, Pai MM, Madhyastha PS. Effect of Prenatal stress and serotonin depletion on postnatal serotonin metabolism in Wistar rats. Iranian J Pharmacol Ther 2008; 7: 71-77.
25. Marklund S, Marklund G. Involvement of the superoxide anion radical in the autoxidation of pyrogallol and a convenient assay for superoxide dismutase. Eur J Biochem 1974; 47: 469-474.
26. Michelsen KA, van den Hove DlLA, Schmitz C, Segers O, Prickaerts J, Steinbusch HWM. Prenatal stress and subsequent exposure to chronic mild stress influence dendritic spine density and morphology in the rat medial prefrontal cortex. BMC Neurosci 2007; 8: 107.
27. Moron MS, Depierre JW, Mannervik B. Levels of glutathione, glutathione reductase and glutathione- S-transferase activities in rat lung and liver. Biochim Biophys Acta 1979; 582: 67-78.
28. Murmu MS, Salomon S, Biala Y, Weinstock M, Braun K, Bock Jr. Changes of spine density and dendritic complexity in the prefrontal cortex in offspring of mothers exposed to stress during pregnancy. Eur J Neurosci 2006; 24: 1477-1487.
29. Nehru B, Kanwar S. N-acetylcysteine exposure on lead-induced lipid peroxidative damage and oxidative defense system in brain regions of rats. Biol Trace Elem Res 2004; 101: 257-264.
30. Novais ARB, Guiramand J, Cohen-Solal C, Crouzin N, de Jesus Ferreira MC, Vignes M, Barbanel G, Cambonie G. N-acetyl-cysteine prevents pyramidal cell disarray and reelin-immunoreactive neuron deficiency in CA3 after prenatal immune challenge in rats. Pediatr Res 2013; 73: 750-755.
31. Ohkawa H, Ohishi N, Yagi K. Assay for lipid peroxides in animal tissues by thiobarbituric acid reaction. Anal Biochem 1979; 95: 351-358.
32. Ou P, Nourooz-Zadeh J, Tritschler H-J, Wolff S. Activation of aldose reductase in rat lens and metal-ion chelation by aldose reductase inhibitors and lipoic acid. Free Radic Res 1996; 25: 337-346.
33. Paintlia MK, Paintlia AS, Barbosa E, Singh I, Singh AK. N-acetylcysteine prevents endotoxin-induced degeneration of oligodendrocyte progenitors and hypomyelination in developing rat brain. J Neurosci Res 2004; 78: 347-361.

34. Rauchova H, Vokurkova M, Koudelova J. Hypoxia-induced lipid peroxidation in the brain during postnatal ontogenesis. Physiol Res 2012; 61: S89.

35. Rehncrona S, Mela L, Siesj BK. Recovery of brain mitochondrial function in the rat after complete and incomplete cerebral ischemia. Stroke 1979; 10: 437-446.

36. Sahin E, Gümüşlü S. Alterations in brain antioxidant status, protein oxidation and lipid peroxidation in response to different stress models. Behav Brain Res 2004; 155: 241-248.

37. Sastre J, Asensi M, Rodrigo F, Pallardo F, Vento M, Vina J. Antioxidant administration to the mother prevents oxidative stress associated with birth in the neonatal rat. Life Sci 1994; 54: 2055-2059.

38. Semple BD, Blomgren K, Gimlin K, Ferriero DM, Noble-Haeusslein LJ. Brain development in rodents and humans: Identifying benchmarks of maturation and vulnerability to injury across species. Prog Neurobiol 2013; 106: 1-16.

39. Sudhanshu Sahu SM, Gayathri Rao. Effect of prenatal stress on expression of glutathione system in neonatal rat brain. Turk Neurosurg 22: 576-582.

40. Takahashi LK, Turner JG, Kalin NH. Prenatal stress alters brain catecholaminergic activity and potentiates stress-induced behavior in adult rats. Brain Res 1992; 574: 131-137.

41. Talge NM, Neal C, Glover V. Antenatal maternal stress and long term effects on child neurodevelopment: how and why? J Child Psychol Psychiatry 2007; 48: 245-261.

42. Weinstock M. The long-term behavioural consequences of prenatal stress. Neurosci Biobehav Rev 2008; 32: 1073-1086.

43. Zhu Z, Li X, Chen W, Zhao Y, Li H, Qing C, Jia N, Bai Z, Liu J. Prenatal stress causes gender dependent neuronal loss and oxidative stress in rat hippocampus. J Neurosci Res 2004; 78: 837-844.

44. Ziment I. Acetylcysteine: a drug that is much more than a mucokinetic. Biomed Pharmacother 1987; 42: 513-519.

Failure of the vascular hypothesis of multiple sclerosis in a rat model of chronic cerebrospinal venous insufficiency

Maha M.A. Zakaria[1], Shahira Y. Mikhael[1], Azza K. Abu Hussein[1], Rania A. Salah El-din[1], Hany W. Abd El-Malak[1], Iman H. Hewedi[2], Hany S. Nadim[1]

[1]Department of Anatomy, Faculty of Medicine, Ain Shams University, Cairo, [2]Department of Pathology, Faculty of Medicine, Ain Shams University, Cairo, Egypt

Abstract

Chronic cerebrospinal venous insufficiency (CCSVI) is a series of stenotic malformations in the cerebrospinal venous outflow routes, which is postulated to cause multiple sclerosis (MS). The hypotheses assumed that CCSVI leads to iron deposition which triggers inflammation and demyelination in MS. Invasive endovascular treatment of CCSVI was initiated based on the previous theory. The present study was designed to validate this hypothesis using a rat model of CCSVI. Bilateral jugular vein ligation (JVL) was performed on female albino rats (n = 15), and sham-operated rats (n = 15) were used as a control group. The rats were followed clinically for eight months and neurological examination detected no weakness or paralysis in the operated rats. At the end of the experiment, the rats were sacrificed and the brains were processed for histopathological examination of tissue sections stained by hematoxylin and eosin, myelin stain, silver impregnation, iron stain and immunohistochemical preparations for GFAP, CD68 and CD45. Semithin sections stained with toluidine blue were also examined. In the JVL group, increased iron deposition in the white matter was detected. An increase in the size and number of astrocytes along with increased GFAP immunoreactivity denoting reactive gliosis was also noted in the JVL group. However, no signs of demyelination, inflammation or axonopathy were detected. This study revealed that iron deposition in the JVL group as a model for CCSVI was not associated with cardinal histopathological findings of MS. It is therefore recommended that the invasive endovascular treatment of CCSVI should be reconsidered and further controlled clinical studies be carried out to provide a better understanding of the pathogeneses of MS.

Key words: CCSVI, multiple sclerosis, animal model, jugular veins, iron overload.

Introduction

Chronic cerebrospinal venous insufficiency (CCSVI) comprises a series of stenotic malformations affecting the extracranial cerebrospinal venous outflow routes, mainly the internal jugular and azygous veins [33]. The chronic insufficient venous drainage occurring in the course of CCSVI was postulated to cause multiple sclerosis (MS) through the deposition of iron in the walls of the congested veins and in the brain tissue [43]. Multiple sclerosis is a chronic incurable demyelinating disease of the central nervous system, which affects up to 2.5 million people worldwide [15].

Maha M.A. Zakaria, Shahira Y. Mikhael, Azza K. Abu Hussein, Rania A. Salah El-din, Hany W. Abd El-Malak, Iman H. Hewedi, Hany S. Nadim

Multiple sclerosis is described as focal inflammatory demyelination that leads to slowing or loss of impulse transmission [35]. The development of MS occurs in three stages: inflammation, demyelination and axonal damage [23].

Iron overload is hypothesized to act as a causal factor in the development of MS lesions [41], either directly via oxidative stress or indirectly by causing the primary activation of the autoimmune cascade [32].

The potential link between the pathogenesis of MS and CCSVI has generated tremendous interest in the scientific community and in the news media [17].

To date, a limited trial has been attempted to create an animal model of CCSVI, bilateral jugular venous ligation have been performed and the mice models have been evaluated for inflammation and demyelination. However, detection of iron and explaining its role in the pathological changes attributed to CCSVI was never attempted [3].

Given the insufficient evidence and the conflicting data concerning the role of CCSVI in the etiology of MS and the source of iron in the course of MS, the present study aims to clarify if CCSVI has any role in MS pathogenesis in a rat model.

Material and methods

Animals and ethics statement

After approval of the CARE (Committee of animal research ethics) of the Faculty of Medicine, Ain Shams University, thirty female adult six-month-old Wistar rats of an average weight of 160 gm were obtained from the animal house of the Medical Research Center (MRC) of the Faculty of Medicine, Ain Shams University and were randomly assigned to either a jugular vein ligation group ($n = 15$) or a sham-operated group ($n = 15$). The animals were given a standard diet and tap water *ad libitum*, housed as three rats/cage and kept in a temperature-controlled room ($23 \pm 1°C$) with a 12 : 12 hours light/dark cycle.

Jugular veins ligation

Under anesthesia using an intraperitoneal injection of ketamine 75 mg/kg and intramuscular chlorpromazine hydrochloride 20 mg/kg and complete aseptic conditions [45], a midline neck incision was performed taking care not to injure the rat salivary glands. The external jugular veins were exposed

bilaterally and ligated in their upper portion just distal to its formation by the union of the anterior and posterior facial veins to avoid blockage of salivary glands drainage using sterile silk 4-0 sutures. The skin closure was done using absorbable vicryl sutures. For six successive postoperative days, wound cleaning was performed and Cefotaxime 40 mg/kg intramuscular injection was given twice daily.

A control group (sham-operated group) was exposed to the same operative procedures and postoperative precautions but without jugular veins ligation.

Neurological examination

The rats were followed up clinically using the standard 5-point "Experimental autoimmune encephalomyelitis" staging system according to Chen *et al.* [9], starting from one month post-surgery: 0 = no signs, 1 = complete tail limpness without limb weakness, 2 = limb weakness without obvious paralysis on ambulation, 3 = one limb with partial paralysis (voluntary movements are still possible), 4 = one limb with complete paralysis, and 5 = moribund.

Tail limpness was tested by fixation of the tail base and observing the tone of the tail, limb weakness was defined by an impaired righting reflex; the rats have difficulty turning over after being laid down on their back, complete paralysis was defined as a total loss of righting reflex.

Obtaining brain tissue for assessment

After eight months and under anesthesia using ketamine 75 mg/kg IP and chlorpromazine hydrochloride 20 mg/kg IM [45], perfusion fixation of the rat brain was performed; and thoracotomy was done and 4% warm formalin in phosphate buffer saline was infused in the rat's left ventricle [14]. Decapitation was done, then the skull was opened and the brain was extracted.

A coronal segment of the brain was cut between a level of 8 mm to 15.3 mm from the beginning of the olfactory bulb which is equivalent to bregma 1 mm to bregma –6.3 mm according to stereotaxic coordinates by Paxinos and Watson [30]. The selected segment comprises most of the brain white matter bundles. The brain segment was immersed in 10% formalin in phosphate buffer saline for processing of paraffin blocks.

For preparation of semithin sections, samples of white matter (1 mm³) from various areas were har-

vested and fixed in a solution of 3% phosphate buffered glutaraldehyde (pH 7.3) overnight at 4°C.

Histopathological examination and histochemical staining

6-8 μm sections were prepared from paraffin blocks for the following stains:

1. Hematoxylin and Eosin (H&E) stain for routine histopathological assessment: the major white matter tracts observed in the coronal brain tissue sections were carefully examined.
2. Luxol fast blue-cresyl violet stain for myelin using the luxol fast blue-cresyl echt violet stain kit (American Master kit, USA) [42].
3. Silver axonal staining using modified Glees technique [5] and Bielschowsky's technique [11].
4. Perls Prussian blue stain for iron [5].

Immunohistochemical staining

Immunohistochemical staining was carried out on 4 μm sections of formalin-fixed paraffin embedded tissue using Dako autostainer with standard labeled streptavidin- biotin-peroxidase complex technique and diaminobenzidine (DAB) served as the chromogen. Staining was performed applying a polyclonal rabbit antibody against glial fibrillary protein (GFAP) (Dako, Code IS524, ready-to-use), monoclonal mouse antibody against CD68 (Dako, Code IS609, Clone KP1, ready-to-use), monoclonal mouse antibody against CD45 (Dako, Code IS751, Clones 2B11 + PD7/26, ready-to-use). Rat brain, rat tonsil and rat spleen tissues were used as positive control for GFAP, CD68, CD45 immunostains, respectively. Negative control was achieved by performing the staining procedures with omission of the primary antibody.

Toluidine blue staining of semithin sections from resin-embedded blocks

The samples were washed off the fixative preparation in phosphate buffer for a period of 4 hours, then post fixed in 1% buffered osmium tetroxide for 1-2 hours at 4°C. The tissue pieces were subsequently washed twice in phosphate buffer and then dehydrated in ascending grades of ethanol. Clearing was done in propylene oxide for 20 minutes at room temperature. Infiltration was then done by using equal parts of propylene oxide and Epon 812 for overnight. The specimens were embedded in gelatin capsules filled with fresh Epon. The capsules were placed in

the oven at 60°C for 48 hours to allow polymerization. Finally, semithin sections were cut at one-micron thickness with a glass knife and were stained with 1% toluidine blue stain dissolved in 1% borax for approximately 30-60 seconds at 60-70°C.

Computer image analysis

"TS View" computer image analysis software version 6.2.4.5 was used to quantitate the number of myelinated fibers and the number of astrocytes per microscopic field as well as the surface area of the astrocytic cell.

NIH "Image J" computer image analysis software version 1.40 g was used to measure the area of iron deposits, area of stained myelin as well as area stained immunohistochemically by GFAP per microscopic field.

For each of the previous entries, measurements were taken from six microscopic fields per slide, six slides per rat and six rats per group.

Counting the myelinated fibers in semithin sections per microscopic field was done using the 100X objective lens. The number of astrocytes per microscopic field was counted using the 40× objective lens. The surface area of astrocytes in square micrometer was measured using the 100× objective lens (6 astrocytes were measured for each case and the mean surface area of the individual astrocyte was then calculated). For measurement of area percentage of iron and GFAP per microscopic field, the 4× objective lens was used.

Calibration of the software was done for each microscopic magnification in order to translate pixels into micrometers. This was done with the aid of a stage micrometer.

For measurement of area percentage per microscopic field used for quantitation of iron and GFAP, images were split into RGB stacks, then the red stack was chosen and adjusted to grey scale threshold to mark the stained areas-areas of positive immunoreactivity with a red-colored binary mask. Then, the percentage of these areas in relation to the microscopic field was subsequently calculated.

Statistical analysis

SPSS software (Version 13.0) was used. Comparison of means between the control and experimental groups was done using independent-samples t-test with p value of < 0.05 was considered significant and < 0.01 was considered highly significant.

Maha M.A. Zakaria, Shahira Y. Mikhael, Azza K. Abu Hussein, Rania A. Salah El-din, Hany W. Abd El-Malak, Iman H. Hewedi, Hany S. Nadim

Results

Chronic cerebrospinal venous insufficiency in rats does not result in neurological deficit

Clinical follow-up of the rats performed using the standard 5-point "Experimental autoimmune encephalomyelitis" staging system revealed no neurological signs in both the sham-operated control group and the jugular vein ligation group. Monthly follow-up started one month post-surgery revealed preserved tone and movement of the rat tail on fixation of the base of the tail with no paralysis or flaccidity. Normal righting reflex was observed.

Histopathological examination and histochemical staining results

Examination of white matter tracts at the level of bregma 1 mm, bregma –1.4 mm, and bregma –2.8 mm as they appeared craniocaudally and dorsoventrally included the cingulum, the corpus callosum, the external capsule, the discrete patches of fibers dispersed in the caudate-putamen, the anterior commissure, the medial forebrain bundle, the lateral olfactory tract, the ventral hippocampal commissure, the dorsal hippocampal commissure, the stria medullaris thalami, the fimbria, the stria terminalis, the internal capsule, the fornix, the mammillothalamic tract, and the optic tract. The following were also examined: the white matter structures apparent at the level of the superior colliculus of the midbrain corresponding to bregma –6.3 mm comprised of the superior colliculus, the medial longitudinal fasciculus, cerebral peduncle, the medial lemniscus, and the alveus.

Histopathological examination by H&E

The examined white matter tracts in both jugular vein ligation group and sham-operated control group exhibited normal appearing white matter with no detectable hypodense patches suggesting demyelination. No signs of congestion or inflammatory cell infiltration were noted in both groups. Mild widening of perivascular Virchow Robin space with surrounding mild brain tissue edema was observed in the jugular vein ligation group compared to the sham-operated control group.

Myelin luxol fast blue/cresyl violet stain

The white matter showed reserved integrity with no foci of demyelination on light microscopic exam-ination of Luxol fast blue/cresyl violet stained rat brain coronal sections in both the sham-operated control group and jugular vein ligation group (Fig. 1A-B). Sharp discrimination between the white matter, which was stained deep blue, and grey matter, which acquired light blue color, was exhibited by the stain.

Computerized image analysis revealed that the percentage of areas stained for myelin per microscopic field in the sham-operated group and in the JVL group were 21.86% ± 10.93% and 23.15% ± 11.73%, respectively. The difference between the two groups was statistically non-significant ($p = 0.813$) (Fig. 2).

Silver stains

Light microscopic examination of silver stained coronal sections of the rat brain in the JVL group revealed similar results to the control group. No alteration in the organization of the major white matter structures with no apparent tangles or swellings in the fibers were noted with Bielschowsky stain and modified Glees technique (Fig. 1C-D).

Iron Perls Prussian blue stain

Light microscopic examination of Perls Prussian blue stained coronal sections of the brain of the rats in the sham-operated control group showed minimal or negative iron deposits (Fig. 1E). On higher magnification, this trivial iron deposition was observed within the oligodendrocytes, the endothelial lining of the blood vessels as well as in the surrounding brain tissue.

Regarding the jugular vein ligation group, markedly increased iron deposition was noted (Fig. 1F). The iron deposits were aggregated mainly in white matter tracts including the corpus callosum, the cingulum, and the external capsule, the white matter tracts within the caudate-putamen complex, and the anterior commissure. Moderate iron deposits were seen in the fimbria and the internal capsule and the stria terminalis, minimal deposits were observed in the optic tract, the fornix, the mammillothalamic tract and the medial longitudinal bundle. On higher magnification, the iron deposits were observed within the oligodendrocytes as well as intercellular deposits. The blood vessels captured on higher magnification photomicrographs showed extensive iron deposits in the endothelial lining of the blood vessels as well as a marked increase in iron in the surrounding brain tissue.
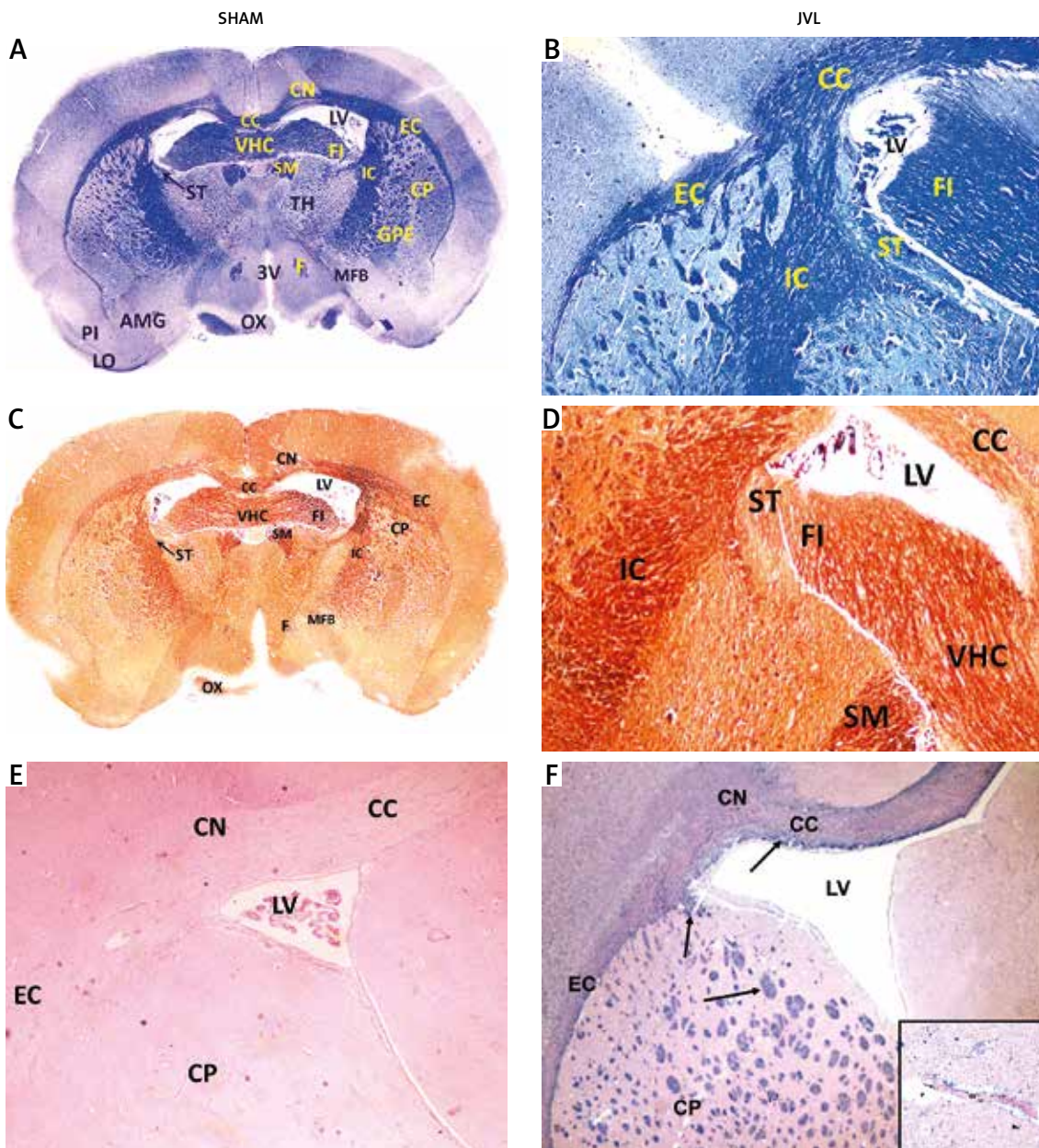
Fig. 1. Reserved white matter integrity with no foci of demyelination in both sham-operated control group (**A**: reconstructed picture) and JVL group (**B**); Luxol fast blue/cresyl violet stain. No alteration in the organization of the major white matter structures with no apparent tangles or swellings in the fibers in both sham-operated control group (**C**: reconstructed picture) and JVL group (**D**); Bielschowsky silver stain. No apparent iron deposit in sham-operated control group (**E**), while a marked increase in iron deposition is noted in the JVL group, mainly noted in white matter tracts (arrows) (**F**), inset shows iron deposits in endothelial cells (arrows) of a blood vessel "BV" and intercellular deposit in surrounding brain tissue (arrowheads) with mild widening of the perivascular space "P"; Perls Prussian Blue stain. Site of sections at coronal levels corresponding to bregma –1.4 mm for **A, B, C,** and **D** and bregma –1.2 mm for **E** and **F**; original magnification for all ×40 and ×1000 for inset. Abbreviations: amygdaloid complex (AMG), corpus callosum (CC), cingulum (CN), caudate-putamen (CP), external capsule (EC), fimbria (FI), fornix (F), internal capsule (IC), globus pallidus externa (GPE), lateral olfactory tract (LO), lateral ventricle (LV), medial forebrain bundle (MFB), optic chiasma (OX), piriform cortex (PI), stria medullaris thalamai (SM), stria terminalis (ST), thalamus (TH), ventral hippocampal commissure (VHC), third ventricle (3V).
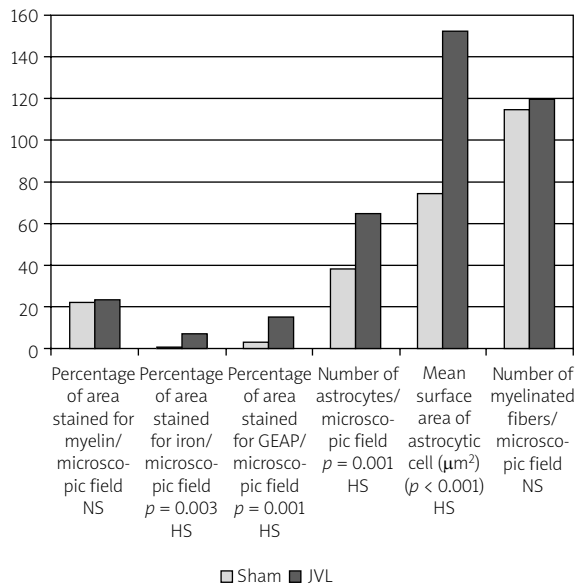
Maha M.A. Zakaria, Shahira Y. Mikhael, Azza K. Abu Hussein, Rania A. Salah El-din, Hany W. Abd El-Malak, Iman H. Hewedi, Hany S. Nadim

Fig. 2. Myelin content, iron content, GFAP immunohistochemical results, and number of myelinated fibers in the sham-operated group and JVL group as assessed by computerized image analysis; NS – non-significant; HS – highly significant.

Upon computer image analysis, the percentage of areas stained for iron per microscopic field in the sham-operated group was 0.93% ± 1.37% compared to 7% ± 5.66% in the JVL group. This difference was statistically highly significant ($p = 0.003$) (Fig. 2).

Immunohistochemical staining results

GFAP immunostaining reveal astrogliosis in rats with CCSVI

The stain highlighted the astrocytic cells mainly in the perivascular localization with apparent astrogliosis observed in the JVL group compared to the sham-operated group. The reactive astrocytes were distributed rather evenly in the white tracts examined with a slight increase in numbers at the corpus callosum and external capsule. This astrogliosis is evidenced as a marked increase in size and number of reactive astrocytes in the JVL group compared to the sham-operated group which appeared as large cells with highly branching thick and intensely staining processes.

This astrogliosis observed by light microscopic examination of the GFAP stained section in the JVL group was further confirmed upon comparing the

JVL group to the sham-operated group regarding the area percentage of GFAP immunoreactivity per microscopic field (14.81 ± 6.2 vs. 3.21 ± 0.55) and the number of astrocytes per microscopic field (64.67 ± 8.62 vs. 37.83 ± 7.94), as well as the mean surface area of the astrocyte in μ2 (152.88 ± 61.44 vs. 74.37 ± 42.39) via computerized image analysis with a highly significant statistical difference, $p < 0.001$ (Figs. 2 and 3).

CD68 and CD45 immunostaining reveal lack of inflammatory response in rats with CCSVI

Neither microglial/macrophage nor lymphocytes could be detected in either perivascular or brain-parenchymal localization in both sham-operated and JVL groups (Fig. 4).

Results of semithin toluidine blue stained sections examination

Light microscopic examination of toluidine blue stained semithin sections from the rat brain of both the sham-operated control group and the JVL group revealed similar findings with unremarkable myelinated nerve fibers, oligodendrocytes, and astrocytes (Fig. 5). Examination of nerve fibers in the corpus callosum and the caudate-putamen showed myelination of most of the fibers with the myelin appearing as a continuous dense cuff surrounding the axons with no apparent vacuolation or thinning. The axons appeared pale and homogenous (Fig. 5).

Computerized image analysis revealed no statistical significant difference between the number of myelinated fibers per microscopic field in the JVL group (119.83 ± 29.2) compared to the sham-operated group (114.5 ± 32.24), $p = 0.770$ (Fig. 2).

Discussion

This study was designed to validate the hypothesis that CCSVI leads to inflammation and demyelination in MS through the deposition of iron in the brain.

The present study showed that even though the rat model of CCSVI showed extensive iron deposition and reactive astrogliosis mostly in white matter, no signs of demyelination were detected. Also no signs of inflammation were observed as confirmed by negative immunoreactivity for both CD68 and CD45. The neurological follow-up of the JVL group and the sham-operated group showed similar results with no paralysis or weakness and intact righting reflex.
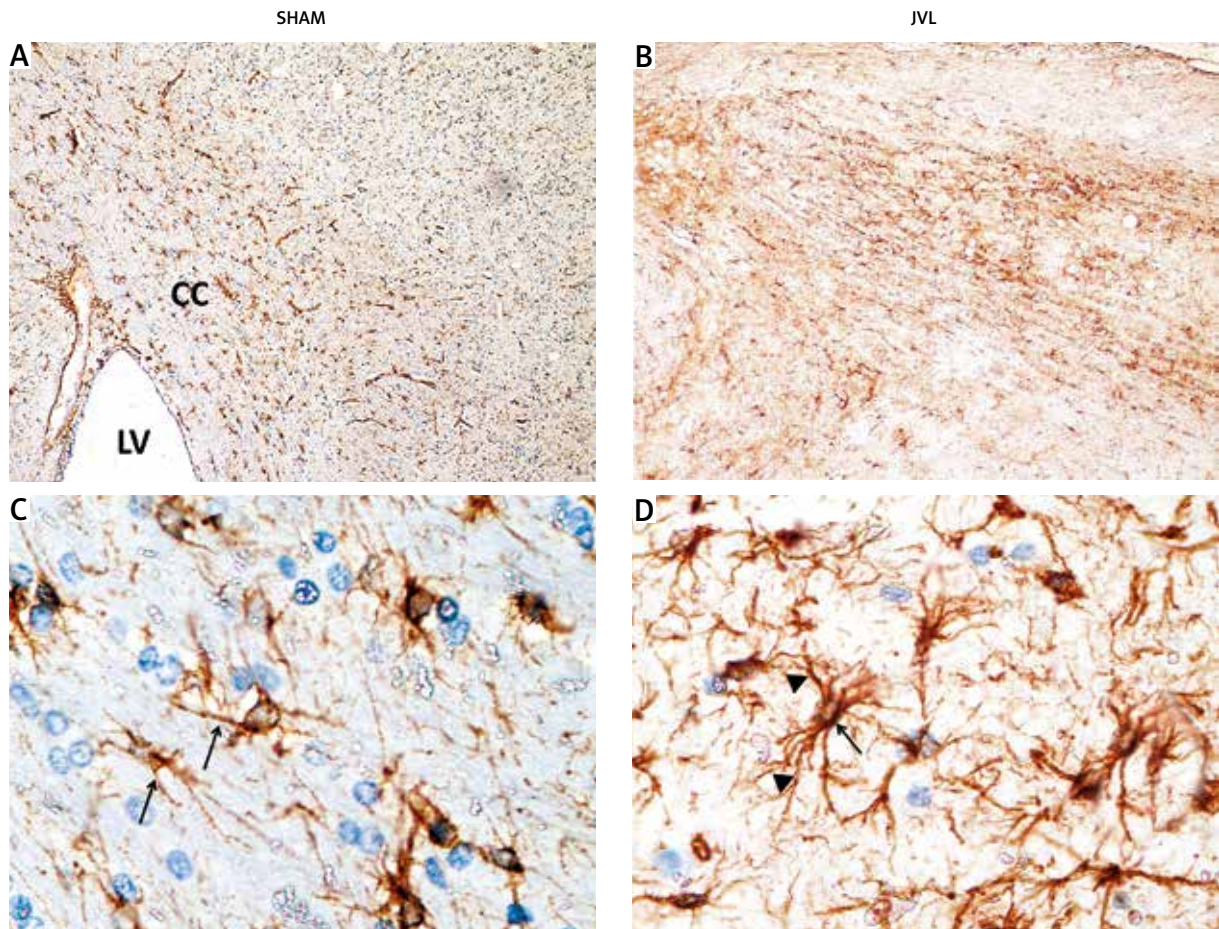
Fig. 3. GFAP immunostaining: apparent moderate positive staining of white matter in the sham-operated group (**A**); while intense staining was noted in corpus callosum (CC) adjacent to the lateral ventricle (LV) from the JVL group (**B**); original magnification × 100. Reactive astrocytes in the sham-operated group (**C**) and JVL group (**D**) with apparent astrogliosis observed in the JVL group evidenced as a marked increase in size and number of astrocyte with highly branching thick and intensely staining processes; original magnification ×1000.
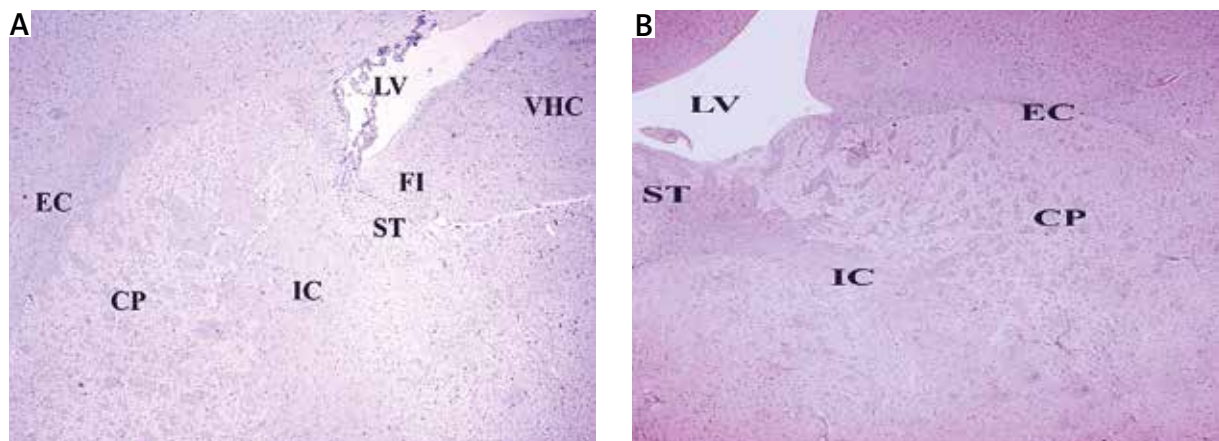
Fig. 4. No detectable inflammatory response with lack of microglial/macrophage (**A**) and lymphocytes (**B**) as assessed by CD68 and CD45 immunostaining, respectively, in the JVL group; the site of section at coronal levels corresponding to bregma –1.4 and –2.8 mm, respectively, original magnification ×40. Abbreviation: caudate-putamen (CP), external capsule (EC), fimbria (FI), internal capsule (IC), stria terminalis (ST), lateral ventricle (LV), ventral hippocampal commissure (VHC).
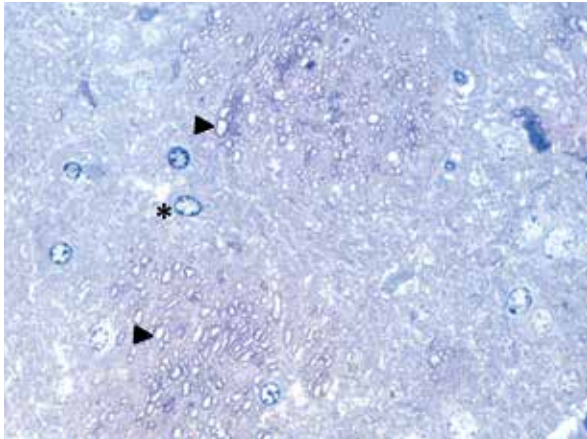
Maha M.A. Zakaria, Shahira Y. Mikhael, Azza K. Abu Hussein, Rania A. Salah El-din, Hany W. Abd El-Malak, Iman H. Hewedi, Hany S. Nadim

Fig. 5. Semithin section examination of nerve fibers in the caudate-putamen in the JVL group exhibited myelination of the nerve fibers (arrowheads) with no apparent vacuolation or thinning, astrocytes (*) are also observed; Toluidine blue stain. Original magnification ×1000.

Jugular vein stenosis was found in some studies to exist in 91% of MS patients with 14% showing bilateral stenosis [26,52]. The cerebral venous outflow in the rat is carried mainly by the external jugular vein with contribution from the vertebral vein, unlike human circulation, the internal jugular vein is almost vestigial in the rat [4]. In the present study, total ligation of the external jugular vein bilaterally in the rat model was performed to maximize the effect on the cerebral venous circulation.

Bilateral jugular vein stenosis in CCSVI was associated with activation of the cervical and intracranial collateral circles shunting the blood towards the superior vena cava and the azygos venous system, respectively [48]. The activation of these collateral circuits was confirmed by CT venogram in the JVL animal model used by Atkinson *et al.* [3]; in the present study, the rat model was used replacing the original mouse model, the cerebral venous drainage in both species is similar as well as the brain structure with few minor differences [29,44].

Mimicking the exact pattern of the venous malformations in CCSVI in a rat model was inaccessible due to the difficulty and high mortality encountered with ligation of the azygos or vertebral veins in rats.

The head position in humans differs from that of the rat which impacts the cerebral venous drainage. In humans the upright position places the internal jugular veins above the heart causing their collapse

and shifts the cerebral venous drainage towards the vertebral vein and azygos system [46]. As rats are quadrupeds, the jugular veins are less liable to compression and play a major role in the cerebral venous outflow [29], which accounts for the use of the jugular veins in the present study.

Although the study of Atkinson *et al.* [3], which employed mice as an animal model of CCSVI, extended over a period of six months, the present experiment extended over a period of eight months in rats. This period covers almost one third of the life span of albino rats [38]. In addition, this time period should be sufficient for the occurrence of pathological manifestations of MS i.e. inflammation, demyelination and axonal injury. Taking into consideration the occurrence of MS in humans in their third or fourth decade [27] and that in the present experiment JVL was performed bilaterally and the venous occlusion was complete, and this would enhance the occurrence of such manifestations if the hypothesis of Zamboni *et al.* [51] was valid.

Areas of the rat brain drained by the external jugular vein comprise the dorsal and the ventral aspects of the brain excluding the caudal part of the brainstem and the cerebellum which is drained mainly by the vertebral and the small internal jugular vein [29]. The coronal brain segment examined in the present study was limited to the areas drained chiefly by the external jugular vein. This segment comprised the periventricular areas, the major white matter tracts as well as the optic tract and optic chiasma. Multiple sclerosis is a disease of the white matter, the cortical lesions are typically periventricular in 80% of patients [13].

The present study showed that CCSVI led to iron deposition in the brain, which is consistent with the findings of Zivadinov *et al.* [53] using MRI in humans. The iron deposits in the present work were recognized mainly in the white matter and the perivascular zones and were detected in oligodendrocytes, a finding similar to the distribution of iron deposits in the brains of more than 30% of MS patients in a study by Adams [2].

However, the distribution of iron deposits in the present study was different from the normal distribution of iron in the rat brain described by Hill and Switzer [19], in their study iron was mainly localized in the circumventricular organs, the pyriform cortex, the globus pallidus, the caudate-putamen and the substantia nigra.

Studies showed that chronic venous disease typically leads to iron deposition in tissues [1,48], which is in accordance with the present study.

The iron deposition that was detected in the current study could be explained by reviewing the findings of Sakata et al. [37] who stated that jugular vein ligation alters cerebral venous volume and the findings of Yura et al. [49] that revealed that jugular vein ligation leads to decreased cerebral blood perfusion. Also, decreased CSF reabsorption was linked to bilateral jugular vein ligation [21]. Hypoxic states were shown to facilitate iron uptake [28] and this uptake by the brain is regulated by the blood-brain barrier (BBB) and the blood-cerebrospinal fluid barrier [31]. Such derangement in the CSF flow dynamics might contribute to the iron deposition observed in the present study.

It was suggested that iron initiates the demyelination sequence in MS either directly through the release of free radicals and reactive oxygen [53], or indirectly by acting as a potent chemotactic factor for macrophages and causing the initial activation of T-cell autoimmune cascade [32].

The lesions in MS are characterized by disturbance of the blood-brain barrier, local edema and demyelination; elements which point to an inflammatory process [12]. The inflammatory process in MS is initiated by the expression of adhesion molecules, followed by the passage of T-lymphocytes and macrophages or microglia cells across the blood-brain barrier [23]. In the areas of active damage, different populations of lymphocytes dominated by CD8+ T-cells as well as cytotoxic T-cells are found, these cells as well as macrophages and activated microglia are closely attached to degenerating myelin sheaths and axons, the inflammatory cells are believed to play a major role in the demyelination and axonal injury [23].

In spite of the iron deposition detected in the present study, there was no observable demyelination or inflammation in the JVL group which was in agreement with Williams et al. [47] who reported that iron deposits in an animal model of MS were found to be independent of the lesions or the inflammation. These results are contrary to the hypotheses proposed by Zamboni [50] that the deposition of iron as a result of deranged cerebral venous return is capable of inducing signs of MS.

Also in the present study, iron deposits were not seen in macrophages, which is contrary to the findings observed typically in inflammatory diseases [40].

Moreover, it was proposed that the source of perivenular iron deposits in the course of MS is extravasated red blood cells that occur as a consequence to alteration in the blood flow pattern resulting in microbleeds [39]. However, the present study did not reveal the presence of extravasated red blood cells.

The results of the present study were consistent with those rendered by Atkinson et al. [3]. In both studies, bilateral jugular vein ligation resulted in no signs of demyelination with absence of activated microglia and lymphocytes. In both studies, neurological assessment of the rats showed no signs of neurological impairment which was in agreement with the histopathological findings. These findings can explain the existence of CCSVI in up to 30% of healthy individuals [22,24]. These results provide evidence that iron deposition resulting from the venous reflux in CCSVI is not a direct causal factor for inflammatory and demyelinating diseases, which explains its occurrence in disease-free individuals.

The present study showed an increase in the number and size of astrocytes as detected by image analysis of GFAP stained sections, this finding is in accordance with the astrogliosis observed in the course of MS [16]. However, the pattern of astrogliosis in the present study was diffuse while in MS, hypertrophied astrocytes were typically seen inside the acute and chronic lesions and form a limiting zone surrounding chronic and inactive plaques [34].

The occurrence of astrogliosis in the current study could be explained by a decrease in cerebral perfusion [8,37] and decreased regional cerebral oxygen saturation [46]. In another study, Román et al. [36] revealed that gliosis was detected in the brain after incomplete ischemic injuries.

The presence of macrophages and lymphocytes in the active MS lesion was established in several studies [7,25] and immunostaining for CD68 and CD45 to highlight such inflammatory cells in brain tissue was previously reported [10]. However, the present study revealed that both CD68 and CD45 showed no detectable inflammatory response in the JVL group.

In conclusion, there is little convincing evidence to confirm a cause-and-effect relationship between venous insufficiency and the pathophysiological cascade underlying MS using the current animal model of CCSVI. Further studies are recommended in order to assess the possible relation between CCSVI and MS by comparing the effect of induction of CCSVI in

Maha M.A. Zakaria, Shahira Y. Mikhael, Azza K. Abu Hussein, Rania A. Salah El-din, Hany W. Abd El-Malak, Iman H. Hewedi, Hany S. Nadim

a chemically-induced rat model of MS, in comparison to an isolated MS model.

Disclosure

Authors report no conflict of interest.

References

1. Ackerman Z, Seidenbaum M, Loewenthal E, Rubinow A. Overload of iron in the skin of patients with varicose ulcers: Possible contributing role of iron accumulation in progression of the disease. Arch Dermatol 1988; 124: 1376-1378.

2. Adams CW. Perivascular iron deposition and other vascular damage in multiple sclerosis. J Neurol Neurosurg Psychiatry 1988; 51: 260-265.

3. Atkinson W, Forghani R, Wojtkiewicz GR, Pulli B, Iwamoto Y, Ueno T, Waterman P, Truelove J, Oklu R, Chen JW. Ligation of the jugular veins does not result in brain inflammation or demyelination in mice. PLoS One 2012; 7: e33671.

4. Aurboonyawat T, Suthipongchai S, Pereira V, Ozanne A, Lasjaunias P. Patterns of Cranial Venous System from the Comparative Anatomy in Vertebrates Part I, Introduction and the Dorsal Venous System. Interv Neuroradiol 2007; 13: 335-344.

5. Bancroft JD, Gamble M. Theory and practice of histological techniques, 6th ed. Churchill Livingstone, United Kingdom 2008.

6. Bartolomei I, Salvi F, Galeotti R, Salviato E, Alcanterini M, Menegatti E, Mascalchi M, Zamboni P . Hemodynamic patterns of chronic cerebrospinal venous insufficiency in multiple sclerosis: Correlation with symptoms at onset and clinical course. Int Angiol 2010; 29: 183-188.

7. Battistini L, Piccio L, Rossi B, Bach S, Galgani S, Gasperini C, Ottoboni L, Ciabini D, Caramia MD, Bernardi G, Laudanna C, Scarpini E, McEver RP, Butcher EC, Borsellino G, Constantin G. CD8+ T cells from patients with acute multiple sclerosis display selective increase of adhesiveness in brain venules: a critical role for P-selectin glycoprotein ligand-1. Blood 2003; 101: 4775-4782.

8. Bousser MG, Chiras J, Bories J, Castaigne P. Cerebral venous thrombosis: a review of 38 cases. Stroke 1985; 16: 199-213.

9. Chen JW, Breckwoldt MO, AikawaE, Chiang G, Weissleder R. Myeloperoxidase-targeted imaging of active inflammatory lesions in murine experimental autoimmune encephalomyelitis. Brain 2008; 131: 1123-1133.

10. Cosenza-Nashat MA, Kim MO, Zhao ML, Suh HS, Lee SC. CD45 Isoform Expression in Microglia and Inflammatory Cells in HIV-1 Encephalitis. Brain Pathol 2006; 4: 256-265.

11. Drury R, Wallington E. Carleton's histological techniques. 5th ed. Oxford University Press, England 1980.

12. Hemmer B, Archelos J J, Hartung H P. New concepts in the immunopathogenesis of multiple sclerosis. Nature Rev Neurosci 2002; 3: 291-301.

13. Frohman EM1, Goodin DS, Calabresi PA, Corboy JR, Coyle PK, Filippi M, Frank JA, Galetta SL, Grossman RI, Hawker K, Kachuck NJ, Levin MC, Phillips JT, Racke MK, Rivera VM, Stuart WH. The utility of MRI in suspected MS: report of the Therapeutics and Technology Assessment Subcommittee of the American Academy of Neurology. Neurology 2003; 61: 602-611.

14. Gage GJ, Kipke DR, Shain W. Whole animal perfusion fixation for rodents. J Vis Exp 2012; 65: e3564.

15. Ganesh A, Stahnisch FW. On the historical succession of vessel-based therapies in the treatment of multiple sclerosis. Eur Neurol 2013; 70: 48-58.

16. Genain CP, Cannella B, Hauser SL, Raine CS. Identification of autoantibodies associated with myelin damage in multiple sclerosis. Nat Med 1999; 5: 170-175.

17. Ghahari S, Forwell S J. Social Media Representation of Chronic Cerebrospinal Venous Insufficiency Intervention for Multiple Sclerosis. Int J MS Care 2016; 18: 49-57.

18. Ghezzi A, Annovazzi P, Amato M, Capello E, Cavalla P, Cocco E, Falcini M, Gallo A, Patti F, Perini P, Rodegher ME, Rovaris M, Rottoli MR, Comi G, MS Study Group-Italian Society of Neurology. Adverse events after endovascular treatment of chronic cerebro-spinal venous insufficiency (CCSVI) in patients with multiple sclerosis. Mult Scler 2013; 19: 961-963.

19. Hill JM, Switzer RC. The regional distribution and cellular localization of iron in the rat brain. Neuroscience 1984; 11: 595-603.

20. Khan O, Filippi M, Freedman MS, Barkhof F, Dore-Duffy P, Lassmann H, Trapp B, Bar-Or A, Zak I, Siegel MJ, Lisak R. Chronic cerebrospinal venous insufficiency and multiple sclerosis. Ann Neurol 2010; 67: 286-290.

21. Kotani J, Nitta K, Sakuma Y, Sugioka S, Fujita N, Ueda Y. Effects of bilateral jugular vein ligation on intracranial pressure and cerebrospinal fluid outflow resistance in cats. Br J Oral Maxillofac Surg 1992; 30: 171-173.

22. Lanzillo R, Mancini M, Liuzzi R, Di Donato O, Salvatore E, Maglio V, Vacca G, Amato L, D'Anna G, Brunetti A, Brescia Morra Vl. Chronic cerebrospinal venous insufficiency in multiple sclerosis: a highly prevalent age-dependent phenomenon. BMC Neurol 2013; 13: 20.

23. Lassmann H. Recent neuropathological findings in MS – implications for diagnosis and therapy Introduction. J Neurol 2004; 251: 2-5.

24. Leone MA, Raymkulova O, Naldi P, Lochner P, Bolamperti L, Coppo L, Stecco A, Liboni W. Chronic cerebrospinal venous insufficiency is not associated with multiple sclerosis and its severity: a blind-verified study. PLoS One 2013; 8: e56031.

25. Lucchinetti C, Brück W, Parisi J, Scheithauer B, Rodriguez M, Lassmann H. Heterogeneity of multiple sclerosis lesions: implications for the pathogenesis of demyelination. Ann Neurol 2000; 47: 707-717.

26. Mandolesi S, Niglio T, Orsini A, De Sio S, d'Alessandro A, Mandolesi D, Fedele F, d'Alessandro A. Venous compression syndrome of internal jugular veins prevalence in patients with multiple sclerosis and chronic cerebro-spinal venous insufficiency. Ann Ital Chir 2016; 87:406-410.

27. Noseworthy JH, Lucchinetti C, Rodriguez M, Weinshenker BG. Multiple sclerosis. N Engl J Med 2000; 343: 938-952.

28. Omori N, Maruyama K, Jin G, Li F, Wang SJ, Hamakawa Y, Sato K, Nagano I, Shoji M, Abe K.Targeting of post-ischemic cerebral endothelium in rat by liposomes bearing polyethylene glycol-coupled transferrin. Neurol Res 2003; 25: 275-279.

29. Paxinos G. The rat nervous system, 4th ed. Academic Press, USA 2014.

30. Paxinos G, Watson C. The Rat Brain in Stereotaxic Coordinates. 7th ed. Academic Press, USA 2013.

31. Pinero DJ, Connor JR. Iron and brain function. In: Lieberman HR, Kanarek RB, Prasad C (eds.). Nutritional Neuroscience. CRC Press, Florida 2005; pp. 235-260.

32. Porto G, De Sousa M. Iron overload and immunity. World J Gastroenterol 2007; 13: 4707-4715.

33. Rae-Grant AD, Wong C, Bernatowicz R, Fox RJ. Observations on the brain vasculature in multiple sclerosis: A historical perspective. Mult Scler Relat Disord 2014; 3: 156-162.

34. Raine CS, Scheinberg L, Waltz JM. Multiple sclerosis: oligodendrocyte survival and proliferation in an active established lesion. Lab Invest 1981; 45: 534-546.

35. Reipert B. Multiple sclerosis: a short review of the disease and its differences between men and women. J Men's Health Gen 2004; 1: 334-340.

36. Román GC, Tatemichi TK, Erkinjuntti T, Cummings JL, Masdeu JC, Garcia JH, Amaducci L, Orgogozo JM, Burn A, Hofman A, Moody DM, O'Brien MD, Yamaguchi T, Grafman J, Drayer BP, Bennett DA, Fisher M, Ogata J, Kokmen E, Bermejo F, Wolf PA, Gorelick PB, Bick KL, Pajeau AK, Bell MA, De Carli C, Culebras A, Korczyn AD, Bogousslavsky J, Hartmann A, Scheinberg P. Vascular dementia: diagnostic criteria for research studies. Report of the NINDS-AIREN International Workshop. Neurology 1993; 43: 250-260.

37. Sakata K, Endo Y, Kimura F, Yamamoto I. Effects of bilateral jugular vein ligation on local cerebral blood flow. Skull Base Surg 1999; 9: 207-210.

38. Sengupta P. The Laboratory Rat: Relating Its Age With Human's. Int J Prev Med 2013; 4: 624-630.

39. Sfagos C, Makis AC, Chaidos A, Hatzimichael EC, Dalamaga A, Kosma K, Bourantas KL. Serum ferritin, transferrin and soluble transferrin receptor levels in multiple sclerosis patients. Mult Scler 2005; 11: 272-275.

40. Sindrilaru A, Peters T, Wieschalka S, Baican C, Baican A, Peter H, Hainzl A, Schatz S, Qi Y, Schlecht A, Weiss JM, Wlaschek M, Sunderkotter C, Scharffetter-Kochanek K. An unrestrained proinflammatory M1 macrophage population induced by iron impairs wound healing in humans and mice. J Clin Invest 2011; 121: 985-997.

41. Singh AV, Zamboni P. Anomalous venous blood flow and iron deposition in multiple sclerosis. J Cereb Blood Flow Metab 2009; 29: 1867-1878.

42. Sofic E, Paulus W, Jellinger K, Riederer P, Youdim MB. Selective increase of iron in substantia nigra zona compacta of parkinsonian brains. J Neurochem 1991; 56: 978-982.

43. Tsivgoulis G, Faissner S, Voumvourakis K, Katsanos AH, Triantafyllou N, Grigoriadis N, Gold R, Krogias C. "Liberation treatment" for chronic cerebrospinal venous insufficiency in multiple sclerosis: the truth will set you free. Brain Behav 2015; 5: 3-12.

44. Watson C, Paxinos G, Puelles L. The mouse nervous system. 1st ed. Academic Press, USA 2012.

45. Waynforth HB, Flecknell P. Experimental and Surgical Technique in the Rat. 2nd ed. Academic Press, USA 1992.

46. Weir B. Multiple Sclerosis – A Vascular Etiology? Can J Neurol Sci 2010; 37: 745-757.

47. Williams R, Rohr AM, Wang WT, Choi IY, Lee P, Berman NE, Lynch SG, LeVine SM. Iron deposition is independent of cellular inflammation in a cerebral model of multiple sclerosis. BMC Neurosci 2011; 12: 59.

48. Yeoh-Ellerton S, Stacey MC. Iron and 8-isoprostane levels in acute and chronic wounds. J Invest Dermatol 2003; 121: 918-925.

49. Yura S, Sako K, Yonemasu Y. The effect of disturbance of cerebral venous drainage on focal cerebral blood flow and ischemic cerebral edema. No to Shinkei 1990; 42: 269-275 [abstract].

50. Zamboni P. The Big Idea: Iron-dependent inflammation in venous disease and proposed parallels in multiple sclerosis. J R Soc Med 2006; 99: 589-593.

51. Zamboni P, Consorti G, Galeotti R, Gianesini S, Menegatti E, Tacconi G, Carinci F. Venous Collateral Circulation of the Extracranial Cerebrospinal Outflow Routes. Curr Neurovasc Res 2009; 6: 204-212.

52. Zamboni P, Galeotti R, Menegatti E, Malagoni AM, Tacconi G, Dall'Ara S, Bartolomei I, Salvi F. Chronic cerebrospinal venous insufficiency in patients with multiple sclerosis. J Neurol Neurosurg Psychiatry 2009; 80: 392-399.

53. Zivadinov R, Schirda C, Dwyer MG, Haacke ME, Weinstock-Guttman B, Menegatti E, Heininen-Brown M, Magnano C, Malagoni AM, Wack DS, Hojnacki D, Kennedy C, Carl E, Bergsland N, Hussein S, Poloni G, Bartolomei I, Salvi F, Zamboni P. Chronic cerebrospinal venous insufficiency and iron deposition on susceptibility-weighted imaging in patients with multiple sclerosis: a pilot case-control study. Int Angiol 2010; 29: 158-175.

Folia
Neuropathologica

Three cases of ectopic sphenoid sinus pituitary adenoma

Ernest Jan Bobeff[1], Karol Wiśniewski[1], Wielisław Papierz[2], Ludomir Stefańczyk [3], Dariusz Jan Jaskólski[1]

[1]Department of Neurosurgery and Neuro-Oncology, Medical University of Lodz, Barlicki University Hospital, Łódź, [2]Institute of Health Sciences, State School of Professional Education in Plock, Płock, [3]Department of Radiology, Medical University of Lodz, Barlicki University Hospital, Łódź, Poland

Abstract

Introduction: Ectopic sphenoid sinus pituitary adenoma is a rare tumour originating from embryologic remnants of Rathke's pouch. Although it is considered a clinically benign neoplasm, necrosis is encountered in 25% of cases and it can invade adjacent bone structures.
Aims: To establish clinical, radiological and histopathological features of ectopic sphenoid sinus pituitary adenoma.
Material and methods: Analysis of three cases: two females and one man, aged 61-70.
Results: One patient presented with a unilateral hearing loss, the other two with headache and vertigo. They all suffered from type 2 diabetes mellitus. Neurological examination revealed no abnormality. Radiological imaging showed a sphenoid sinus space-occupying soft-tissue lesion with bone erosion in 2 cases and empty sella in 2 patients whereas one had a normal pituitary gland. All were operated on via the transnasal approach. Total resection was achieved in one patient and subtotal in two; in two cases we observed intact sellar dura and in one intact sellar floor. Histopathology showed immunoreactivity for synaptophysin in all cases and cytokeratin in two. The Ki-67 index was less than 2%. Immunohistochemical staining demonstrated growth hormone cells in all cases whereas prolactin and adrenocorticotropin in two. The patients were discharged home in good condition with no neurological deficits.
Conclusions: Ectopic sphenoid sinus pituitary adenoma should always be considered in differential diagnosis of sphenoid sinus lesion in the elderly, especially in coexistence with empty sella or type 2 diabetes mellitus. Since ectopic sphenoid sinus pituitary adenoma is a benign lesion, surgical removal is an effective treatment.

Key words: sphenoid sinus, empty sella, neuroendocrine markers, plurihormonal, ectopic pituitary adenoma.

Introduction

Pituitary adenoma (PA) is a common entity in the sellar region, it accounts for approximately 12% of primary brain tumours [16]. Its ectopic localization in sphenoid sinus is seen in 0.48% of cases [17]. Although ectopic sphenoid sinus pituitary adenomas (ESSPAs) are benign neoplasms, necrosis is encountered in 25% of them [17]. They are either characterized by well-defined radiological margins [17,19] or described as bone invading expansile lesions [4,15]. They originate from embryologic remnants of Rathke's pouch, which prematurely terminated their migration to the pituitary fossa [2,4,10,15,17,19].

Communicating author:
Ernest Jan Bobeff, Department of Neurosurgery and Neuro-Oncology, Medical University of Lodz, Barlicki University Hospital, 22 Kopcińskiego St., 90-153 Łódź, Poland, phone: +48 42 677 67 70, e-mail: ernestbobeff@gmail.com

Material and methods

In order to reveal clinical, radiological and histo-pathological features of ESSPA, we analysed three cases: two females and one male, aged 61-70.

Results

Patient 1, a 64-year-old-female, presented with a unilateral left-sided insidious hearing loss of one year's duration. Her medical history was notable for mild hypertension (HT) and type 2 diabetes mellitus (DM II). Additionally she had a past medical history of hypothyroidism, glaucoma, and menopause at the age of 25. The radiological imaging showed a space-occupying soft-tissue lesion within the sphenoid sinus protruding into the left choana (Fig. 1). It had irregular enhancement after gadolinium administra-

tion. Empty sella and bone erosion were observed (Fig. 2). The sella turcica was slightly deepened, lined with a 2 mm thick strand of the pituitary gland and the narrowed pituitary stalk. We performed a sub-total resection of the tumour via the transnasal approach. It presented as a necrotic mass, tender in consistency and with blurred margins. Despite the erosion of adjacent bone structures including sellar floor, it was possible to recognise the intact sellar dura. She was discharged home in good condition with no neurological deficits.

Patient 2, a 70-year-old woman, was referred for evaluation of a 2-cm heterogeneous sphenoid sinus mass discovered when a magnetic resonance scan was obtained to evaluate H/A and vertigo. She offered no other complaints. She had a past medical history of DM II and HT treated medically. On mag-
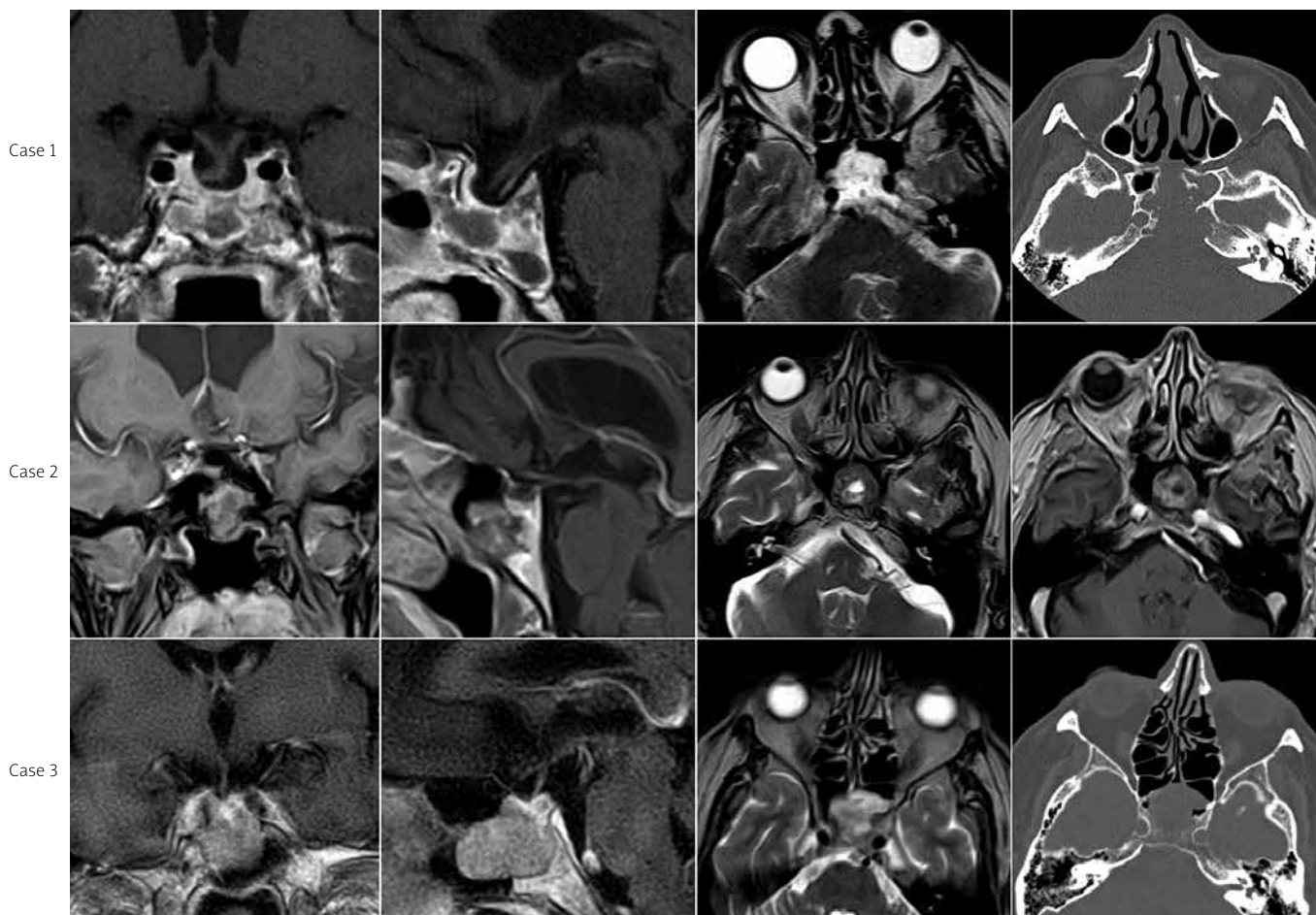

Fig. 1. Post-gadolinium T1-weighted (coronal and midline sagittal) and T2-weighted (axial) MR images of three cases of ectopic sphenoid sinus pituitary adenoma before surgery – column 1-3; CT scans showing bone erosion in patients 1 and 3, and post-gadolinium T1-weighted axial MR image of case 2 (column 4).

Ernest Jan Bobeff , Karol Wiśniewski, Wielisław Papierz, Ludomir Stefańczyk , Dariusz Jan Jaskólski

Fig. 2. Computed tomography midline sagittal scan showing bone erosion in patient 1 **(A)**; 3D reconstruction **(B)**.

netic resonance (MR) images after administration of gadolinium enhancement, we observed an irregular soft-tissue lesion within the sphenoid sinus, with a liquid cyst located interiorly (Fig. 1). It had well-defined margins and there was a normal pituitary gland located inside the sella turcica. She was operated on via the transnasal approach and the lesion was totally removed. The bone borders of the sphenoid sinus were confirmed intact. She was discharged home in good condition with no neurological deficits.

Patient 3, a 61-year-old man, was referred to the neurology clinic for evaluation of chronic H/A and episodes of vertigo. He had modest comorbidities such as mild HT and DM II, well-controlled with medications. Radiological studies revealed a space-occupying soft-tissue lesion within the sphenoid sinus with increased bone turnover, and suspected empty sella (Fig. 1). After gadolinium administration it had regular enhancement. The patient was operated on via the transnasal approach; we performed a subtotal resection of the lesion. The intact sellar dura was confirmed. He was discharged home in good condition with no neurological deficits.

The initial histopathological examination showed small fragments of tissue with alternating mucoid and fibrous, hyalinized stroma in all cases (Fig. 3). The tumours consisted of small, monomorphic cells with hyperchromatic nuclei and scant cytoplasm.

In the first case, necrosis was found in the central zone. The neoplastic cells were arranged in nests and separated by thin-walled vessels and poorly vascularized connective tissue. Haemorrhage was focally observed. All tumours showed no cytologic features of malignancy, with the Ki-67 labelling index of less than 2% and no mitotic figures. Immunohistochemical staining for the transcription termination factor and CD68 were negative in all cases, while cytokeratin was positive in the second and third case. Immunoreactivity for neuroendocrine markers including synaptophysin, neuron-specific enolase, chromogranin A and CD56 was observed. In the first case, the tumour demonstrated some S100-positive cells. The above immunophenotypes indicated a neuroendocrine tumour without cytologic features of malignancy and suggested a differential diagnosis between pituitary adenoma and paraganglioma. We performed immunohistochemical staining for pituitary hormones, which demonstrated growth hormone (GH) cells in all cases whereas prolactin (PRL) and adrenocorticotropic hormone (ACTH) in two. Hence, the final diagnoses of pituitary adenoma were established.

In the first case, hormone tests revealed a slightly increased prolactin level. The patients remain under surveillance for further growth symptoms by MRI and were referred to an endocrinologist for medical treatment.
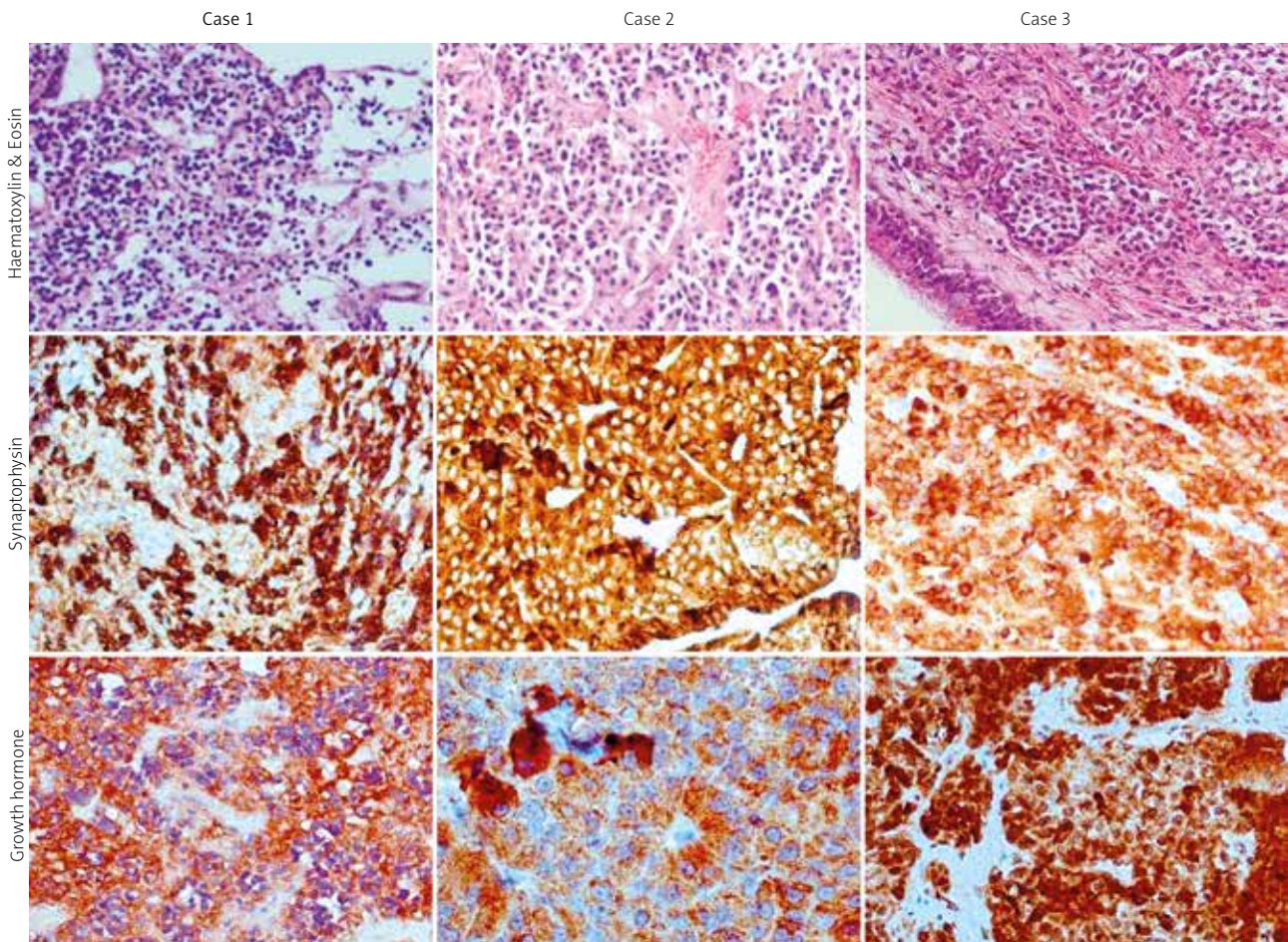
Fig. 3. The initial histopathological examination with haematoxylin and eosin (line 1); immunoreactivity for synaptophysin (line 2); immunohistochemical staining for pituitary hormones demonstrating growth hormone cells in all cases (line 3).

Discussion

The pathogenesis of ectopic pituitary adenoma (EPA) is not fully understood. It is hypothesized that neoplastic transformation occurs within the ectopic pituitary tissue located along the path of migration of Rathke's pouch, that is in the craniopharyngeal canal, or in the adjacent area [2,4,10,15,17,19]. Most frequently this tissue may be found in the sphenoid sinus, and then is called 'ectopic intrasphenoid hypophysis' [7,18]. Consequently, the coexistence with the primary empty sella in such cases results from premature termination of migration of Rathke's pouch, before reaching the pituitary fossa [4,10,15,19]. As it was shown in a recent review by Liang *et al.* [10] (Table I), to date only 15 cases of ESSPA associated with an empty sella have been reported in the literature [2,4-6,9-12,19].

The largest series of ESSPA in the literature by Thompson *et al.* included 32 cases [17] (Table I). The authors revealed that the mean age of diagnosis was greater than in typical pituitary adenoma by approximately 10 years. They indicated most sensitive neuroendocrine markers that are synaptophysin and CD56, which were also positive in our study.

Ectopic sphenoid sinus pituitary adenomas encompasses a wide range of symptomatology: acromegaly, Cushing's syndrome, sexual dysfunction, amenorrhea, MEN-1 syndrome (multiple endocrine neoplasia type 1), nasal obstruction, rhinorrhoea and epistaxis, H/A, vertigo, and ear symptoms such as hearing loss. All those although mentioned in the literature, can hardly be related to a lesion limited to the sphenoid sinus. We are of the opinion that also in our series the tumours were incidental findings.

Ernest Jan Bobeff , Karol Wiśniewski, Wielisław Papierz, Ludomir Stefańczyk , Dariusz Jan Jaskólski

Table I. Results of the study and review of the literature

Factor	Case 1	Case 2	Case 3	Thompson *et al.* 2012 [16]	Liang *et al.* 2014 [10]
Sex	Female	Female	Male	16 males, 16 females	4 males, 6 females, 5 unknown
Age	64	70	61	Mean age 57.1	Unknown
Clinical summary	Unilateral hearing loss, DM II, HT	H/A and vertigo, DM II, HT	H/A and vertigo, DM II, HT	Asymptomatic H/A Chronic sinusitis Obstructive symptoms Visual disturbances Mass Nerve changes Balance or hirsutism	Acromegaly Cushing's syndrome Sexual dysfunction Amenorrhea MEN-1 syndrome Nasal obstruction Rhinorrhoea & epistaxis Unilateral hearing loss
Imaging studies					
Empty sella	+	−	+	−	100% (15/15)
Bone involvement	+	−	+	66% (21/32)	Unknown
Intact sellar dura	+	+	+	Unknown	87% (13/15)
Intact sellar floor	−	+	−	Unknown	Unknown
Size	32 mm	20 mm	28 mm	Mean size 34 mm	Unknown
Resection	Subtotal	Total	Subtotal	Unknown	Unknown
Pathology					
Necrosis	+	−	−	25% (8/32)	Unknown
PRL	+	+	−	59% (13/22)	4/9
ACTH	+	−	+	33% (6/18)	1/9
GH	+	+	+	26% (5/19)	3/9
TSH	−	−	−	29% (5/17)	Unknown
FSH	−	−	−	47% (9/19)	Unknown
Synaptophysin	+	+	+	97% (29/30)	Unknown
Neuron-specific enolase	+	+	+	76% (13/17)	Unknown
Chromogranin A	+	+	+	71% (17/24)	Unknown
CD56	+	+	+	91% (10/11)	Unknown
S100	+	−	−	7% (1/15)	Unknown
Pan-cytokeratin	−	+	+	79% (22/28)	Unknown
Ki-67	< 1%	< 1%	< 2%	All < 3%	Unknown
Hormone tests	Slightly ↑PRL	Normal	Normal		

Regarding the differential diagnosis, invasive pituitary adenoma is an important consideration. Initial intrasellar localization of a pituitary adenoma with a following localized or diffuse destruction of sellar floor and extension into the sphenoid sinus – grade 3 and 4 in modified Hardy's system – is expected in 35% and 10% of cases, respectively [13]. Although MRI may help to confirm the integrity of sellar dura and sellar floor [4,10,12,19], the gold standard is an intraoperative verification [2,5,6,9-11,15]. In case of bone erosion of sphenoid, the evidence of ESSPA seems less justifiable. In our series, computed tomography (CT) scans demonstrated erosion of the sellar floor in two patients, with preserved integrity of dural lining on MRI which was later confirmed on surgery. In one case (patient 2), the sphenoid bone was intact.

In the first case, a slightly increased prolactin concentration was observed, possibly related to the empty sella, rather than to the secreting nature of the tumour. Hyperprolactinaemia is seen in 21% of ESSPA [17] and in 15% of the empty sella syndromes [1]. Some authors suggest it is due to the stalk effect observed in the intrasellar hypertension and consists of impaired dopamine delivery [1,3]. Continuity of the pituitary stalk is essential for adequate development and well-functioning of the pituitary gland [8]. We inferred that the process of developing adenoma in
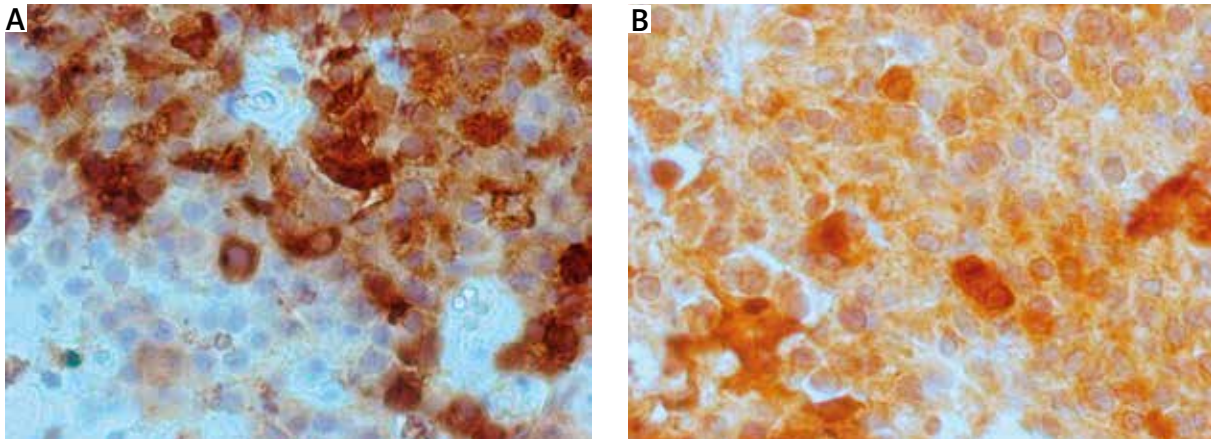
Fig. 4. Plurimorphous pituitary adenoma observed in patient 3: immunohistochemical staining revealed positive reaction for adrenocorticotropic hormone **(A)** and growth hormone **(B)** cells.

the ectopic pituitary gland may be a direct corollary of lack of the hypothalamic regulation of pituitary development during embryogenesis and subsequent impaired dopamine delivery.

A significant proportion of PA is plurihormonal. Plurimorphous PA, however, defined as showing more than one cell type, is a very rare entity [14]. In our study, we observed 2 cases (patient 1 and 3) of non-functioning PA, which were simultaneously locally positive for both ACTH and GH (Fig. 4).

Currently, there is no established treatment for ESSPA [2]. Thompson *et al.* postulated that surgical removal is a treatment of choice independently of hormone test results [17]. Preoperative medical therapy may be considered in prolactin-secreting pituitary adenomas as it can effectively reduce the size of the tumour. Additional characteristics that might support the conservative treatment are lack of symptoms (incidental finding) and elderly age of a patient.

Ectopic sphenoid sinus pituitary adenoma is a rare tumour that should always be considered in differential diagnosis of a sphenoid sinus lesion in the elderly, especially in coexistence with empty sella, DM II and HT. It can be commonly characterised by radiological and histopathological features of invasiveness – bone erosion and necrosis – despite its clinically benign nature. Surgical confirmation of the intact sellar floor or sellar dura is required to differentiate ESSPA from invasive PA. Surgical removal is an effective treatment.

Disclosure

Authors report no conflict of interest.

References

1. Agarwal JK, Sahay RK, Bhadada SK, Reddy V, Agarwal NK. Empty Sella syndrome. J Indian Acad Clin Med 2001; 2: 198-201.
2. Ajler P, Bendersky D, Hem S, Campero A. Ectopic prolactinoma within the sphenoidal sinus associated with empty sella. Surg Neurol Int 2012; 3: 260-263.
3. Bergsneider M, Mirsadraei L, Yong WH, Salamon N, Linetsky M, Wang MB, McArthur DL, Heaney AP. The pituitary stalk effect: is it a passing phenomenon? J Neurooncol 2014; 117: 477-484.
4. Das CJ, Seith A, Gamanagatti S, Goswami R. On the AJR view-box. Ectopic pituitary adenoma with an empty sella. AJR Am J Roentgenol 2006; 186: 1468-1469.
5. Gondim JA, Schops M, Ferreira E, Bulcão T, Mota JI, Silveira C. Acromegaly due to an ectopic pituitary adenoma in the sphenoid sinus. Acta Radiol 2004; 45: 689-691.
6. Hong J, Ding X, Wang S. Coexistence of ectopic pituitary adenoma and empty sella in a patient with acromegaly: a case report and review of literature. Neurol India 2012; 60: 304-306.
7. Jinkins JR. Atlas of Neuroradiologic Embryology, Anatomy, and Variants. LWW, Philadelphia 2000.
8. Kelberman D, Rizzoti K, Lovell-Badge R, Robinson IC, Dattani MT. Genetic Regulation of Pituitary Gland Development in Human and Mouse. Endocr Rev 2009; 30: 790-829.
9. Kusano Y, Horiuchi T, Oya F, Miyaoka Y, Oguchi K, Takemae T, Hongo K. Ectopic pituitary adenoma associated with an empty sella: a case report and review of the literature. J Neuroimaging 2013; 23: 135-136.
10. Liang J, Libien J, Kunam V, Shao C, Rao C. Ectopic pituitary adenoma associated with an empty sella presenting with hearing loss: case report with literature review. Clin Neuropathol 2014; 33: 197-202.
11. Matsuno A, Katayama H, Okazaki R, Toriumi M, Tanaka H, Akashi M, Tanaka K, Murakami M, Tanaka H, Nagashima T. Ectopic pituitary adenoma in the sphenoid sinus causing acromegaly associated with empty sella. ANZ J Surg 2001; 71: 495-498.

Ernest Jan Bobeff , Karol Wiśniewski, Wielisław Papierz, Ludomir Stefańczyk , Dariusz Jan Jaskólski

12. Naswa N, Das CJ, Sharma P, Karunanithi S, Bal C, Kumar R. Ectopic pituitary adenoma with empty sella in the setting of MEN-1 syndrome: detection with 68Ga-DOTANOC PET/CT. Jpn J Radiol 2012; 30: 783-786.

13. Oruçkaptan HH, Senmevsim O, Ozcan OE, Ozgen T. Pituitary adenomas: results of 684 surgically treated patients and review of the literature. Surg Neurol 2000; 53: 211-219.

14. Rasul FT, Jaunmuktane Z, Khan AA, Phadke R, Powell M. Plurihormonal pituitary adenoma with concomitant adrenocorticotropic hormone (ACTH) and growth hormone (GH) secretion: a report of two cases and review of the literature. Acta Neurochir 2014; 156: 141-146.

15. Slonim SM, Haykal HA, Cushing GW, Freidberg SR, Lee AK. MRI appearances of an ectopic pituitary adenoma: case report and review of the literature. Neuroradiology 1993; 35: 546-548.

16. Thapar K, Kovacs K, Scheithauer BW, Lloyd RV. Diagnosis and Management of Pituitary Tumors. Humana Press, Totowa 2001.

17. Thompson LD, Seethala RR, Müller S. Ectopic Sphenoid Sinus Pituitary Adenoma (ESSPA) with Normal Anterior Pituitary Gland: A Clinicopathologic and Immunophenotypic Study of 32 Cases with a Comprehensive Review of the English Literature. Head Neck Pathol 2012; 6: 75-100.

18. Tortori-Donati P, Rossi A. Pediatric Neuroradiology – Brain. Head, Neck and Spine. Springer, New York 2005.

19. Yang BT, Chong VF, Wang ZC, Xian JF, Chen QH. Sphenoid sinus ectopic pituitary adenomas: CT and MRI findings. Br J Radiol 2010; 83: 218-224.

Folia
Neuropathologica

GRN mutation in a patient with a behavioral variant of frontotemporal lobar degeneration (bvFTD)

Sylwia Walczysková[1], Pavel Ressner[2], Šárka Hilscherová[1], Jaroslav Kotlas[3], Jiří Konrád[4], Věnceslava Svobodová[5]

[1]Department of Medical Genetics, University Hospital Ostrava, Ostrava, [2]Neurology Clinic, University Hospital Ostrava, Ostrava, [3]Institute of Biology and Medical Genetics, General University Hospital, Prague, [4]Psychiatric Hospital Havlíčkův Brod, Gerontopsychiatry, Havlíčkův Brod, [5]KlinNeuro Prague Ltd, Neurology, Physiotherapy, Neurosurgery, Prague, Czech Republic

Abstract

The clinical spectrum of frontotemporal lobar degeneration (FTLD) is characterized by personality changes, language impairment, and executive function deficits. About 40% of FTLD cases have a family history of the disease, and the GRN gene is currently the most frequent genetic determinant. In cases of inherited FTLD with GRN mutations, parkinsonism is often an early sign due to greater grey matter atrophy in the caudate nucleus and bilateral atrophy in the thalamus. We investigated a female patient with signs of frontotemporal lobe atrophy and unilateral caudate nucleus atrophy on MRI. DNA was isolated from peripheral blood leukocytes and tested for GRN gene mutations. A pathogenic splice donor site mutation, c.708+1G>A, was found in the GRN gene. MRI showed unilateral caudate nucleus atrophy. This report extends the evidence for phenotypic and neuropathological heterogeneity in FTLD spectrum disorders due to splicing mutations in the GRN gene.

Key words: caudate nucleus atrophy, frontotemporal dementia, GRN gene, splicing mutation.

Introduction

Patients < 65 years old with presenile dementia make up 5-15% of all patients with dementia. Frontotemporal lobar degeneration (FTLD) is the second most common cause of early onset dementia after Alzheimer's disease. Frontotemporal lobar degeneration is a highly heritable disorder, with about 25-50% of patients having a positive family history and about 10% showing clear autosomal-dominant inheritance, even though a genetic cause can be demonstrated in less than 20% of patients [2]. This neurodegenerative disorder shows genetic and pathological heterogeneity, is characterized by behavior and language distur-

bances, and is associated with variable frontal, temporal, and basal ganglia atrophy with neuronal loss and gliosis [2,16]. The redefined clinical criteria recognize different phenotypes based on the clinical symptoms at presentation, including a possible behavioral variant of FTLD (bvFTD), two language variants, primary progressive nonfluent aphasia (PNFA), and a semantic variant. Notably, all variants can overlap with atypical Parkinsonian disorders such as progressive supranuclear palsy and corticobasal degeneration [5,12,14].

Frontotemporal lobar degeneration has been linked to mutations in seven genes (*TARDBP*, *FUS*, *MAPT*,

Sylwia Walczysková, Pavel Ressner, Šárka Hilscherová, Jaroslav Kotlas, Jiří Konrád, Věnceslava Svobodová

GRN, *VCP*, *CHMP2B*, and *C9ORF72*), three of which account for the vast majority of familial FTLD cases and for a proportion of sporadic FTLD cases: the *MAPT* gene (microtubule-associated protein Tau), the *GRN* gene (also known as *PGRN*, progranulin), and the *C9ORF72* gene (expanded hexanucleotide repeat in a non-coding region of chromosome 9 open reading frame 72). About 95% of individuals who are diagnosed with FTLD with a pathogenic mutation in the *GRN* gene (FTLD-GRN) have an affected parent. The age of clinical onset varies widely in GRN mutation carriers, even within the same family, and it is currently not possible to predict the exact age of disease onset in an asymptomatic individual. The proportion of cases caused by *de novo* mutation is unknown but is estimated to be 5% or less [11]. The *GRN* gene encodes a secreted multifunctional growth factor that is involved in a wide range of biological processes, such as development, wound repair, and the immune response, among others [7,16]. In the FTD patient population, the *GRN* mutation frequency ranges from 5% to 26%, and FTLD-GRN is inherited in an autosomal dominant manner. Pathogenic mutations in the *GRN* gene are typically loss-of-function, nonsense, frame shift, or splice-site mutations that lead to GRN haploinsufficiency (null mutations). Studies have shown that the GRN levels in cerebrospinal fluid (CSF) do not differ in patients with a variety of types of primary neurodegenerative dementias. However, the plasma PGRN level (up to 35-75% reduction in mutation carriers with respect to controls), which can be used to detect GRN mutation carriers, is one of the best examples of a reliable plasma biomarker in neurodegenerative diseases [6,17]. Subcortical and deep cortical involvement is a key feature of FTLD and especially of GRN-related disease, which shows a significantly higher degree of atrophy bilaterally in the caudate nucleus and thalamus compared to FTLD patients without a *GRN* mutation. This may explain the parkinsonism that is frequently associated with the disease even in its early stages. There are some case reports describing the loss of pigmented neurons from the substantia nigra [9,15,19]. Here we describe a case of a patient with a rare splicing mutation in the *GRN* gene and unilateral caudate nucleus atrophy.

Case report

The patient was a right-handed Caucasian woman (III-2) with 18 years of formal education who began to exhibit memory and cognitive impairment, behavioral changes, and slight language disturbances (word finding difficulties) in 2005 when she was 59 years old. There was a strong family history of dementia in the proband's family (Fig. 1A); specifically, her father (II-1) (deceased at the age of 72 years) and grandmother (I-2) had histories of dementia, as reported by relatives. The woman had 3 sons (IV-1 – IV-3), the oldest born in 1974; to date, all are healthy. The proband was otherwise healthy (i.e. no somatic disorders), with a normal full blood count and metabolic, renal, and hepatic function. She had no history of alcohol or drug abuse, not even nicotinism.

In 2005, the proband's family began to notice behavioral changes, such as wandering, instead of going to the work (finally that was the reason for her dismissal), she began to be dissocial (unsociable and indecent in her behavior) and insensitive to the others, and she began telling lies profusely. She exhibited mild executive function disturbances, began to have problems with cooking (she was cooking from rotten or unsuitable ingredients). She reduced food intake due to lack of appetite. At that time she had found herself healthy and refused to visit any physician. She also became forgetful, language problems appeared, she had difficulties finding words and repeated sentences and phrases (perseverations). She repeatedly got lost in her hometown. She was unaware that she was having these issues (anosognosia).

The patient worked as a teacher until 2008. In 2010, her behavior worsened (unreasonable conduct), and she began running away from home with getting lost in the city. At home and lately in the hospital she was walking back and forth permanently in the corridor and opening/closing doors and drawers repetitively. She was not able to do activities of daily living (dressing, self-care, cooking, gadget use), began to lose social inhibition (changing clothes at a parking place abroad), she lost insight. On the basis of clinical symptoms she met criteria for bvFTD diagnosis.

Psychological testing performed in 2010 showed the following scores: MMSE, 26/30; Raven's Progressive Matrices IQ, 117; Wechsler Memory Test MIQ, 77; in Clock Drawing Test the numbers were written correctly, only handed in a slightly incorrect position and, she was unable to distinguish accurately the hour and minute hand. In 2011, her speech became very poor and telegraphic, and she was unable to recall words and phrases, she used agrammatisms, words in wrong and senseless combinations (phonemic paraphasia),
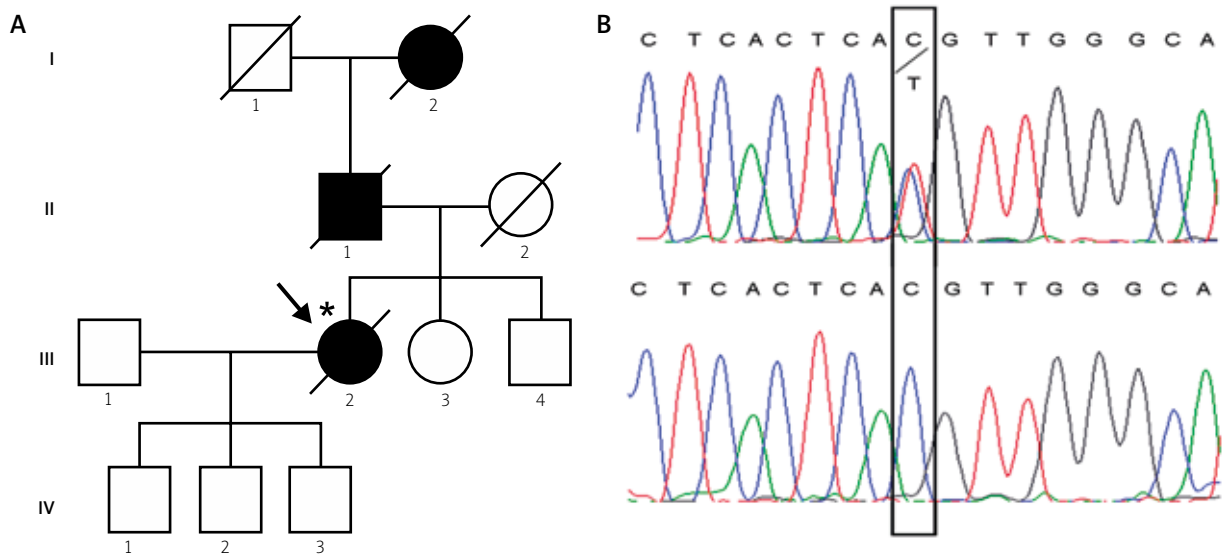
Fig. 1. A) The pedigree of the Czech family showing the inheritance of frontotemporal dementia. Affected individuals are shown as filled symbols and the arrow points to the proband. **B)** Reverse DNA sequence fragment of the GRN gene. The upper panel shows the pathogenic mutation c.708+1G>A in intron 7, and the lower panel shows the normal sequence.

without dysarthria, with accented perseverations, losing ability to write and read, then she lost capability of forming sentences, in a logopedic exam she was diagnosed as expressive non-fluent aphasia (Broca aphasia). An MRI of her brain revealed left frontotemporal atrophy with ventricular dilatation that was more prominent in the temporal region with atrophy of hippocampus and insula and left caudate nucleus atrophy (Fig. 2).

Over the next year, the speech problems were profusely pronounced and there was a clinical overlap with progressive non-fluent aphasia (nfvPAA). She could understand only very simple instructions, and, for example, she stood up and walked away under the directions. She also had urinary and fecal incontinence.

In 2012, she lost the ability of spontaneous speech; she could only say simple phrases like "You go", and she gradually became mute. In 2013, she needed complete personal care and a nasogastric tube feeding towards the end of the disease, in 2015. She passed away at the age of 69 years from pneumonia related to her disorder. The disease duration was about 8 years.

Two of the woman's three sons were interested in presymptomatic DNA testing and underwent extensive genetic counseling.

Material and methods

Genomic DNA was extracted from the patient's whole blood using standard procedures. Informed consent to genetic analysis for diagnostic and research purposes was obtained from the patient's legal guardian. Due to the clinical course and strong family history of the disease, we performed mutation analysis of the *PSEN1, PSEN2, APP* (exons 16, 17 only) and *GRN* genes. All coding exons and flanking sequences of these genes were amplified using primers, which are available upon request. The amplified fragments were sequenced in both directions using standard protocols and the BigDye Terminator v3.1 Cycle Sequencing Kit and an ABI PRISM3130 genetic analyzer. The sequences were analyzed using SeqScape® software v2.5 (Applied Biosystems, Life Technologies, Carlsbad, CA, USA); NCBI Ref. sequence NM_002087.3. The available brain MRI exams (Magnetom Avanto 1,5 T; Siemens) were analyzed visually. There were 2 independent DNA samples from two sons of the proband available for testing (with informed consent) and for potential confirmation of the mutation.

Results

Sequence analysis of the patient's *GRN* gene identified a pathogenic splice donor site mutation,

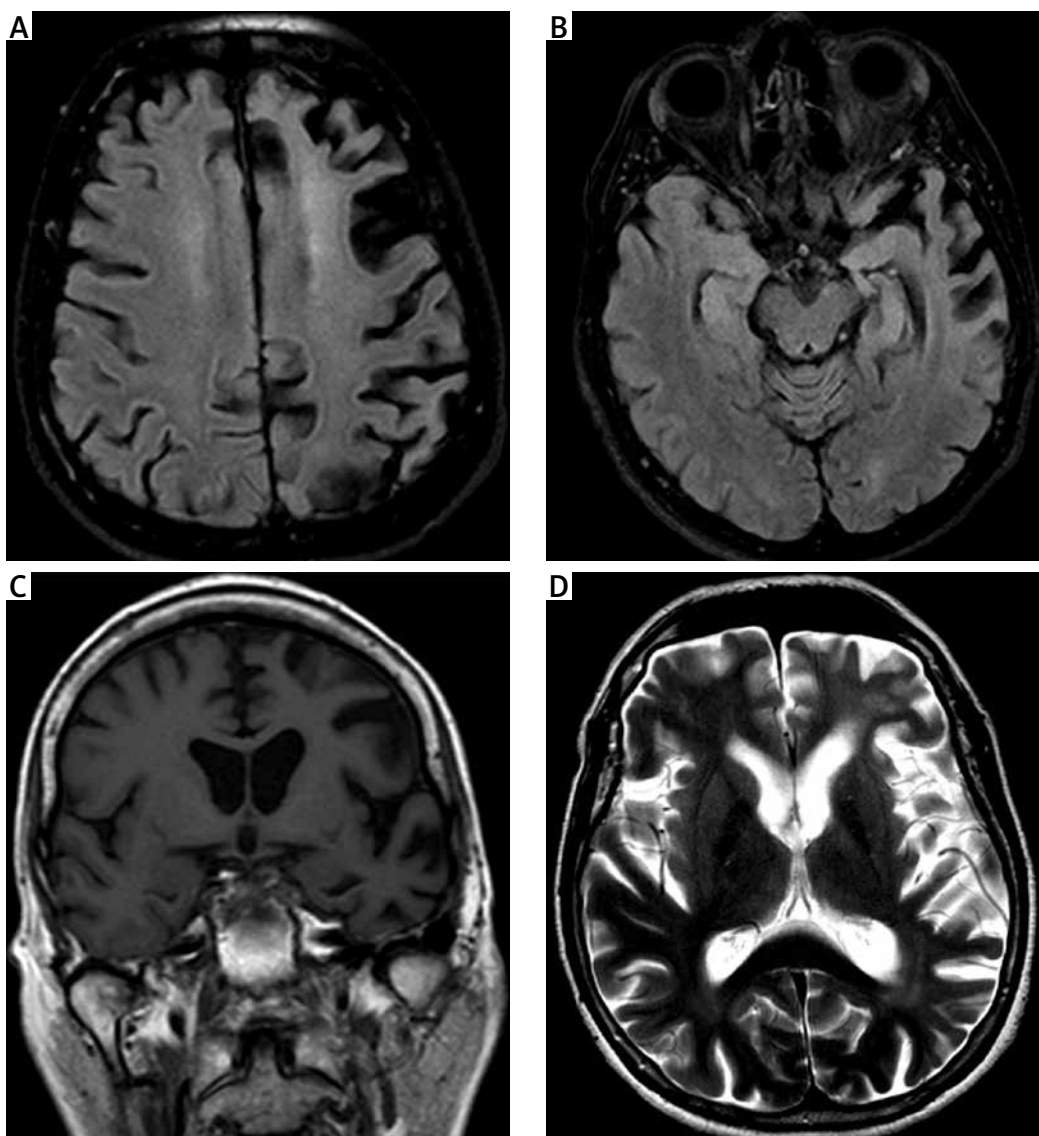Sylwia Walczysková, Pavel Ressner, Šárka Hilscherová, Jaroslav Kotlas, Jiří Konrád, Věnceslava Svobodová

Fig. 2. Magnetic resonance imaging of the patient at 64 years of age. **A)** FLAIR parietal and frontal atrophy. **B)** Temporal atrophy that is more marked on the left side. **C)** T1 coronal image. **D)** T2 caput caudate nucleus atrophy on the left side.

c.708+1G>A, in intron 7 (Fig. 1B). The mutation was heterozygous and was predicted to have dramatic consequences on the maturation of GRN mRNA, leading to the removal of exon 7 and thus creating a frame shift that would result in a truncated protein half of its normal length (protein level, p.Val-200GlyfsX18) [16].

Discussion

Here we report a patient with a pathogenic splice site mutation c.708+1G>A in the *GRN* gene. This intronic mutation was described previously by Masellis *et al.* (2006) in 2 of 12 siblings that were been affected by corticobasal syndrome (CBS). That report described the evolution of the patients' dementia, motor decline (including rigidity, dystonia, and apraxia), cortical sensory loss, visuospatial dysfunction, behavioral changes, and extrapyramidal features. The caudate nucleus and putamen were atrophic, while the hippocampus was normal in size. Although both family members were diagnosed with CBS, their clinical courses showed important differences. Notably, there

was no history of dementia or parkinsonism in either parent. Another report described another French family of Caucasian origin with 2 affected members but no family history of the disease [17]. The signs of disease onset included tachyphemia and behavioral disorders such as apathy. In addition, the two had attention disorders, impulsivity, joviality, memory deficits, tachyphemia, and reduction of spontaneous language. These cases were considered a behavioral type of FTLD. The mean age at disease onset in both of these families was at 53-72 years old, and the mean disease duration was about 2-8 years according to the Alzheimer Disease & Frontotemporal Dementia Mutation database.

Researchers and healthcare providers often consider patterns such as repetitive locomotion following circuitous path or back and forth, as well as random ambulation to be aimless and dementia-related behavioral disturbances [4]. Some of these patterns are associated with running away, wandering or getting lost [4]. Our proband had a family history of dementia and showed personality and language deterioration along with attempts of running away from home and stereotypic behavior (repetitive walking back and forth, opening the doors and drawers in the corridor). Otherwise she had no specific health problems.

Volumetric studies that compared the rate of brain atrophy in FTD-GRN versus FTD caused by mutations in the *MAPT* gene (FTD-MAPT) showed that individuals with pathogenic *GRN* variants have a higher rate (3.5% vs. 2.4% per year) of whole-brain atrophy that is more asymmetrically pronounced than those with *MAPT*-related FTLD [20]. The 2010 brain MRI examination of our proband revealed not only asymmetric involvement with pronounced brain atrophy of the left temporal and frontal lobes and asymmetric caudate nucleus atrophy, which is in agreement with the literature [3,14], but also revealed greatly pronounced caudate nucleus and gyrus rectus atrophy on the left side, with virtually normal findings for the right caudate nucleus, and it would have been very interesting to follow the changes in asymmetry over time. Such a finding appears to be, according to some authors, a typical finding in bvFTD [8]. However, the asymmetric atrophy of the left hemisphere with predominance in temporal and frontal lobes, hippocampi and insula including subcortical atrophy with basal ganglia and the large atrophy of the left caudate nucleus indi-

cate the diagnosis of bvFTD in our case. The shape deflation of the left caudate nucleus, which corresponded to afferent connections from the dorsolateral prefrontal mediofrontal/anterior cingulate and orbitofrontal cortex, correlated with worsening disease severity [14]. Our proband with dementia and pathogenic mutation in the *GRN* gene and a clinical manifestation of the disease fulfilled the diagnostic criteria for bvFTD.

Five years after the disease onset, according to psychological and logopedic examinations, there was a clear progress in speech impairment with agrammatisms, anomia and phonemic paraphasia, later on with speech fluency impairment – almost no spontaneous speech, she was only repeating words sporadically. This was in agreement with progressive non-fluent aphasia (non-fluent PPA) (nfvPPA). Such a course may suggest that types of FTD can overlap in certain stages of disease.

In a report by Harris *et al.* (2016) it was found that over 90% of patients with FTLD pathology exhibited a combination of at least one behavioral and one language feature [10]. It would have been interesting to repeat the MRI, but it was not possible due to the death of the patient in 2015. In the above reports by Masellis *et al.* (2006) and Le Ber *et al.* (2008), the tested patients were diagnosed with behavioral variants of FTLD. Our patient showed the typical signs of this variant in the early stages of the disease, though the later speech problems suggested the progressive nonfluent aphasia variant. In relation to these initial symptoms, we consider our patient as probable bvFTD. There might be some modifier genes and/or environmental influences, epigenetic factors, ethnicity that prevail over a particular manifestation of one variant of FTLD over another.

In conclusion, this case report highlights the variety of MRI characteristics that are found in patients with frontotemporal dementia and the c.708+1G>A mutation in the *GRN* gene. The age of clinical onset and survival can vary widely in *GRN* mutation carriers, even within the same family [1]. A precise diagnosis must be made through genetic testing.

Acknowledgements

Sylwia Walczysková, Pavel Ressner, Šárka Hilscherová, Jaroslav Kotlas, Jiří Konrád, Věnceslava Svobodová

Disclosure

Authors report no conflict of interest.

References

1. Armstrong RA. Survival in the pre-senile dementia frontotemporal lobar degeneration with the TDP-43 proteinopathy: effects of genetic, demographic and neuropathological variables. Folia Neuropathol 2016; 24: 137-148.
2. Benussi A, Padovani A, Borroni B. Phenotypic heterogeneity of monogenic frontotemporal dementia. Front Aging Neurosci 2015; 7: 171.
3. Buhour MS, Doidy F, Laisney M, Pitel AL, de La Sayette V, Viader F, Eustache F, Desgranges B. Pathophysiology of the behavioral variant of frontotemporal lobar degeneration: a study combining MRI and FDG-PET. Brain Imaging Behav 2016; 1-13.
4. Cipriani G, Lucetti C, Nuti A, Danti S. Wandering and dementia. Psychogeriatrics 2014; 14: 135-142.
5. Dewer B, Rogers P, Ricketts J, Mukonoweshuro W, Zeman A. The radiological diagnosis of frontotemporal dementia in everyday practice: an audit of reports, review of diagnostic criteria, and proposal for service improvement. Clin Radiol 2016; 71: 40-47.
6. Finch N, Baker M, Crook R, Swanson K, Kuntz K, Surtees R, Bisceglio G, Rovelet-Lecrux A, Boeve B, Petersen RC, Dickson DW, Younkin SG, Deramecourt V, Crook J, Graff-Radford NR, Rademakers R. Plasma progranulin levels predict progranulin mutation status in frontotemporal dementia and asymptomatic family members. Brain 2009; 132: 583-591.
7. Fontana F, Siva K, Denti MA. A network of RNA and protein interactions in frontotemporal dementia. Front Mol Neurosci 2015; 8: 9.
8. Frings L, Yew B, Flanagan E, Lam BYK, Hüll M, Huppertz J, Hodges JR, Hornberger M. Longitudinal grey and white matter changes in frontotemporal dementia and Alzheimer's disease. PLoS Ona 2014; 9: e90814.
9. Gijselinck I, Van Broeckhoven C, Cruts M. Granulin mutations associated with frontotemporal lobar degeneration and related disorders: An update. Hum Mutat 2008; 29: 1373-1386.
10. Harris JM, Jones M, Gall C, Richardson AMT, Neary D, du Plessis D, Pal P, Mann DMA, Snowden JS, Thompson JC. Co-Occurrence of Language and Behavioural Change in Frontotemporal Lobar Degeneration. Dement Geriatr Cogn Disord Extra 2016; 6: 205-213.
11. Hsiung GYR, Feldman HH. GRN-related frontotemporal dementia. In: GeneReviews® [Internet]. Pagon RA et al. (eds.). University of Washington, Seattle 2007; pp. 1993-2016.
12. Lashley T, Rohrer JD, Mead S, Revesz T. Review: an update on clinical, genetic and pathological aspects of frontotemporal lobar degenerations. Neuropathol Appl Neurobiol 2015; 41: 858-881.
13. Le Ber I, Camuzat A, Hannequin D, Pasquier F, Guedj E, Rovelet-Lecrux A, Hahn-Barma V, van der Zee J, Clot F, Bakchine S, Puel M, Ghanim M, Lacomblez L, Mikol J, Deramecourt V, Lejeune P, de la Sayette V, Belliard S, Vercelletto M, Meyrignac Ch, Van Broeckhoven Ch, Lambert JCh, Verpillat P, Campion D, Habert MO, Dubois B, Brice A. Phenotype variability in progranulin muta-

tion carriers: a clinical, neuropsychological, imaging and genetic study. Brain 2008; 131: 732-746.
14. Macfarlane MD, Jakabek D, Walterfang M, Vestberg S, Velakoulis D, Wilkes FA, Nilsson C, van Westen D, Looi JC, Santillo AF. Striatal atrophy in the behavioral variant of frontotemporal dementia: correlation with diagnosis, negative symptoms and disease severity. PLoS One 2015; 10: e0129692.
15. Mackenzie IRA, Baker M, Pickering-Brown S, Hsiung GYR, Lindholm C, Dwosh E, Gass J, Cannon A, Rademakers R, Hutton M, Feldman HH. The neuropathology of frontotemporal lobar degeneration caused by mutations in the progranulin gene. Brain 2006; 129: 3081-3090.
16. Masellis M, Momeni P, Meschino W, Heffner Jr R, Elder J, Sato Ch, Liang Y, St George-Hyslop P, Hardy J, Bilbao J, Black S, Rogaeva E. Novel splicing mutation in the progranulin gene causing familial corticobasal syndrome. Brain 2006; 129: 3115-3123.
17. Morenas-Rodríguez E, Cervera-Carles L, Vilaplana E, Alcolea D, Carmona-Iragui M, Dols-Icardo O, Ribosa-Nogué R, Muñoz-Llahuna L, Sala I, Sánchez-Saudinós MB, Blesa R, Clarimón J, Fortea J, Lleó A. Progranulin protein levels in cerebrospinal fluid in primary neurodegenerative dementias. J Alzheimers Dis 2016; 50: 539-546.
18. Po K, Leslie FVC, Gracia N, Bartley L, Kwok JBJ, Halliday GM, Hodges JR, Burrell JR. Heritability in frontotemporal dementia: more missing pieces? J Neurol 2014; 261: 2170-2177.
19. Premi E, Garibotto V, Gazzina S, Formenti A, Archetti S, Gasparotti R, Padovani A, Borroni B. Subcortical and deep cortical atrophy in frontotemporal dementia due to granulin mutations. Dement Geriatr Cogn Dis Extra 2014; 4: 95-102.
20. Whitwell JL, Weigand SD, Gunter JL, Boeve BF, Rademakers R, Knopman DS, Wszolek ZK, Petersen RC, Jack CR, Josephs KA. Trajectories of brain and hippocampal atrophy in FTD with mutations in MAPT or GRN. Neurology 2011; 77: 393-398.

Multiple cerebral fusiform aneurysms involving the posterior and anterior circulation including the anterior cerebral artery: a case report

Sumit Das, Tibor Valyi-Nagy

Department of Pathology, University of Illinois at Chicago, United States

Abstract

Multiple fusiform aneurysms occurring in a single patient are very uncommon. Fusiform aneurysms affecting the anterior circulation are extremely rare and reported cases involve the middle cerebral artery and internal carotid artery. We report here a case of a 55-year-old African American male who had a history of multiple strokes and who was found unresponsive prior to his latest hospital admission. Neuroimaging was remarkable for multiple fusiform aneurysms involving segments of the anterior, middle and posterior cerebral arteries as well as subarachnoid and intraparenchymal hemorrhage. Unfortunately even after aggressive medical management, the patient did not show any signs of recovery and further management entailed comfort care measures only. The patient passed away shortly thereafter. Post-mortem examination confirmed the presence of multiple fusiform aneurysms with involvement of both the posterior and anterior circulation including the anterior cerebral artery as well as subarachnoid and intraparenchymal hemorrhage. Interestingly, there was no apparent site of aneurysm rupture identified to explain the hemorrhage. Our case is unusual in that the multiple fusiform aneurysms were found to extensively involve both the anterior and posterior circulation. Furthermore, our case demonstrates involvement of the anterior cerebral artery by fusiform aneurysms, which is also a very rare event.

Key words: aneurysm, multiple, hemorrhage, risk factors, pathogenesis.

Introduction

An aneurysm is a focal dilation of the arterial wall. The majority of aneurysms are of a saccular type. Fusiform aneurysms are nonsaccular dilations involving the entire arterial wall for a short distance [12]. They have different pathological features, anatomic distribution and natural histories [3]. They are formed from ectatic and tortuous basal arteries and typically arise in the middle part of the basilar artery [12].

Potential causes of fusiform aneurysms include atherosclerosis, dissection, disorders of collagen, and infection. Fusiform aneurysms affecting the anterior circulation are extremely rare and reported cases involve the middle cerebral artery and internal carotid artery [12]. Multiple fusiform aneurysms occurring in a single patient are also very uncommon [6,7]. We present here an unusual case of a patient with multiple fusiform aneurysms involving both the posterior and anterior circulation including the anterior cerebral artery with

Communicating author:

Sumit Das, MD, Department of Pathology, University of Illinois at Chicago, 640 South Wood Street, 60612 Chicago, United States, e-mail: sumitk.das9276@gmail.com

pathology confirmed on post-mortem examination. Our case is aimed to raise awareness of the possibility of diffuse involvement of the circle of Willis blood vessels by fusiform aneurysms and also describes the rare involvement of the anterior cerebral artery by this type of aneurysm.

Case report

A 55-year-old African American male with a past medical history of hypertension and multiple episodes of stroke first presented at an outside hospital with acute onset of right-sided extremity weakness, right facial droop, and slurred speech. Neurological examination was notable for mild dysarthria, expressive aphasia, mild facial droop, and clonus in the right ankle. Neuroimaging performed at the outside hospital revealed an infarction in the vascular territory of the left anterior cerebral artery. CT angiogram revealed multiple fusiform aneurysms along with severe stenosis of the right M2 and left M2 segments, occlusion of the right A2 and A1 segments, and intracranial portion of the left vertebral artery. The patient underwent pipeline stenting of the right P2 segment.

Six months later, the patient was found unresponsive at his home with surrounding evidence of emesis. He was subsequently transported to the outside hospital where he was intubated. CT angiogram revealed subarachnoid hemorrhage within the basilar cisterns and intraparenchymal hemorrhage involving the pons,

midbrain and right basal ganglia. At this point the patient was transferred to our hospital for neurosurgical evaluation and management. Treatment for his aneurysms was held off pending improvement of his neurologic status. Unfortunately no such recovery was noted. One week later, the patient's family opted to switch the mode of care to comfort measures. The next morning he was noted to be in asystole. Pupils were fixed and dilated with no heart or lung sounds. No spontaneous movements were appreciated either. He was subsequently pronounced deceased.

Post-mortem examination

General autopsy was notable for moderate calcific atherosclerotic deposits in the abdominal aorta and bilateral common iliac arteries, cardiomegaly with globular shaped heart and bilateral ventricular hypertrophy along with moderate occlusion of the left anterior descending coronary artery.

Neuropathologic examination

The whole brain was examined both during the general autopsy and after formalin fixation. Extensive subarachnoid hemorrhage was identified predominantly over the ventral aspect of the brain but also involving parts of the cerebral convexity and cerebellar hemisphere. Dissection of the circle of Willis vessels confirmed the presence of multiple unruptured fusiform aneurysms involving segments of the anterior,
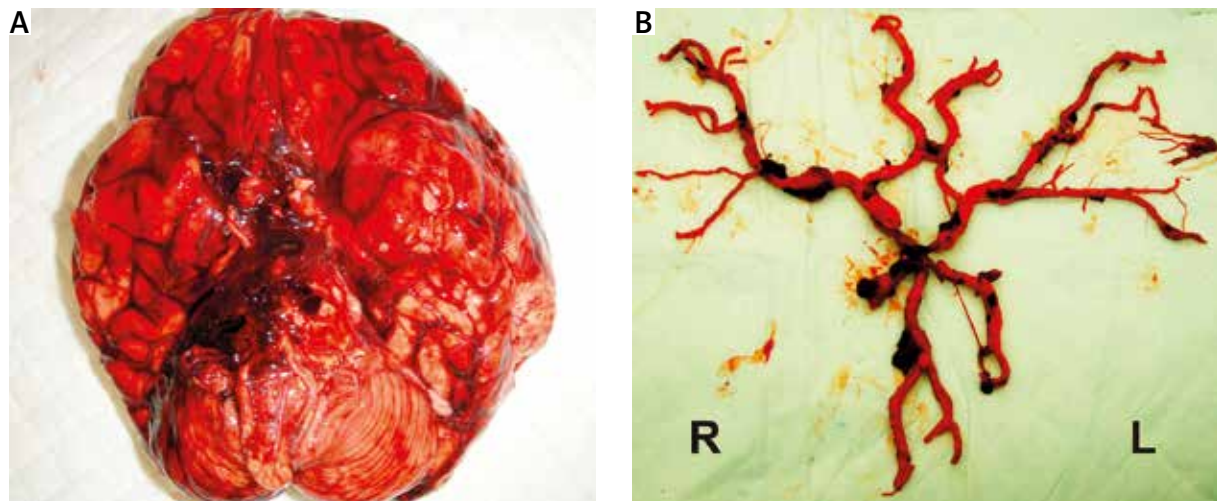

Fig. 1. A) Unfixed brain showing diffuse subarachnoid haemorrhage involving the ventral aspect of the brain including the brainstem and cerebellum. **B)** Vessels of the circle of Willis dissected out of the unfixed brain demonstrating multiple fusiform aneurysms, including involvement of the anterior cerebral artery.

middle and posterior cerebral arteries as well as the basilar artery (Fig. 1). Severe atherosclerosis was also noted throughout the circle of Willis blood vessels.

Coronal sectioning of the cerebrum revealed bilateral intraparenchymal hemorrhage extending to the lateral ventricles. Hemorrhagic infarcts were noted in the anterior-medial aspect of the frontal lobe extending to the posterior parietal lobe and inferiorly to the basal ganglia. Portions of the thalamus and brainstem were also involved by hemorrhage. Intraparenchymal hemorrhage was also seen in the right cerebellum.

Microscopic sections confirmed the presence of aneurysms with the aid of elastic staining, which showed focal loss of the internal elastic lamina. The walls of the blood vessels involved by the aneurysms showed prominent atherosclerotic changes in the form of cholesterol clefts, scattered calcification and intimal hyperplasia. Prominent arteriolosclerosis was noted throughout sections of the cerebral hemisphere.

Subacute to chronic infarcts were observed in the sampled sections of the frontal cortex and mesiotemporal region. Sections of the midbrain and pons revealed extensive hemorrhagic infarcts.

Discussion

Fusiform aneurysm is a localized or diffuse dilation of an artery involving intima, media and adventitia.

It is formed from ectatic, often tortuous, basal arteries. Most aneurysms occur in the basilar artery but are rare in the anterior circulation. When they do occur in the later, they are most commonly found in the middle cerebral artery and internal carotid artery [12]. Fusiform aneurysms that involve the anterior cerebral artery as in our patient are also extremely rare [1,2,4]. Typical presentations of fusiform aneurysms include brain stem and/or cranial nerve compression (basilar artery aneurysm), ischemia secondary to thrombosis, brain stem/cerebellar infarcts with a basilar artery aneurysm or hemorrhage.

Although definite risk factors for multiple aneurysms have not been clearly identified, reported associations include older age, female sex, hypertension, and cigarette smoking [8]. As previously mentioned, our patient had a long history of hypertension. Proposed etiologic factors of fusiform aneurysms include atherosclerosis, vessel dissection, collagen vascular disease, and fibromuscular dysplasia [13].

It has been suggested that the initial event in formation of a fusiform aneurysm is lipid deposition in and below the intima leading to disruption of the internal elastic membrane and infiltration of the muscular wall [5,13]. The resultant atrophy of the elastic substance and musculature then leads to tortuosity of the vessel due to intravascular pressure causing the ectatic vessel to expand in diameter and length. The increasing luminal diameter results in turbulent blood flow, which in turn can lead to thrombus for-
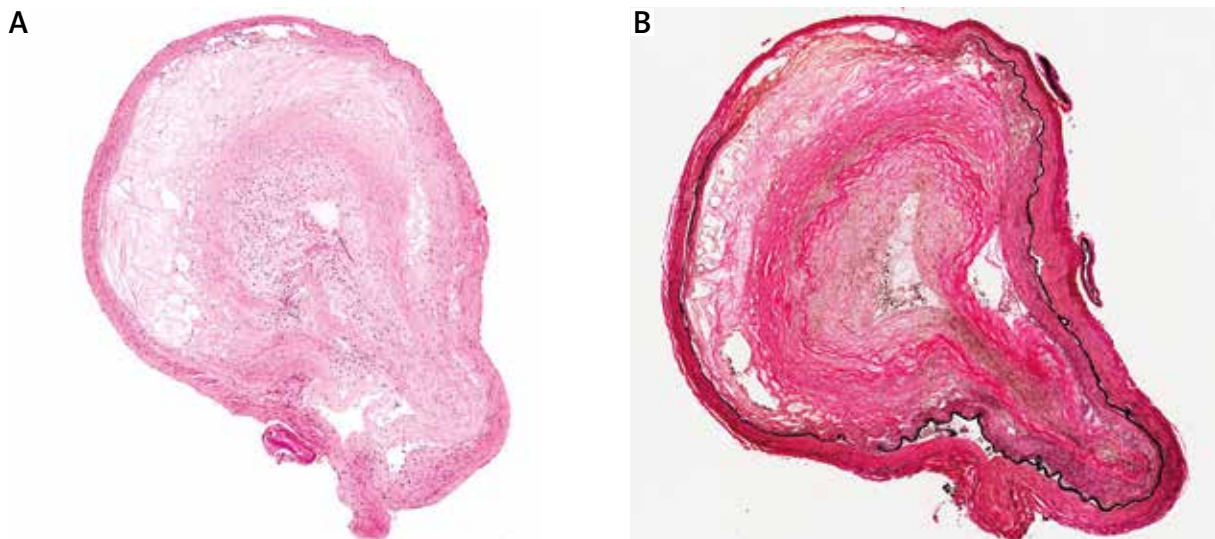

Fig. 2. A) Hematoxylin and eosin stained section from one of the major vessels demonstrating circumferential bulging and atheroma. **B)** Elastic stain demonstrating focal loss of internal elastic lamina.

mation resulting in further intimal disruption and vessel distortion [5,13,14]. In our patient, multiple cerebral vessels were involved by significant atherosclerosis, which may have been the main pathogenic factor in the development of the observed fusiform aneurysms by causing significant weakening of the vessel walls. Histologic examination of the vessels involved by fusiform aneurysms also revealed significant atherosclerotic changes in the form of cholesterol clefts, calcification and intimal hyperplasia. We did not find any pathologic evidence of arterial dissection or any apparent collagen deposition within the walls of the blood vessels. The absence of obvious collagen deposition within the arterial wall made fibromuscular dysplasia or collagen vascular disease less likely factors in the formation of fusiform aneurysms in our patient.

Day (2003) conducted a review of 102 cases of spontaneous fusiform aneurysms based on which he proposed that spontaneous fusiform MCA aneurysms usually develop as a result of arterial dissection. He also suggested that spontaneous fusiform aneurysms in the anterior circulation, especially those involving the MCA, are more often found in younger patients. His review did not include aneurysms associated with trauma, infection, inflammation, and neoplasia. The study also did not touch on fusiform aneurysms occurring in the anterior cerebral artery territory. This raises the question of whether the clinical course of fusiform aneurysms differs depending on where in the anterior circulation they occur and if the mode of management differs in any way.

There are also very few reports of multiple fusiform aneurysms diffusely involving the cerebral vessels as they did in our patient [9]. The clinical course of such extensive involvement is therefore not fully understood and may warrant further study, which in turn can help guide future management and follow-up.

Hemorrhage resulting from rupture of fusiform aneurysms is rare although it has been suggested that fusiform aneurysms of the vertebral artery and internal carotid artery frequently present with hemorrhage [3]. In our case, a site of aneurysmal rupture was not found, leading us to presume that our patient's subarachnoid and intraparenchymal hemorrhages were likely secondary to uncontrolled hypertension.

In summary, we report here a very unusual case of multiple fusiform aneurysms affecting both the posterior and anterior circulation in a single patient with involvement of the anterior cerebral artery, which can pose a treatment challenge. Follow-up studies are needed to better understand the clinical course and determine appropriate management for such patients.

Disclosure

Authors report no conflict of interest.

References

1. Alba AA, Lawton MT. Anterior cerebral artery bypass for complex aneurysms: an experience with intrcranial-intracranial reconstruction and review of bypass options. J Neurosurg 2014; 120: 1364-1377.

2. Chang HW, Youn SW, Jung C, Kang S, Sohn CH, Kwon BJ, Han MH. Technical strategy in endovascular treatment of proximal anterior cerebral artery aneurysms. Acta Neurochir 2011; 153: 279-285.

3. Day AL, Gaposchkin CG, Yu CJ, Rivet DJ, Dacey Jr RJ. Spontaneous fusiform middle cerebral artery aneurysms: characteristics and a proposed mechanism of formation. J Neurosurg 2003; 99: 228-240.

4. Dunn G, Gerrard J, Jho D, Ogilvy C. Surgical treatment of a large fusiform distal anterior cerebral artery aneurysm with in situ end-to-side A3-A3 bypass graft and aneurysm trapping: case report and review of the literature. Neurosurgery 2011; 68: E587-591.

5. Echiverri HC, Rubino FA, Gupta, SR, Gujrati M. Fusiform aneurysms of vertebrobasilar arterial system. Stroke 1989; 20: 1741-1747.

6. Endo T, Mori K, Maeda M. Multiple arteriosclerotic fusiform aneurysms of the superficial temporal artery. Neurol Med Chir 2000; 40: 321-323.

7. George KG, Rennie A, Saxena A. Multiple cerebral aneurysms secondary to cardiac myxoma. Br J Neurosurg 2012; 26: 409-411.

8. Hori N, Takahashi N, Furuichi S, Mori K, Onizuka M, Tsutsumi K, Shibata S. Giant fusiform aneurysms in the middle cerebral artery presenting with hemorrhages of different origins. J Neurosurg 2003; 99: 391-396.

9. Jing L, Liu J, Zhang Y, Paliwal N, Meng H, Wang S, Yang X. Analysis of Multiple Intracranial Aneurysms with Different Outcomes in the Same Patient After Endovascular Treatment. World Neurosurgery 2016; 91: 399-408.

10. Juvela S. Risk factors for multiple intracranial aneurysms. Stroke 2000; 31: 392-397.

11. Krings T, Mandell DM, Kiehl TR, Geibprasert S, Tymianski M, Alvarez H, terBrugge KG, Hans FJ. Intracranial aneurysms: from vessel wall pathology to therapeutic approach. Nat Rev Neurol 2011; 7: 547-559.

12. Nobutaka H Nobuaki T, Shoji F, Katshuharu M, Masanari O, Keisuke T, Shobu S. Giant fusiform aneurysms in the middle cerebral artery presenting with hemorrhages of different origins. J Neurosurg 2003; 99: 391-396.

13. Park S, Yim, M, Lee C, Ealmaan Kim E, Son E. Intracranial Fusiform Aneurysms: It's Pathogenesis, Clinical Characteristics and Managements. J Korean Neurosurg 2008; 44: 116-123.

14. Wakabayashi Y, Nakano T, Isono M, Shimomura T, Hori S. Dissecting Aneurysm of the Anterior Cerebral Artery Requiring Surgical Treatment: Case Report. Neurol Med Chir 2000; 40: 624-627.

Folia
Neuropathologica

Pancreatitis in mitochondrial disorders

Josef Finsterer[1], Sinda Zarrouk-Mahjoub[2]

[1]Krankenanstalt Rudolfstiftung, Vienna, Austria, [2]University of Tunis El Manar, Genomics Platform, Pasteur Institute of Tunis, Tunisia

Dear Editor, with interest we read the article by Zhiping *et al.* about 5 patients from a Chinese family with MELAS due to the m.3243A>G mutation of whom 2 also had pancreatitis in the absence of a *PRSS1* mutation [1]. We have the following comments and concerns.

We do not agree with the statement that only six patients carrying an mtDNA mutation have been so far reported with pancreatitis (Table I) [1]. Pancreatitis was reported in at least 16 other MID patients (Table I) [2]. Interestingly, pancreatitis has not been reported in association with mutations in nDNA located genes. Among MID patients carrying the mtDNA mutation m.3243A>G pancreatitis has been reported in at least 8 patients (Table I).

In the abstract it is stated that 7 members of the family carried the m.3243A>G mutation. However, in the clinical data section, only 5 patients are presented. We should be informed about the reason why 2 patients were excluded from the study. A further discrepancy derives from Figure 1 which shows 9 affected patients. What was the reason why 4 patients were excluded? Another inconsistency concerns the *PRSS1* mutation. In the abstract it is mentioned that it was found in all tissue samples of all 5 included patients. However, in the results section it is men-

tioned that no mutations were found in the *PRSS1, SPINK1*, and *CFTR* genes [1].

Proband I/2 is indicated as deceased in Figure 1 [1]. How can this subject have been investigated if he is dead?

The authors mention that they also recorded EEGs of all included patients [1]. How many of the 5 included patients and the 9 clinically affected had epilepsy? What types of seizures were reported, which antiepileptic drugs were administered, and what was the quality of the seizure control? Particularly patient III/1 had epilepsy. Was she put on a ketogenic diet, which has been shown beneficial at least in some patients with mitochondrial epilepsy [3]?

The authors mention that a structured questionnaire was applied but no results are reported [1]. What was the purpose of applying such a questionnaire and what were the results and their interpretation?

It is quite unusual to find the same abnormality in all 5 included patients in the light of the variable heteroplasmy rates [1]. Did truly all 5 patients show up with cytotoxic edema in the internal capsule bilaterally as presented in the results?

Since MELAS is characterised by the occurrence of stroke-like episodes (SLEs) it would be interesting to know if the index case or any of the family members carrying the m.3243A>G mutation had a posi-

Communicating author:
Josef Finsterer, MD, PhD, Postfach 20, 1180 Vienna, Austria, phone: +43-1-71165, fax: +43-1-4781711, e-mail: fifigs1@yahoo.de

Josef Finsterer, Sinda Zarrouk-Mahjoub

Table I. Mitochondrial disorders in which pancreatitis has been reported

Reference	NOP	Age (y)	Sex	Mutation
Ishiyama 2013	2	10	Female	m.8344A>G
		28	Female	m.3243A>G
Duran 2012	1	3	Male	mtDNA deletion
Liu 2012	1	10	Male	mtDNA deletion
Finsterer 2011	1	80	Female	nm
Velinov 2009	1	4	Female	m.9098T>C
Fragaki 2009	1	Newborn	Male	m.15635T>C
Verny 2008	5	nm	nm	m.3243A>G
Debray 2006	1	17	Male	mtDNA deletion
Finsterer 2006	1	58	Male	nm
Finsterer 2004	1	38	Male	m.8381A>G
Toyono 2001	1	10	Female	m.8344A>G
Tsao 2000	1	3 weeks	Male	mtDNA depletion
Schleiffer 2000	1	37	Female	m.3243A>G
Kishnani 1996	1	1.3	Male	m.3243A>G
Oexle 1996	1	nm	Male	m.3254A>G
Montine 1995	1	17	Male	nm (AHD)
Kato 1990	1	10	Male	CIV deficiency

NOP – number of patients, nm – not mentioned, AHD – Alpers-Huttenlocher disease

tive history for a SLE. In this respect we should be also informed about the results of the DWI and the ADC sequences, particularly if there was a vasogenic or cytotoxic edema in the region of the bilaterally symmetric T2-lesions in the internal capsule.

The authors mention hyperlipidemia as a manifestation of the m.3243A>G mutation [1]. Did they regard hyperlipidemia as a result of the mtDNA mutation and if so, how to explain that serum lipids are elevated due to this mutation? Is it conceivable that hyperlipidemia was attributable to their lifestyle or diet?

Overall, this interesting study could profit from clarification of the inconsistencies mentioned above. Also information about the results of all investigations carried out should be provided. Readers should be also informed about the applied treatment of any phenotypic feature and its effect.

Disclosure

Authors report no conflict of interest.

References

1. Zhiping W, Quwen L, Hai Z, Jian Z, Peiyi G. Application of molecular imaging combined with genetic screening in diagnosing MELAS, diabetes and recurrent pancreatitis. Folia Neuropathol 2016; 54: 66-71.
2. Ishiyama A, Komaki H, Saito T, Saito Y, Nakagawa E, Sugai K, Itagaki Y, Matsuzaki K, Nakura M, Nishino I, Goto Y, Sasaki M. Unusual exocrine complication of pancreatitis in mitochondrial disease. Brain Dev 2013; 35: 654-659.
3. Martikainen MH, Päivärinta M, Jääskeläinen S, Majamaa K. Successful treatment of POLG-related mitochondrial epilepsy with antiepileptic drugs and low glycaemic index diet. Epileptic Disord 2012; 14: 438-441.

Editor's Note

Up to December 2016 the authors of the article entitled: "Application of molecular imaging combined with genetic screening in diagnosing MELAS, diabetes and recurrent pancreatitis" did not reply to the comments including in this letter.

Instructions to Authors

This instruction is based upon *Uniform Requirements for Manuscripts Submitted to Biomedical Reviews* (the complete document appears in N Engl J Med 1997; 336, 309-315).

Aims and scope

Folia Neuropathologica is an official journal of the Mossakowski Medical Research Centre Polish Academy of Sciences and the Polish Association of Neuropathologists. The journal publishes original articles and reviews that deal with all aspects of clinical and experimental neuropathology and related fields of neuroscience research. The scope of journal includes surgical and experimental pathomorphology, ultrastructure, immunohistochemistry, biochemistry and molecular biology of the nervous tissue. Papers on surgical neuropathology and neuroimaging are also welcome. The reports in other fields relevant to the understanding of human neuropathology might be considered.

Publication charge

Please note that there is an obligatory charge (250 Euro) for the manuscript being accepted for publication in *Folia Neuropathologica*. We send invoice for payment after the article is accepted for publication. There are no additional charges based on color figures or other elements.

Ethical consideration

Papers describing animal experiments can be accepted for publication only if the experiment conforms to the legal requirements in Poland as well as with the European Communities Council Directive of November 24, 1986 or the National Institute of Health Guide (National Institute of Health Publications No. 80-23, Revised 1978) for the care and use of Laboratory Animals for experimental procedure. Authors must provide a full description of their anesthetics and surgical procedures. Papers describing experiments on human subjects must include a statement that experiments were performed with the understanding and consent of each subject, with the approval of the appropriate local ethics committee.

Submission of manuscripts

Articles should be written in English. All new manuscripts should be submitted through the online submission at http://panel2.termedia.pl/fn
For authors unable to submit their manuscript online, please contact with Prof. E. Matyja, Editor-in-Chief of *Folia Neuropathologica*, ematyja@imdik.pan.pl
The Editorial Board reserves the right to reject a paper without reviewers' opinion if the content or the form of the paper does not meet minimum acceptance criteria or if the subject of the paper is beyond the aims and scope of the journal.

Legal aspects

In sending the manuscript the author(s) confirm(s) that (s)he has (they have) not previously submitted it to another journal (except for abstracts of no more than 400 words) or published it elsewhere. The author(s) also agree(s), if and when the manuscript is accepted for publication, to automatic and free transfer of copyright to the Publisher allowing for the publication and distribution of the material submitted in all available forms and fields of exploitation. The author(s) accept(s) that the manuscript will not be published elsewhere in any language without the written consent of the copyright holder, i.e. the Publisher.
All manuscripts submitted should be accompanied by an authors' statement including signed confirmation of the above and confirming that this publication has been approved by all co-authors (if any), as well as by the responsible authorities at the institution where the work has been carried out. The authors' statement should be signed by ALL co-authors. Additionally, the author(s) confirm(s) that (s)he is (they are) familiar with and will observe the "Instruction to Authors" included in *Folia Neuropathologica* and also that all sources of financial support have been fully disclosed. Materials previously published should be accompanied by written consent for reprinting from the relevant Publishers. In the case of photographs of identifiable persons, their written consent should also be provided. Any potential conflict of interest will be dealt with by the local court specific to the Publisher. Legal relations between the Publisher and the author(s) are in accordance with Polish law and with international conventions binding on Poland.
Authors agree to waive their royalties.

Anonymous review

All manuscripts will be subject to a process of anonymous editorial review.

Preparation of manuscripts

Articles must be written in English, with British spelling used consistently throughout. Authors not entirely familiar with English are advised to correct the style by professional language editors or native English speakers.
• The length of original article should not exceed 20 printed pages including text, illustrations, tables, and references.

- Manuscripts should be typed using 12pts.font, double-spaced, and fully corrected. Allow a margin at least 2.5 cm at the top, bottom and left side of the page. Text should not be justified.
- The title page should contain: the author's full names, title of the paper, all authors' affiliations, full name and address of the communicating author (including e-mail address and fax number), running title (not exceed 40 characters including spaces).
- The abstract should not exceed 350 words. A list of 3–10 key words is recommended below the abstract.
- The manuscript body should be organized in a standard form with separate sections: Introduction, Material and Methods, Results, Discussion, and References. Review articles should be divided into sections and subsections as appropriate without numbering.
- Do not underline in the text. Avoid footnotes.
- All dimensions and measurements must be specified in the metric system.
- The source of any drug and special reagent should be identified.
- Particular attention needs to be paid to the selection of appropriate analysis of data and the results of statistical test should be incorporated in the results section.
- The nomenclature used should conform to the current edition of the Nomina Anatomica or Nomina Anatomica Veterinaria.
- Acknowledgements should be made in a separate sheet following Discussion and before References. These should contain a list of dedications, acknowledgements, and funding sources.
- Legends of figures and tables should be typed on separate pages.
- The editor reserves the right to make corrections.

Tables

- Tables numbered in Roman numerals require a brief but descriptive heading.
- The major divisions of the table should be indicated by horizontal rules.
- Explanatory matter should be included in footnotes, indicated in the body of the table in order of their appearance.
- Tables must not duplicate material in the text or in illustration.

Illustrations

All figures should be supplied electronically at resolution 300dpi in all standard formats (tiff, jpg, Adobe Photoshop, Corel Draw, and EPS). Name your figure files with "Fig" and the figure number, e.g., Fig1.tif
- The maximum figure size is 84 mm or 174 mm for use in a single or double column width, respectively.
- When possible, group several illustrations on one block for reproduction. Like all other figures, block should be prepared within a rectangular frame to fit within a single or double column width of 84 and 174 mm, respectively, and a maximum page height of 226 mm.
- Each figure should include scale magnification bar; do not use magnification factors in the figure legends.
- All figures, whether photographs, graphs or diagrams, should be numbered using Arabic numerals and cited in the text in consecutive numerical order
- **Immunohistochemical study requires color illustrations of very good quality. The papers with white and black immunohistochemistry will not be accepted.**
- **For the paper accepted before 01.04.2016 the publication charge includes only the expense of color illustrations.** The cost of color print for every successive 8 pages is 200 euro irrespective of the number of color pages, i.e., the price remains the same whether there is one or eight pages.
The Publisher makes out the bill to the communicating Author.

References

The list of references (written on a separate page) should include only those publications that are cited in the text. Avoid citation of academic books, manuals and atlases. References may be arranged alphabetically and numbered consecutively. References should be given in square brackets with no space between the comma and the consecutive number, e.g. [3,4,6-12].
References should be written as follows:
Journal papers: initials and names of all authors, full title of paper, journal abbreviation (according to Index Medicus), year of publication, volume (in Arabic numerals), first and last page (example below):
1. Valverde F. The organization of area 18 in the monkey. Anat Embryol 1978; 154: 305-334.
2. Uray NJ, Gona AG. Calbindin immunoreactivity in the auricular lobe and interauricular granular band of the cerebellum in bullfrogs. Brain Behav Evol 1999; 53: 10-19.
Book and monographs: initials and names of all authors, full title, edition, publisher, place, year (examples below):
1. Pollack RS. Tumor surgery of the head and neck. Karger, Basel 1975.
2. Amaral DG, Price JL, Pitkänen A, Carmichael ST. Anatomical organization of the primate amygdaloid complex. In: Aggleton JP (ed.). The amygdala. Wiley-Liss, New York 1992; pp. 1-66.
Reference to articles that are accepted for publication may be cited as „in press" or Epub.

Proofs

Corrections to the proofs should be restricted to printer's errors only; other alterations will be charged to the authors. In order to maintain rapid publication, proofs should be returned within 48 hours, preferably by e-mail, fax or courier mail. If the Publisher receives no response from the authors after 10 days, it will be assumed that there are no errors to correct and the article will be published.

Subscription information

Folia
Neuropathologica

AUTHOR'S STATEMENT

Title of the article

....

....

....

The author(s) hereby confirm(s) that:

☐ The above-mentioned work has not previously been published and that it has not been submitted to the Publishers of any other journal (with the exception of abstracts not exceeding 400 words).

☐ All co-authors named and the relevant authorities of the scientific institutions at which the work has been carried out are familiar with the contents of this work and have agreed to its publication.

☐ In sending the manuscript together with illustrations and tables agree(s) to automatic and free transfer of copyright to the Publisher allowing for the publication and distribution of the material submitted in all available forms and fields of exploitation, without limits of territory or language, provided that the material is accepted for publication. At the same time the author(s) accept(s) that the submitted work will not be published elsewhere and in whatever language without the earlier written permission of the copyright holder, i.e. the Publisher.

☐ (S)he (they) agree to waive his(her)(their) royalties (fees).

☐ (S)he (they) empower(s) the Publisher to make any necessary editorial changes to the submitted manuscript.

☐ All sources of funding of the work have been fully disclosed.

☐ The manuscript has been prepared in accordance with the Publisher's requirements.

☐ (S)he (they) is (are) familiar with the regulations governing the acceptance of works as published in *Folia Neuropathologica* and agree(s) to follow them.

☐ (S)he (they) agree to accept appropriate invoice from the Publisher in case colour illustrations are implemented.

Date   *Signatures of **all** authors*

The covering letter formula can be found at: www.folianeuro.termedia.pl
-The covering letter should be sent to Associate Editor:
Milena Laure-Kamionowska
-Editorial Office of Folia Neuropathologica
Mossakowski Medical Research Centre, Polish Academy of Sciences
Poland Medical Research Centre
ul. Pawinskiego 5
02-106 Warszawa, Poland

CONTENTS